

# An Introduction to Thermal Physics

Daniel V. Schroeder

Weber State University

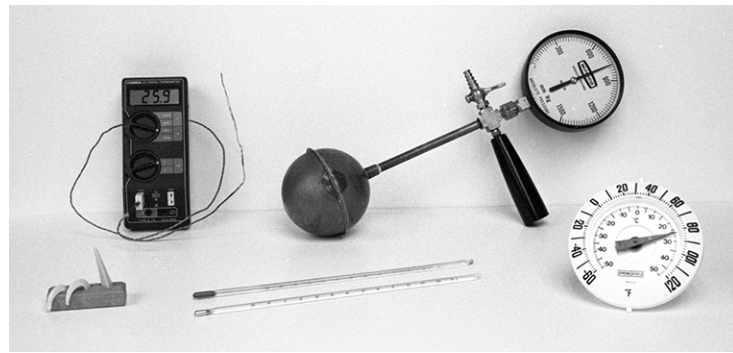
This collection of figures and tables is provided for the personal and classroom use of students and instructors. Anyone is welcome to download this document and save a personal copy for reference. Instructors are welcome to incorporate these figures and tables, with attribution, into lecture slides and similar materials for classroom presentation. Any other type of reproduction or redistribution, including re-posting on any public Web site, is prohibited. All of this material is under copyright by the publisher, except for figures that are attributed to other sources, which are under copyright by those sources.

Copyright ©2000, Addison-Wesley Publishing Company

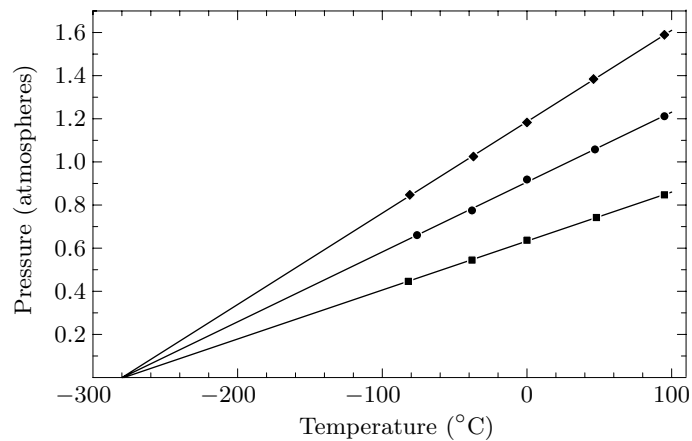
# 1 Energy in Thermal Physics



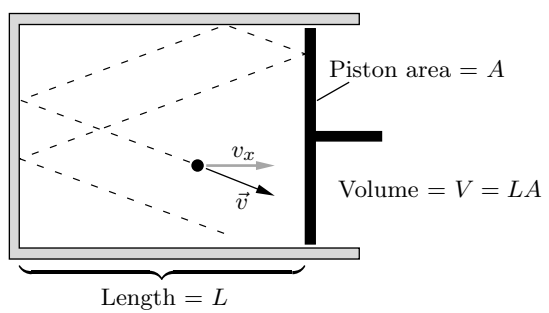
**Figure 1.1.** A hot-air balloon interacts thermally, mechanically, and diffusively with its environment—exchanging energy, volume, and particles. Not all of these interactions are at equilibrium, however. Copyright ©2000, Addison-Wesley.



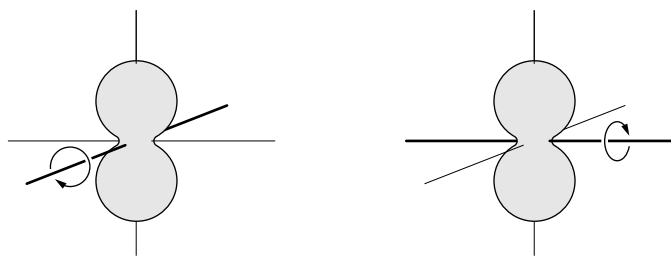
**Figure 1.2.** A selection of thermometers. In the center are two liquid-in-glass thermometers, which measure the expansion of mercury (for higher temperatures) and alcohol (for lower temperatures). The dial thermometer to the right measures the turning of a coil of metal, while the bulb apparatus behind it measures the pressure of a fixed volume of gas. The digital thermometer at left-rear uses a thermocouple—a junction of two metals—which generates a small temperature-dependent voltage. At left-front is a set of three potter's cones, which melt and droop at specified clay-firing temperatures. Copyright ©2000, Addison-Wesley.



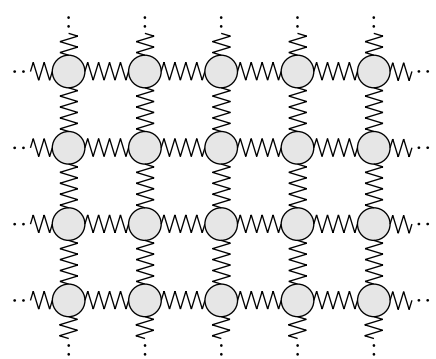
**Figure 1.3.** Data from a student experiment measuring the pressure of a fixed volume of gas at various temperatures (using the bulb apparatus shown in Figure 1.2). The three data sets are for three different amounts of gas (air) in the bulb. Regardless of the amount of gas, the pressure is a linear function of temperature that extrapolates to zero at approximately  $-280^{\circ}\text{C}$ . (More precise measurements show that the zero-point does depend slightly on the amount of gas, but has a well-defined limit of  $-273.15^{\circ}\text{C}$  as the density of the gas goes to zero.) Copyright ©2000, Addison-Wesley.



**Figure 1.4.** A greatly simplified model of an ideal gas, with just one molecule bouncing around elastically. Copyright ©2000, Addison-Wesley.

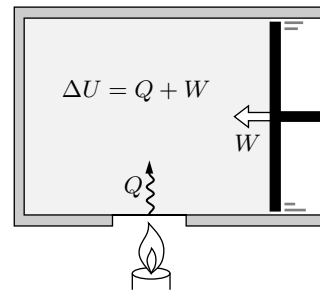


**Figure 1.5.** A diatomic molecule can rotate about two independent axes, perpendicular to each other. Rotation about the third axis, down the length of the molecule, is not allowed. Copyright ©2000, Addison-Wesley.

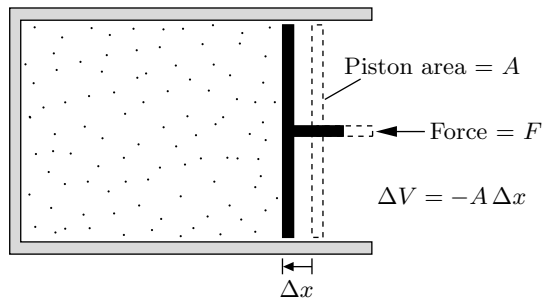


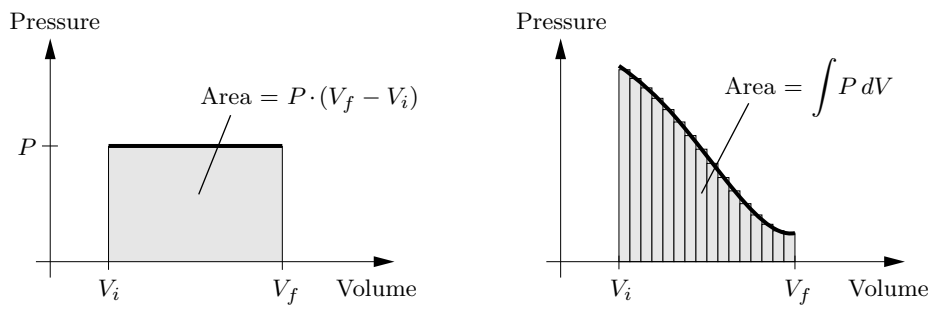
**Figure 1.6.** The “bed-spring” model of a crystalline solid. Each atom is like a ball, joined to its neighbors by springs. In three dimensions, there are six degrees of freedom per atom: three from kinetic energy and three from potential energy stored in the springs. Copyright ©2000, Addison-Wesley.

**Figure 1.7.** The total change in the energy of a system is the sum of the heat added to it and the work done on it. Copyright ©2000, Addison-Wesley.

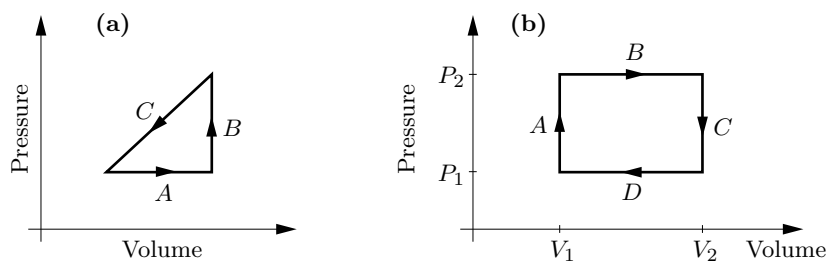


**Figure 1.8.** When the piston moves inward, the volume of the gas changes by  $\Delta V$  (a negative amount) and the work done on the gas (assuming quasistatic compression) is  $-P\Delta V$ . Copyright ©2000, Addison-Wesley.

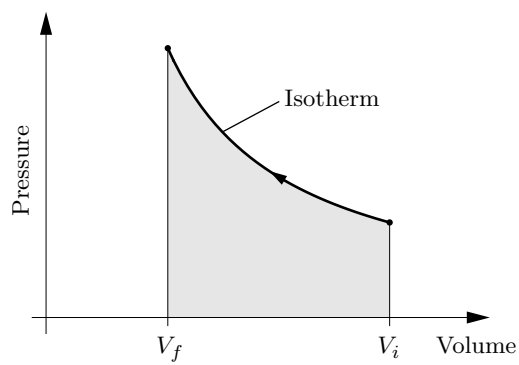




**Figure 1.9.** When the volume of a gas changes and its pressure is constant, the work done on the gas is minus the area under the graph of pressure vs. volume. The same is true even when the pressure is not constant. Copyright ©2000, Addison-Wesley.

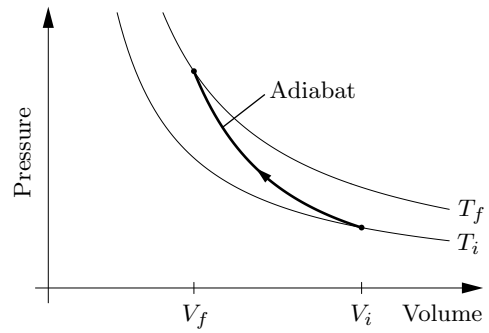


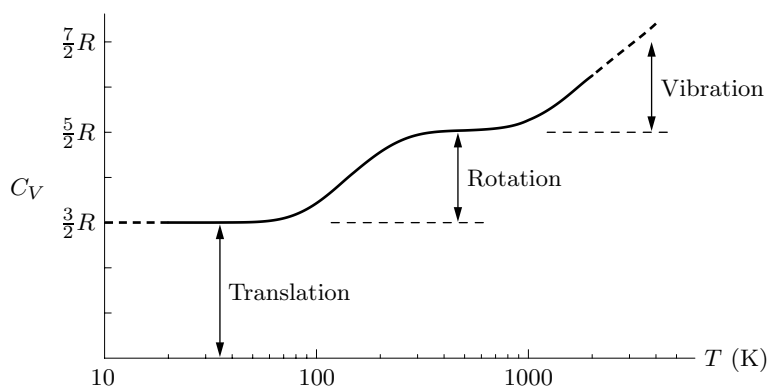
**Figure 1.10.** *PV* diagrams for Problems 1.33 and 1.34. Copyright ©2000, Addison-Wesley.



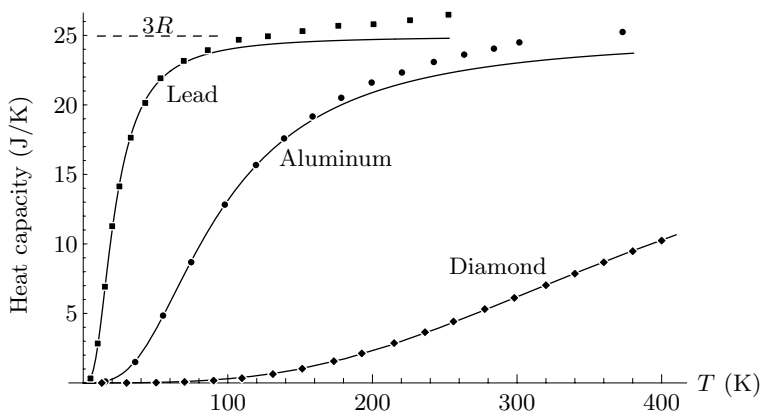
**Figure 1.11.** For isothermal compression of an ideal gas, the  $PV$  graph is a concave-up hyperbola, called an **isotherm**. As always, the work done is minus the area under the graph. Copyright ©2000, Addison-Wesley.

**Figure 1.12.** The  $PV$  curve for adiabatic compression (called an **adiabat**) begins on a lower-temperature isotherm and ends on a higher-temperature isotherm.  
Copyright ©2000, Addison-Wesley.

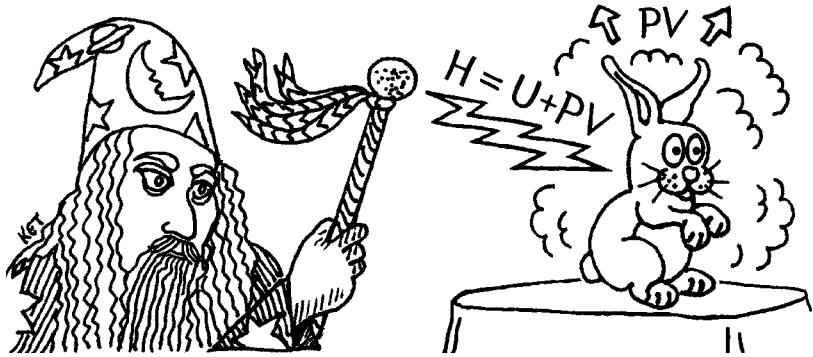




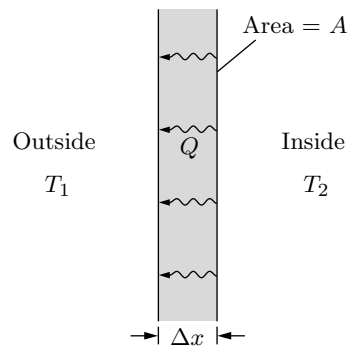
**Figure 1.13.** Heat capacity at constant volume of one mole of hydrogen ( $H_2$ ) gas. Note that the temperature scale is logarithmic. Below about 100 K only the three translational degrees of freedom are active. Around room temperature the two rotational degrees of freedom are active as well. Above 1000 K the two vibrational degrees of freedom also become active. At atmospheric pressure, hydrogen liquefies at 20 K and begins to dissociate at about 2000 K. Data from Woolley et al. (1948). Copyright ©2000, Addison-Wesley.



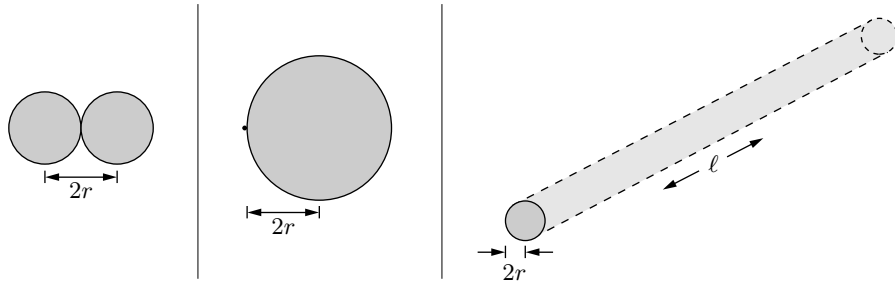
**Figure 1.14.** Measured heat capacities at constant pressure (data points) for one mole each of three different elemental solids. The solid curves show the heat capacity at constant *volume* predicted by the model used in Section 7.5, with the horizontal scale chosen to best fit the data for each substance. At sufficiently high temperatures,  $C_V$  for each material approaches the value  $3R$  predicted by the equipartition theorem. The discrepancies between the data and the solid curves at high  $T$  are mostly due to the differences between  $C_P$  and  $C_V$ . At  $T = 0$  all degrees of freedom are frozen out, so both  $C_P$  and  $C_V$  go to zero. Data from Y. S. Touloukian, ed., *Thermophysical Properties of Matter* (Plenum, New York, 1970). Copyright ©2000, Addison-Wesley.



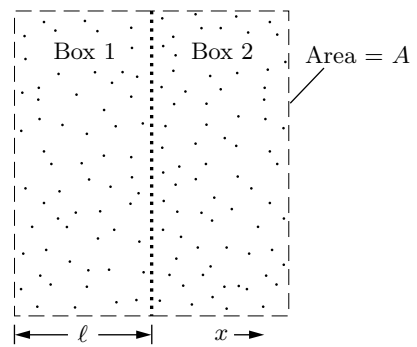
**Figure 1.15.** To create a rabbit out of nothing and place it on the table, the magician must summon up not only the energy  $U$  of the rabbit, but also some additional energy, equal to  $PV$ , to push the atmosphere out of the way to make room. The *total* energy required is the **enthalpy**,  $H = U + PV$ . Drawing by Karen Thurber. Copyright ©2000, Addison-Wesley.



**Figure 1.16.** The rate of heat conduction through a pane of glass is proportional to its area  $A$  and inversely proportional to its thickness  $\Delta x$ . Copyright ©2000, Addison-Wesley.

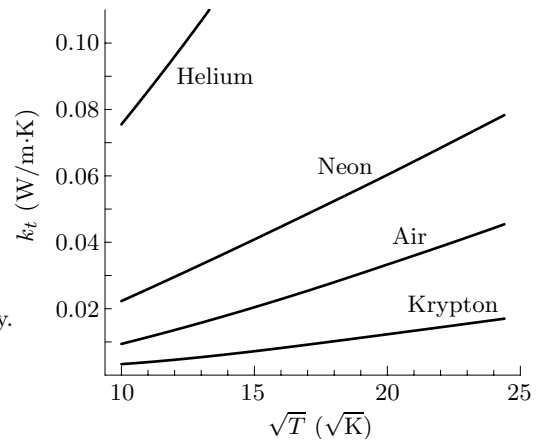


**Figure 1.17.** A collision between molecules occurs when their centers are separated by twice the molecular radius  $r$ . The same would be true if one molecule had radius  $2r$  and the other were a point. When a sphere of radius  $2r$  moves in a straight line of length  $\ell$ , it sweeps out a cylinder whose volume is  $4\pi r^2\ell$ . Copyright ©2000, Addison-Wesley.



**Figure 1.18.** Heat conduction across the dotted line occurs because the molecules moving from box 1 to box 2 have a different average energy than the molecules moving from box 2 to box 1. For free motion between these boxes, each should have a width of roughly one mean free path. Copyright ©2000, Addison-Wesley.

**Figure 1.19.** Thermal conductivities of selected gases, plotted vs. the square root of the absolute temperature. The curves are approximately linear, as predicted by equation 1.65. Data from Lide (1994). Copyright ©2000, Addison-Wesley.



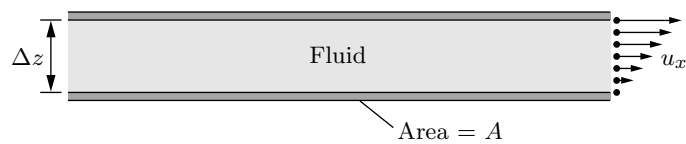
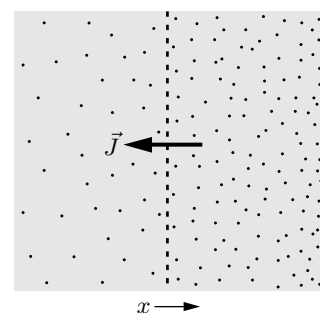


**Figure 1.20.** The simplest arrangement for demonstrating viscosity: two parallel surfaces sliding past each other, separated by a narrow gap containing a fluid. If the motion is slow enough and the gap narrow enough, the fluid flow is **laminar**: At the macroscopic scale the fluid moves only horizontally, with no turbulence.  
Copyright ©2000, Addison-Wesley.

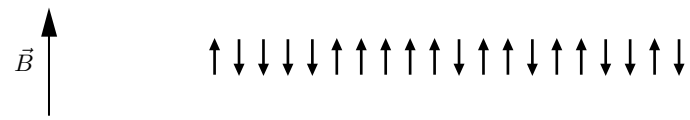
**Figure 1.21.** When the concentration of a certain type of molecule increases from left to right, there will be **diffusion**, a net flow of molecules, from right to left. Copyright ©2000, Addison-Wesley.



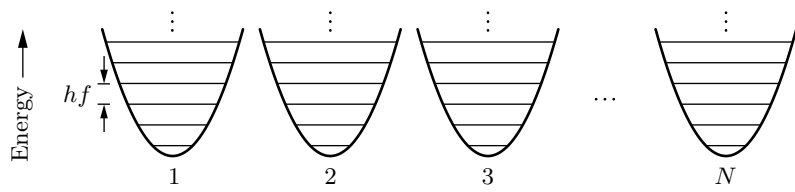
# 2 The Second Law

Penny	Nickel	Dime
H	H	H
H	H	T
H	T	H
T	H	H
H	T	T
T	H	T
T	T	H
T	T	T

**Table 2.1.** A list of all possible “microstates” of a set of three coins (where H is for heads and T is for tails). Copyright ©2000, Addison-Wesley.



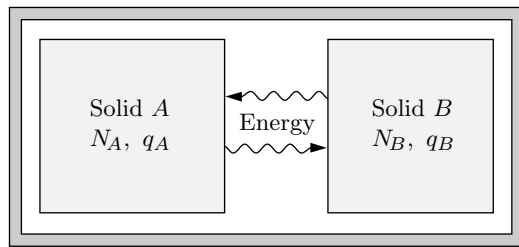
**Figure 2.1.** A symbolic representation of a two-state paramagnet, in which each elementary dipole can point either parallel or antiparallel to the externally applied magnetic field. Copyright ©2000, Addison-Wesley.



**Figure 2.2.** In quantum mechanics, any system with a quadratic potential energy function has evenly spaced energy levels separated in energy by  $hf$ , where  $f$  is the classical oscillation frequency. An Einstein solid is a collection of  $N$  such oscillators, all with the same frequency. Copyright ©2000, Addison-Wesley.

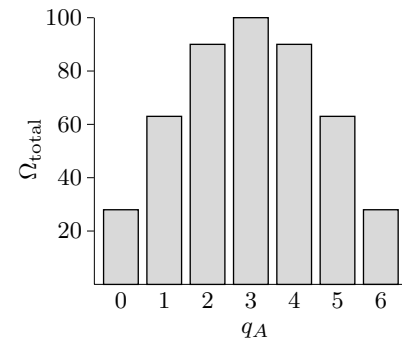
Oscillator:	#1	#2	#3	Oscillator:	#1	#2	#3
Energy:	0	0	0	Energy:	3	0	0
1	0	0		0	3	0	
0	1	0		0	0	3	
0	0	1		2	1	0	
2	0	0		2	0	1	
0	2	0		1	2	0	
0	0	2		0	2	1	
1	1	0		1	0	2	
1	0	1		0	1	2	
0	1	1		1	1	1	

**Table 2.2.** Microstates of a small Einstein solid consisting of only three oscillators, containing a total of zero, one, two, or three units of energy. Copyright ©2000, Addison-Wesley.



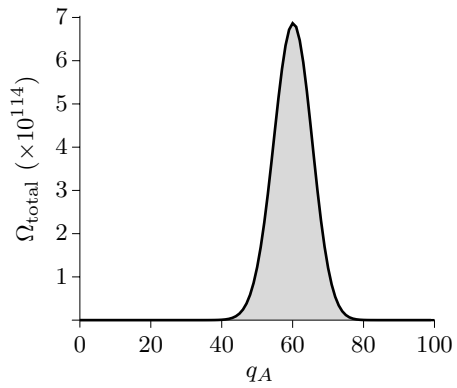
**Figure 2.3.** Two Einstein solids that can exchange energy with each other, isolated from the rest of the universe. Copyright ©2000, Addison-Wesley.

$q_A$	$\Omega_A$	$q_B$	$\Omega_B$	$\Omega_{\text{total}} = \Omega_A \Omega_B$
0	1	6	28	28
1	3	5	21	63
2	6	4	15	90
3	10	3	10	100
4	15	2	6	90
5	21	1	3	63
6	28	0	1	28
$\frac{462}{462} = \binom{6+6-1}{6}$				

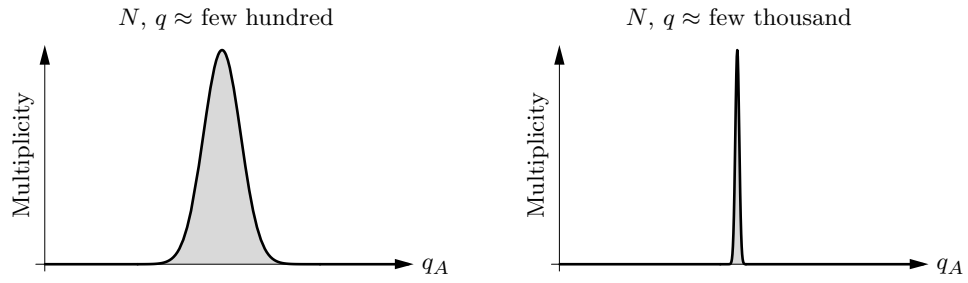


**Figure 2.4.** Macrostates and multiplicities of a system of two Einstein solids, each containing three oscillators, sharing a total of six units of energy. Copyright ©2000, Addison-Wesley.

$q_A$	$\Omega_A$	$q_B$	$\Omega_B$	$\Omega_{\text{total}}$
0	1	100	$2.8 \times 10^{81}$	$2.8 \times 10^{81}$
1	300	99	$9.3 \times 10^{80}$	$2.8 \times 10^{83}$
2	45150	98	$3.1 \times 10^{80}$	$1.4 \times 10^{85}$
3	4545100	97	$1.0 \times 10^{80}$	$4.6 \times 10^{86}$
4	$3.4 \times 10^8$	96	$3.3 \times 10^{79}$	$1.1 \times 10^{88}$
$\vdots$	$\vdots$	$\vdots$	$\vdots$	$\vdots$
59	$2.2 \times 10^{68}$	41	$3.1 \times 10^{46}$	$6.8 \times 10^{114}$
60	$1.3 \times 10^{69}$	40	$5.3 \times 10^{45}$	$6.9 \times 10^{114}$
61	$7.7 \times 10^{69}$	39	$8.8 \times 10^{44}$	$6.8 \times 10^{114}$
$\vdots$	$\vdots$	$\vdots$	$\vdots$	$\vdots$
100	$1.7 \times 10^{96}$	0	1	$\frac{1.7 \times 10^{96}}{9.3 \times 10^{115}}$



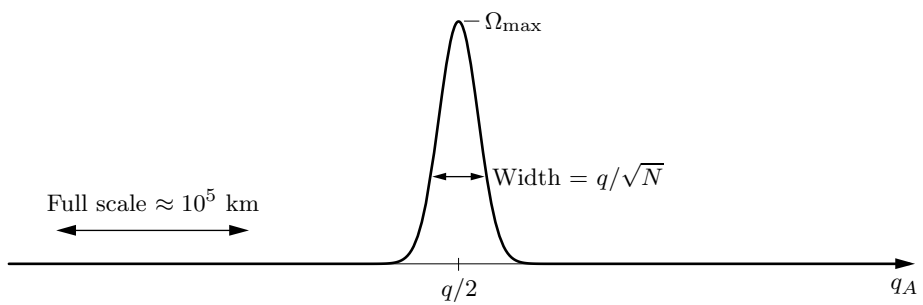
**Figure 2.5.** Macrostates and multiplicities of a system of two Einstein solids, with 300 and 200 oscillators respectively, sharing a total of 100 units of energy.  
Copyright ©2000, Addison-Wesley.



**Figure 2.6.** Typical multiplicity graphs for two interacting Einstein solids, containing a few hundred oscillators and energy units (left) and a few thousand (right). As the size of the system increases, the peak becomes very narrow relative to the full horizontal scale. For  $N \approx q \approx 10^{20}$ , the peak is much too sharp to draw.  
Copyright ©2000, Addison-Wesley.

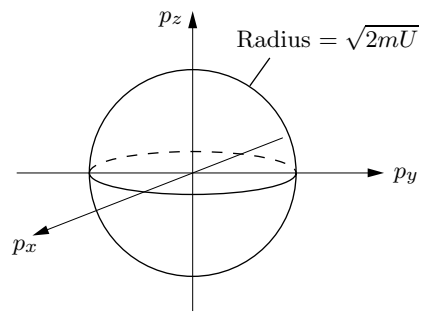
$N$	$N!$	$N^N e^{-N} \sqrt{2\pi N}$	Error	$\ln N!$	$N \ln N - N$	Error
1	1	.922	7.7%	0	-1	$\infty$
10	3628800	3598696	.83%	15.1	13.0	13.8%
100	$9 \times 10^{157}$	$9 \times 10^{157}$	.083%	364	360	.89%

**Table 2.3.** Comparison of Stirling's approximation (equations 2.14 and 2.16) to exact values for  $N = 1, 10$ , and  $100$ . Copyright ©2000, Addison-Wesley.



**Figure 2.7.** Multiplicity of a system of two large Einstein solids with many energy units per oscillator (high-temperature limit). Only a tiny fraction of the full horizontal scale is shown. Copyright ©2000, Addison-Wesley.

**Figure 2.8.** A sphere in momentum space with radius  $\sqrt{2mU}$ . If a molecule has energy  $U$ , its momentum vector must lie somewhere on the surface of this sphere. Copyright ©2000, Addison-Wesley.



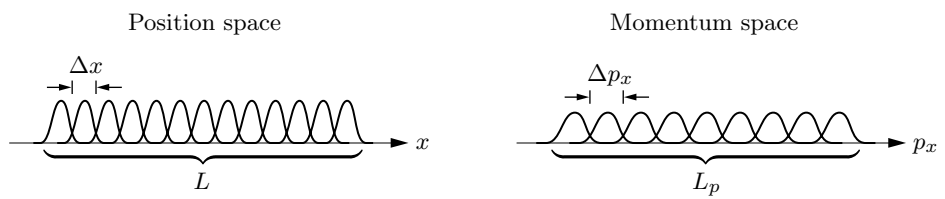


**Figure 2.9.** A number of “independent” position states and momentum states for a quantum-mechanical particle moving in one dimension. If we make the wavefunctions narrower in position space, they become wider in momentum space, and vice versa. Copyright ©2000, Addison-Wesley.

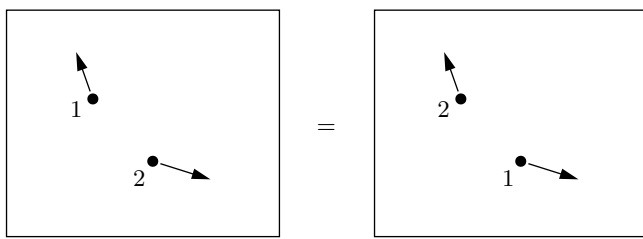


**Figure 2.10.** In a gas of two identical molecules, interchanging the states of the molecules leaves the system in the same state as before. Copyright ©2000, Addison-Wesley.

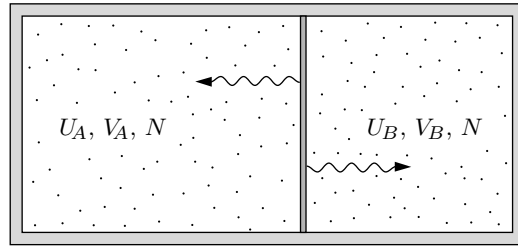


**Figure 2.11.** Two ideal gases, each confined to a fixed volume, separated by a partition that allows energy to pass through. The total energy of the two gases is fixed. Copyright ©2000, Addison-Wesley.

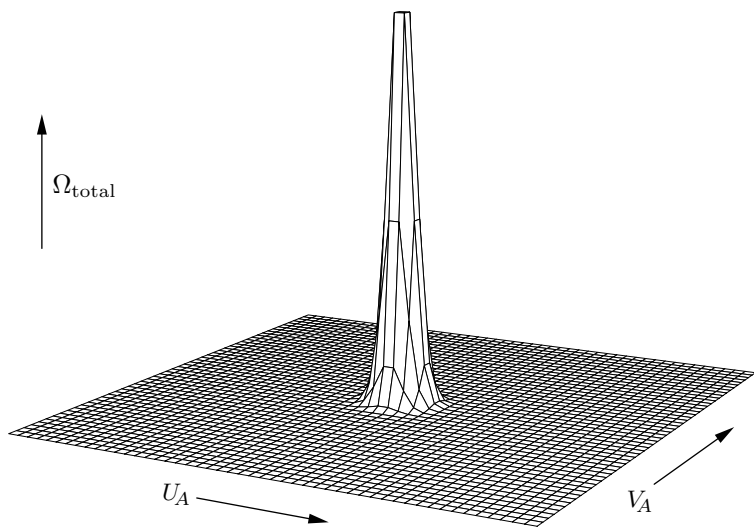


**Figure 2.12.** Multiplicity of a system of two ideal gases, as a function of the energy and volume of gas A (with the total energy and total volume held fixed). If the number of molecules in each gas is large, the full horizontal scale would stretch far beyond the edge of the page. Copyright ©2000, Addison-Wesley.

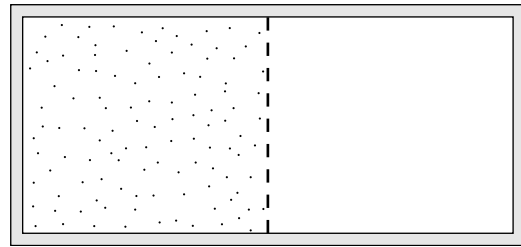


**Figure 2.13.** A very unlikely arrangement of gas molecules. Copyright ©2000, Addison-Wesley.

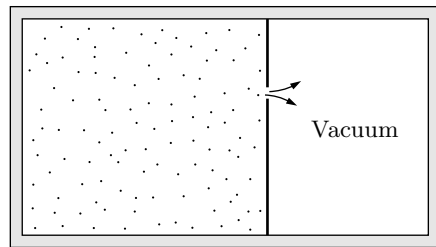


**Figure 2.14.** Free expansion of a gas into a vacuum. Because the gas neither does work nor absorbs heat, its energy is unchanged. The entropy of the gas increases, however. Copyright ©2000, Addison-Wesley.

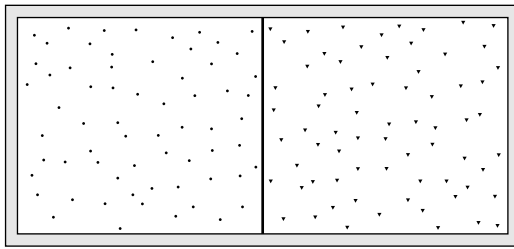


**Figure 2.15.** Two different gases, separated by a partition. When the partition is removed, each gas expands to fill the whole container, mixing with the other and creating entropy. Copyright ©2000, Addison-Wesley.

# 3 Interactions and Implications

$q_A$	$\Omega_A$	$S_A/k$	$q_B$	$\Omega_B$	$S_B/k$	$\Omega_{\text{total}}$	$S_{\text{total}}/k$
0	1	0	100	$2.8 \times 10^{81}$	187.5	$2.8 \times 10^{81}$	187.5
1	300	5.7	99	$9.3 \times 10^{80}$	186.4	$2.8 \times 10^{83}$	192.1
2	45150	10.7	98	$3.1 \times 10^{80}$	185.3	$1.4 \times 10^{85}$	196.0
$\vdots$	$\vdots$	$\vdots$	$\vdots$	$\vdots$	$\vdots$	$\vdots$	$\vdots$
11	$5.3 \times 10^{19}$	45.4	89	$1.1 \times 10^{76}$	175.1	$5.9 \times 10^{95}$	220.5
12	$1.4 \times 10^{21}$	48.7	88	$3.4 \times 10^{75}$	173.9	$4.7 \times 10^{96}$	222.6
13	$3.3 \times 10^{22}$	51.9	87	$1.0 \times 10^{75}$	172.7	$3.5 \times 10^{97}$	224.6
$\vdots$	$\vdots$	$\vdots$	$\vdots$	$\vdots$	$\vdots$	$\vdots$	$\vdots$
59	$2.2 \times 10^{68}$	157.4	41	$3.1 \times 10^{46}$	107.0	$6.7 \times 10^{114}$	264.4
60	$1.3 \times 10^{69}$	159.1	40	$5.3 \times 10^{45}$	105.3	$6.9 \times 10^{114}$	264.4
61	$7.7 \times 10^{69}$	160.9	39	$8.8 \times 10^{44}$	103.5	$6.8 \times 10^{114}$	264.4
$\vdots$	$\vdots$	$\vdots$	$\vdots$	$\vdots$	$\vdots$	$\vdots$	$\vdots$
100	$1.7 \times 10^{96}$	221.6	0	1	0	$1.7 \times 10^{96}$	221.6

**Table 3.1.** Macrostates, multiplicities, and entropies of a system of two Einstein solids, one with 300 oscillators and the other with 200, sharing a total of 100 units of energy. Copyright ©2000, Addison-Wesley.

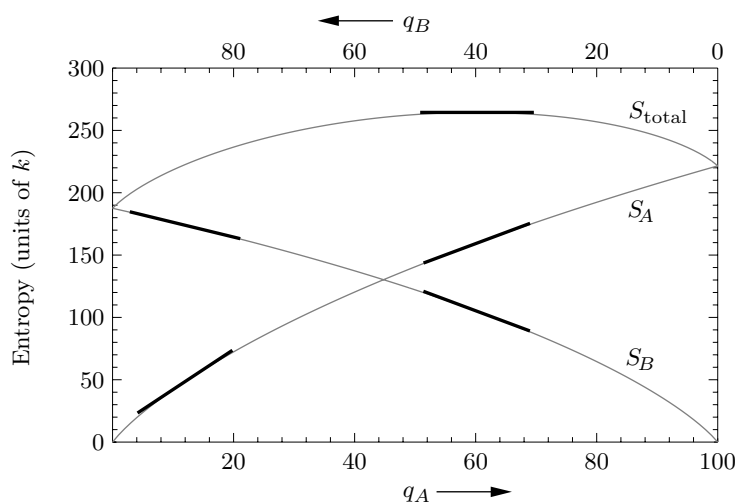


**Figure 3.1.** A plot of the entropies calculated in Table 3.1. At equilibrium ( $q_A = 60$ ), the total entropy is a maximum so its graph has a horizontal tangent; therefore the slopes of the tangents to the graphs of  $S_A$  and  $S_B$  are equal in magnitude. Away from equilibrium (for instance, at  $q_A = 12$ ), the solid whose graph has the steeper tangent line tends to gain energy spontaneously; therefore we say that it has the lower temperature. Copyright ©2000, Addison-Wesley.

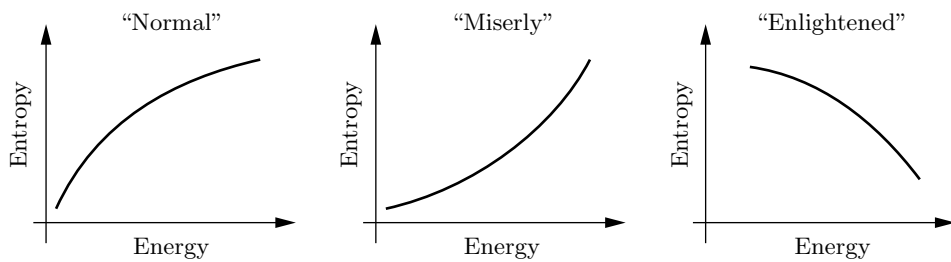


**Figure 3.2.** Graphs of entropy vs. energy (or happiness vs. money) for a “normal” system that becomes hotter (more generous) as it gains energy; a “miserly” system that becomes colder (less generous) as it gains energy; and an “enlightened” system that doesn’t want to gain energy at all. Copyright ©2000, Addison-Wesley.

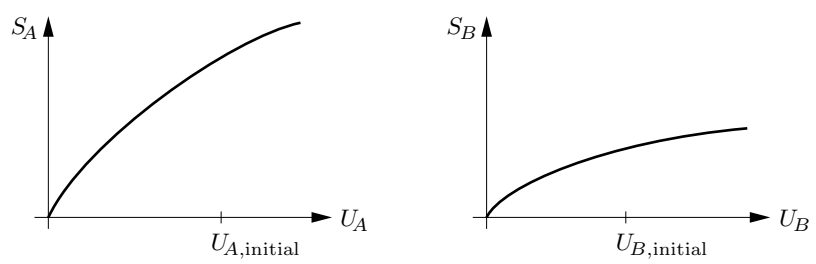


**Figure 3.3.** Graphs of entropy vs. energy for two objects. Copyright ©2000, Addison-Wesley.

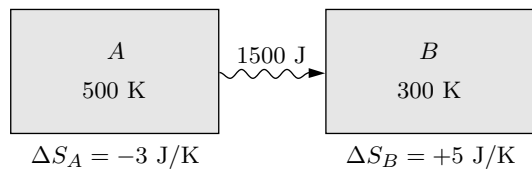


**Figure 3.4.** When 1500 J of heat leaves a 500 K object, its entropy decreases by 3 J/K. When this same heat enters a 300 K object, its entropy increases by 5 J/K.  
Copyright ©2000, Addison-Wesley.

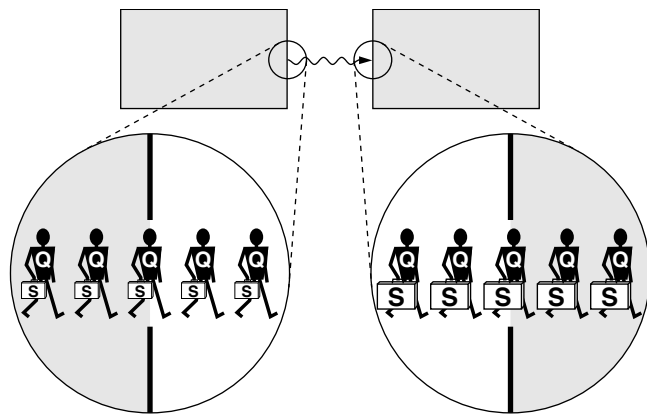


**Figure 3.5.** Each unit of heat energy ( $Q$ ) that leaves a hot object is required to carry some entropy ( $Q/T$ ) with it. When it enters a cooler object, the amount of entropy has increased. Copyright ©2000, Addison-Wesley.

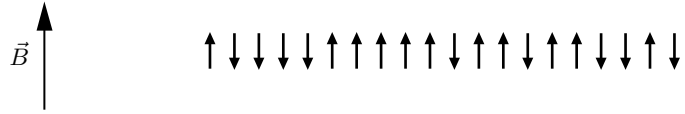
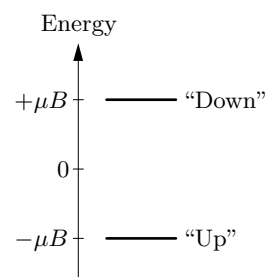


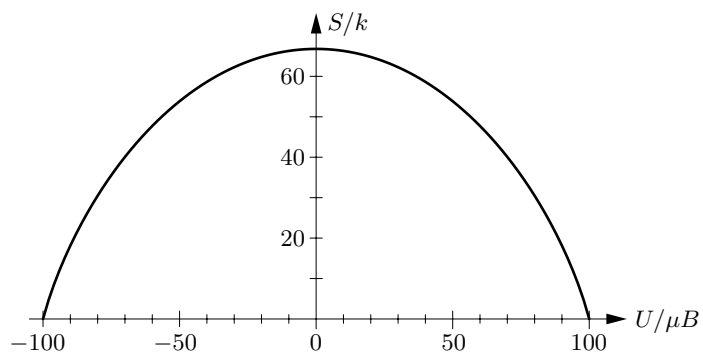
**Figure 3.6.** A two-state paramagnet, consisting of  $N$  microscopic magnetic dipoles, each of which is either “up” or “down” at any moment. The dipoles respond only to the influence of the external magnetic field  $B$ ; they do not interact with their neighbors (except to exchange energy). Copyright ©2000, Addison-Wesley.

**Figure 3.7.** The energy levels of a single dipole in an ideal two-state paramagnet are  $-\mu B$  (for the “up” state) and  $+\mu B$  (for the “down” state). Copyright ©2000, Addison-Wesley.



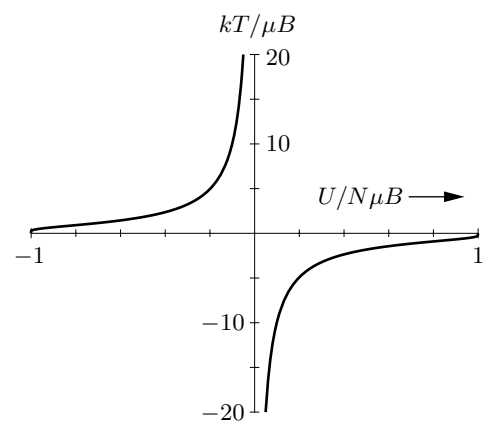
$N_\uparrow$	$U/\mu B$	$M/N\mu$	$\Omega$	$S/k$	$kT/\mu B$	$C/Nk$
100	-100	1.00	1	0	0	—
99	-98	.98	100	4.61	.47	.074
98	-96	.96	4950	8.51	.54	.310
97	-94	.94	$1.6 \times 10^5$	11.99	.60	.365
:	:	:	:	:	:	:
52	-4	.04	$9.3 \times 10^{28}$	66.70	25.2	.001
51	-2	.02	$9.9 \times 10^{28}$	66.76	50.5	—
50	0	0	$1.0 \times 10^{29}$	66.78	$\infty$	—
49	2	-.02	$9.9 \times 10^{28}$	66.76	-50.5	—
48	4	-.04	$9.3 \times 10^{28}$	66.70	-25.2	.001
:	:	:	:	:	:	:
1	98	-.98	100	4.61	-.47	.074
0	100	-1.00	1	0	0	—

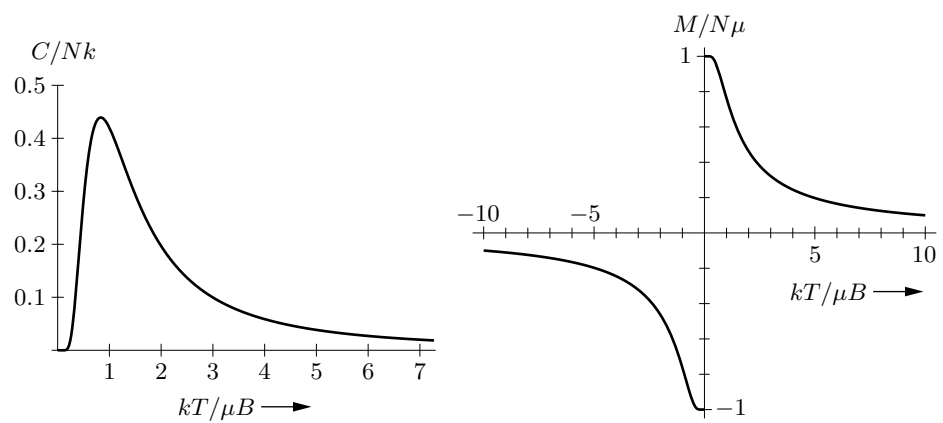
**Table 3.2.** Thermodynamic properties of a two-state paramagnet consisting of 100 elementary dipoles. Microscopic physics determines the energy  $U$  and total magnetization  $M$  in terms of the number of dipoles pointing up,  $N_\uparrow$ . The multiplicity  $\Omega$  is calculated from the combinatoric formula 3.27, while the entropy  $S$  is  $k \ln \Omega$ . The last two columns show the temperature and the heat capacity, calculated by taking derivatives as explained in the text. Copyright ©2000, Addison-Wesley.



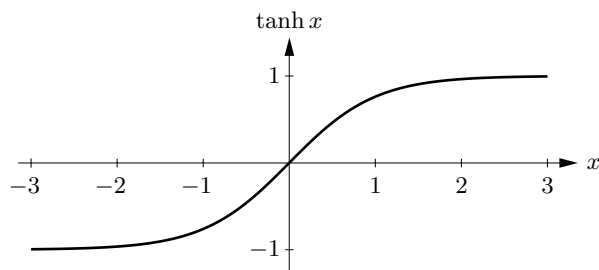
**Figure 3.8.** Entropy as a function of energy for a two-state paramagnet consisting of 100 elementary dipoles. Copyright ©2000, Addison-Wesley.

**Figure 3.9.** Temperature as a function of energy for a two-state paramagnet. (This graph was plotted from the analytic formulas derived later in the text; a plot of the data in Table 3.2 would look similar but less smooth.) Copyright ©2000, Addison-Wesley.

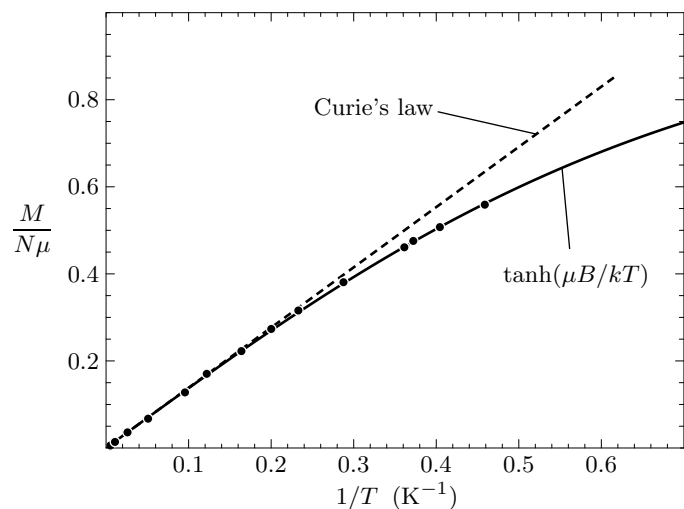




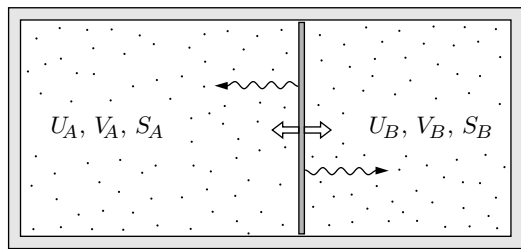
**Figure 3.10.** Heat capacity and magnetization of a two-state paramagnet (computed from the analytic formulas derived later in the text). Copyright ©2000, Addison-Wesley.



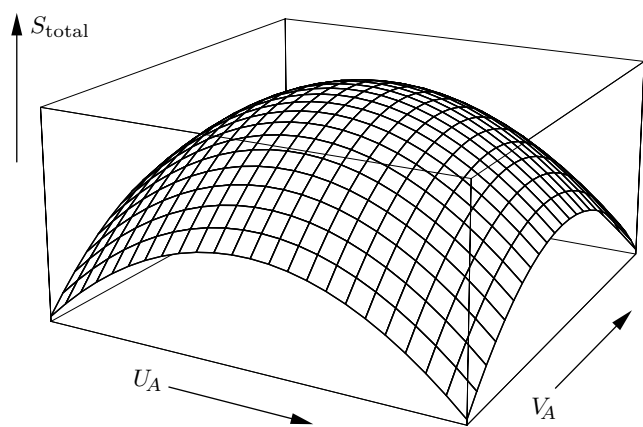
**Figure 3.11.** The hyperbolic tangent function. In the formulas for the energy and magnetization of a two-state paramagnet, the argument  $x$  of the hyperbolic tangent is  $\mu B/kT$ . Copyright ©2000, Addison-Wesley.



**Figure 3.12.** Experimental measurements of the magnetization of the organic free radical “DPPH” (in a 1:1 complex with benzene), taken at  $B = 2.06 \text{ T}$  and temperatures ranging from 300 K down to 2.2 K. The solid curve is the prediction of equation 3.32 (with  $\mu = \mu_B$ ), while the dashed line is the prediction of Curie’s law for the high-temperature limit. (Because the effective number of elementary dipoles in this experiment was uncertain by a few percent, the vertical scale of the theoretical graphs has been adjusted to obtain the best fit.) Adapted from P. Grobet, L. Van Gerven, and A. Van den Bosch, *Journal of Chemical Physics* **68**, 5225 (1978). Copyright ©2000, Addison-Wesley.

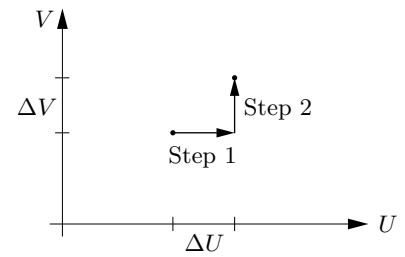


**Figure 3.13.** Two systems that can exchange both energy and volume with each other. The total energy and total volume are fixed. Copyright ©2000, Addison-Wesley.



**Figure 3.14.** A graph of entropy vs.  $U_A$  and  $V_A$  for the system shown in Figure 3.13. The equilibrium values of  $U_A$  and  $V_A$  are where the graph reaches its highest point. Copyright ©2000, Addison-Wesley.

**Figure 3.15.** To compute the change in entropy when both  $U$  and  $V$  change, consider the process in two steps: changing  $U$  while holding  $V$  fixed, then changing  $V$  while holding  $U$  fixed. Copyright ©2000, Addison-Wesley.



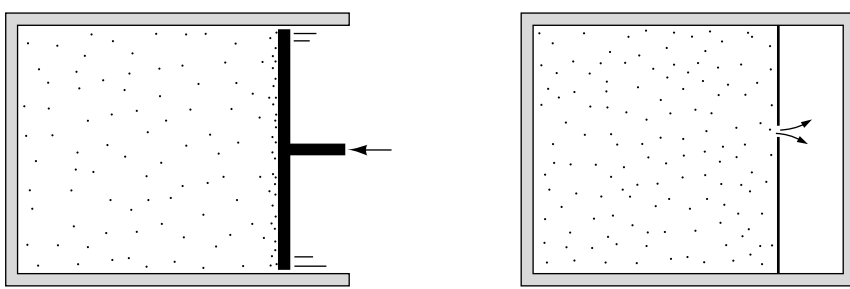


**Figure 3.16.** Two types of non-quasistatic volume changes: very fast compression that creates internal disequilibrium, and free expansion into a vacuum. Copyright ©2000, Addison-Wesley.

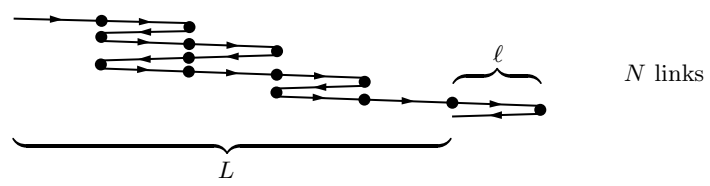


**Figure 3.17.** A crude model of a rubber band as a chain in which each link can only point left or right. Copyright ©2000, Addison-Wesley.

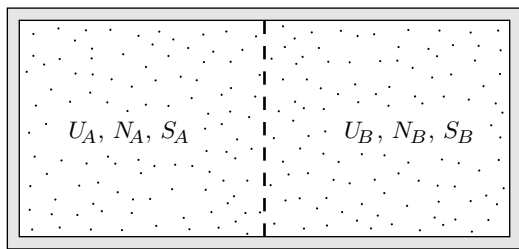


**Figure 3.18.** Two systems that can exchange both energy and particles. Copyright ©2000, Addison-Wesley.

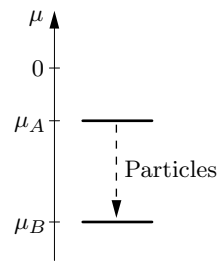


**Figure 3.19.** Particles tend to flow toward lower values of the chemical potential, even if both values are negative. Copyright ©2000, Addison-Wesley.

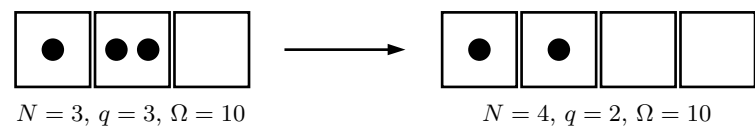


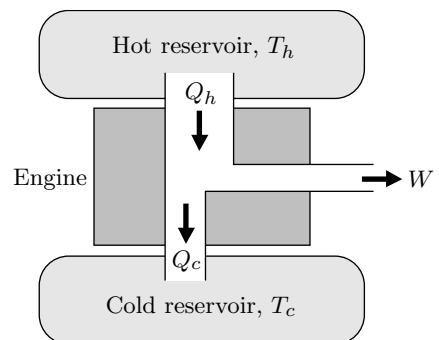
**Figure 3.20.** In order to add an oscillator (represented by a box) to this very small Einstein solid while holding the entropy (or multiplicity) fixed, we must remove one unit of energy (represented by a dot). Copyright ©2000, Addison-Wesley.

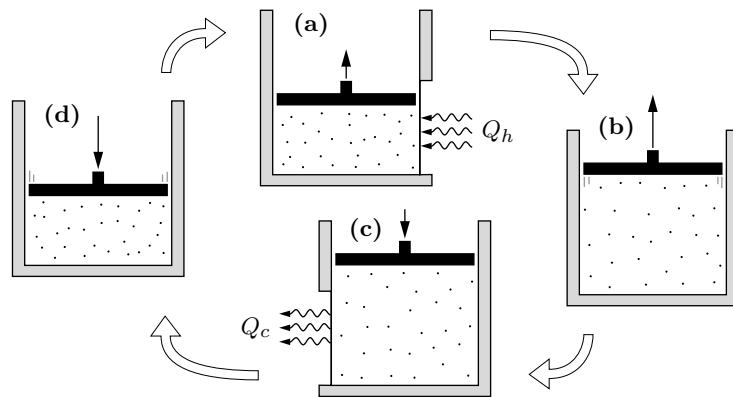
Type of interaction	Exchanged quantity	Governing variable	Formula
thermal	energy	temperature	$\frac{1}{T} = \left( \frac{\partial S}{\partial U} \right)_{V,N}$
mechanical	volume	pressure	$\frac{P}{T} = \left( \frac{\partial S}{\partial V} \right)_{U,N}$
diffusive	particles	chemical potential	$\frac{\mu}{T} = - \left( \frac{\partial S}{\partial N} \right)_{U,V}$

**Table 3.3.** Summary of the three types of interactions considered in this chapter, and the associated variables and partial-derivative relations. Copyright ©2000, Addison-Wesley.

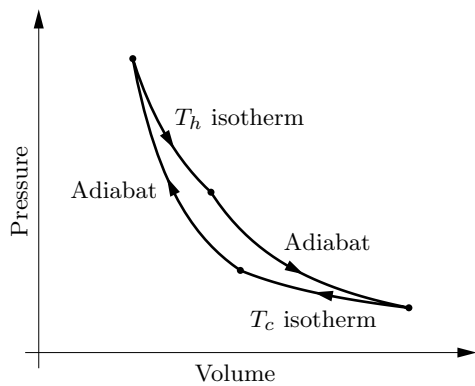
# 4 Engines and Refrigerators

**Figure 4.1.** Energy-flow diagram for a heat engine. Energy enters as heat from the hot reservoir, and leaves both as work and as waste heat expelled to the cold reservoir. Copyright ©2000, Addison-Wesley.



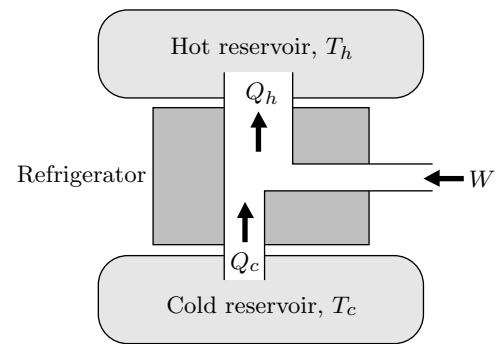


**Figure 4.2.** The four steps of a Carnot cycle: (a) isothermal expansion at  $T_h$  while absorbing heat; (b) adiabatic expansion to  $T_c$ ; (c) isothermal compression at  $T_c$  while expelling heat; and (d) adiabatic compression back to  $T_h$ . The system must be put in thermal contact with the hot reservoir during step (a) and with the cold reservoir during step (c). Copyright ©2000, Addison-Wesley.

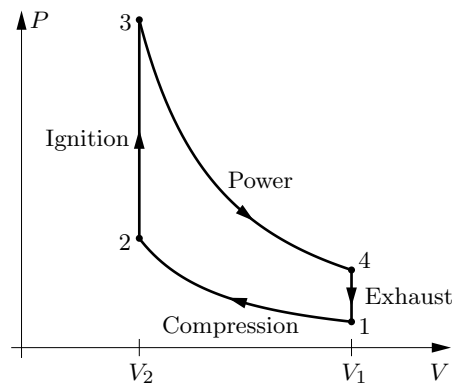


**Figure 4.3.** *PV* diagram for an ideal monatomic gas undergoing a Carnot cycle. Copyright ©2000, Addison-Wesley.

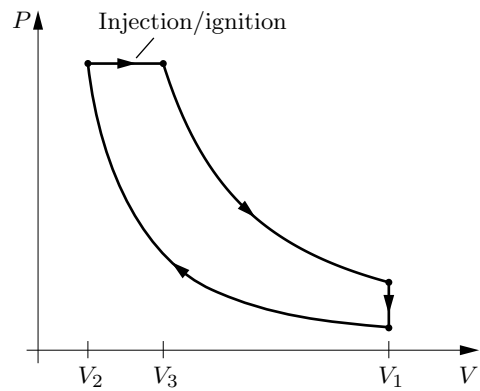
**Figure 4.4.** Energy-flow diagram for a refrigerator or air conditioner. For a kitchen refrigerator, the space inside it is the cold reservoir and the space outside it is the hot reservoir. An electrically powered compressor supplies the work. Copyright ©2000, Addison-Wesley.



**Figure 4.5.** The idealized Otto cycle, an approximation of what happens in a gasoline engine. In real engines the compression ratio  $V_1/V_2$  is larger than shown here, typically 8 or 10. Copyright ©2000, Addison-Wesley.



**Figure 4.6.** *PV* diagram for the Diesel cycle. Copyright ©2000, Addison-Wesley.



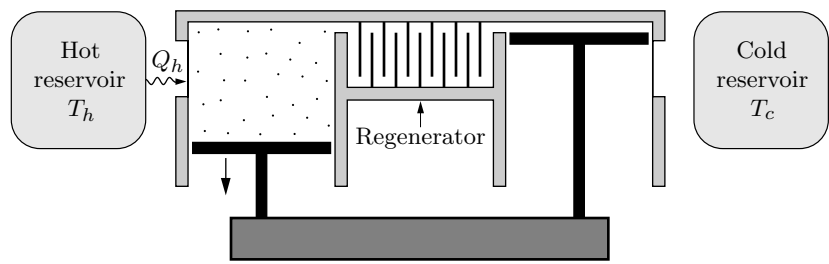


**Figure 4.7.** A Stirling engine, shown during the power stroke when the hot piston is moving outward and the cold piston is at rest. (For simplicity, the linkages between the two pistons are not shown.) Copyright ©2000, Addison-Wesley.

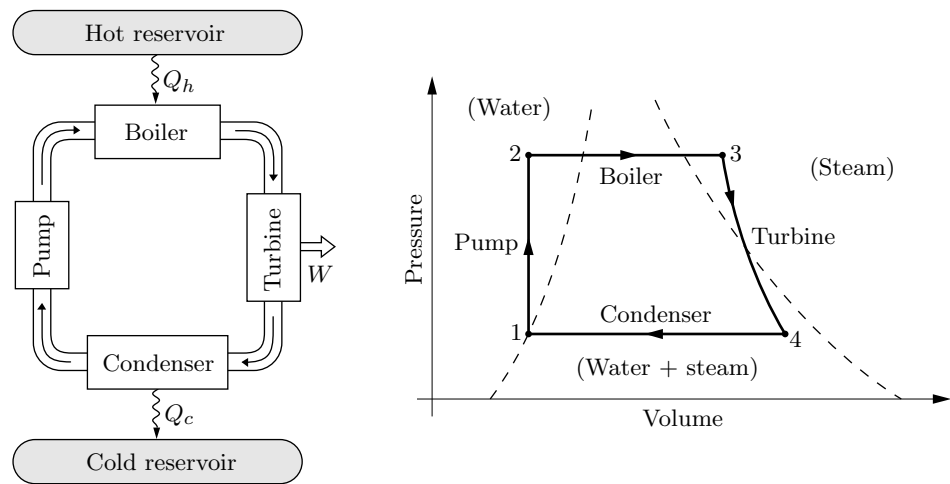


**Figure 4.8.** Schematic diagram of a steam engine and the associated *PV* cycle (not to scale), called the **Rankine cycle**. The dashed lines show where the fluid is liquid water, where it is steam, and where it is part water and part steam. Copyright ©2000, Addison-Wesley.

$T$ (°C)	$P$ (bar)	$H_{\text{water}}$ (kJ)	$H_{\text{steam}}$ (kJ)	$S_{\text{water}}$ (kJ/K)	$S_{\text{steam}}$ (kJ/K)
0	0.006	0	2501	0	9.156
10	0.012	42	2520	0.151	8.901
20	0.023	84	2538	0.297	8.667
30	0.042	126	2556	0.437	8.453
50	0.123	209	2592	0.704	8.076
100	1.013	419	2676	1.307	7.355

**Table 4.1.** Properties of saturated water/steam. Pressures are given in bars, where  $1 \text{ bar} = 10^5 \text{ Pa} \approx 1 \text{ atm}$ . All values are for 1 kg of fluid, and are measured relative to liquid water at the triple point ( $0.01^\circ\text{C}$  and 0.006 bar). Excerpted from Keenan et al. (1978). Copyright ©2000, Addison-Wesley.

$P$ (bar)	Temperature ( $^{\circ}\text{C}$ )				
	200	300	400	500	600
1.0	$H$ (kJ)	2875	3074	3278	3488
	$S$ (kJ/K)	7.834	8.216	8.544	8.834
3.0	$H$ (kJ)	2866	3069	3275	3486
	$S$ (kJ/K)	7.312	7.702	8.033	8.325
10	$H$ (kJ)	2828	3051	3264	3479
	$S$ (kJ/K)	6.694	7.123	7.465	7.762
30	$H$ (kJ)		2994	3231	3457
	$S$ (kJ/K)		6.539	6.921	7.234
100	$H$ (kJ)			3097	3374
	$S$ (kJ/K)			6.212	6.597
300	$H$ (kJ)			2151	3081
	$S$ (kJ/K)			4.473	5.791
					6.233

**Table 4.2.** Properties of superheated steam. All values are for 1 kg of fluid, and are measured relative to liquid water at the triple point. Excerpted from Keenan et al. (1978). Copyright ©2000, Addison-Wesley.

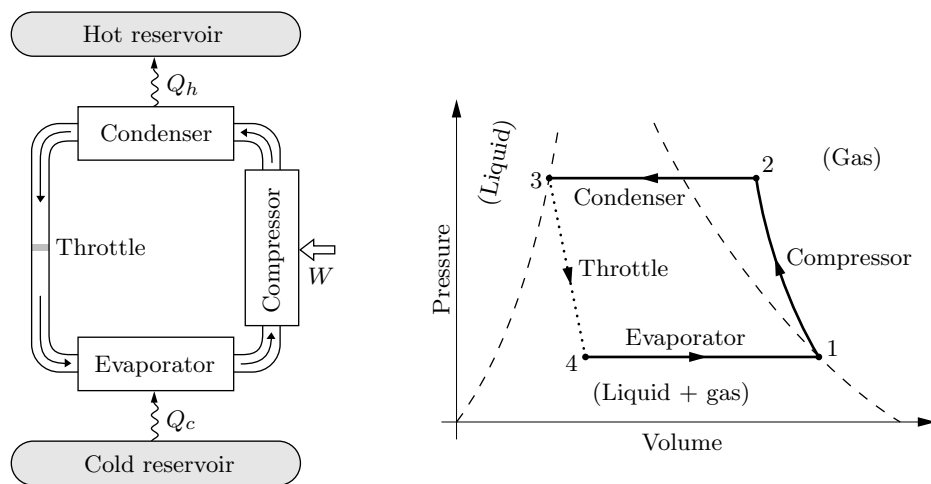


**Figure 4.9.** A schematic drawing and  $PV$  diagram (not to scale) of the standard refrigeration cycle. The dashed lines indicate where the refrigerant is liquid, gas, and a combination of the two. Copyright ©2000, Addison-Wesley.

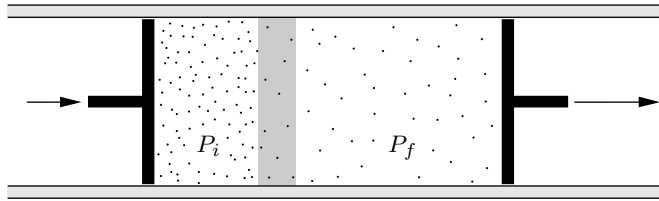


**Figure 4.10.** The throttling process, in which a fluid is pushed through a porous plug and then expands into a region of lower pressure. Copyright ©2000, Addison-Wesley.

$P$ (bar)	$T$ (°C)	$H_{\text{liquid}}$ (kJ)	$H_{\text{gas}}$ (kJ)	$S_{\text{liquid}}$ (kJ/K)	$S_{\text{gas}}$ (kJ/K)
1.0	-26.4	16	231	0.068	0.940
1.4	-18.8	26	236	0.106	0.932
2.0	-10.1	37	241	0.148	0.925
4.0	8.9	62	252	0.240	0.915
6.0	21.6	79	259	0.300	0.910
8.0	31.3	93	264	0.346	0.907
10.0	39.4	105	268	0.384	0.904
12.0	46.3	116	271	0.416	0.902

**Table 4.3.** Properties of the refrigerant HFC-134a under saturated conditions (at its boiling point for each pressure). All values are for 1 kg of fluid, and are measured relative to an arbitrarily chosen reference state, the saturated liquid at -40°C. Excerpted from Moran and Shapiro (1995). Copyright ©2000, Addison-Wesley.

$P$ (bar)	Temperature ( $^{\circ}\text{C}$ )			
	40	50	60	
8.0	$H$ (kJ)	274	284	295
	$S$ (kJ/K)	0.937	0.971	1.003
10.0	$H$ (kJ)	269	280	291
	$S$ (kJ/K)	0.907	0.943	0.977
12.0	$H$ (kJ)		276	287
	$S$ (kJ/K)		0.916	0.953

**Table 4.4.** Properties of superheated (gaseous) refrigerant HFC-134a. All values are for 1 kg of fluid, and are measured relative to the same reference state as in Table 4.3. Excerpted from Moran and Shapiro (1995). Copyright ©2000, Addison-Wesley.

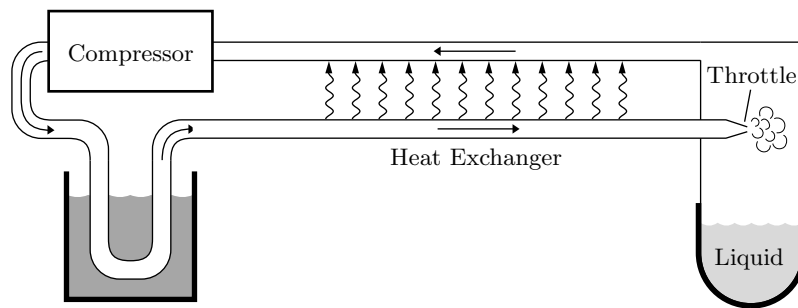
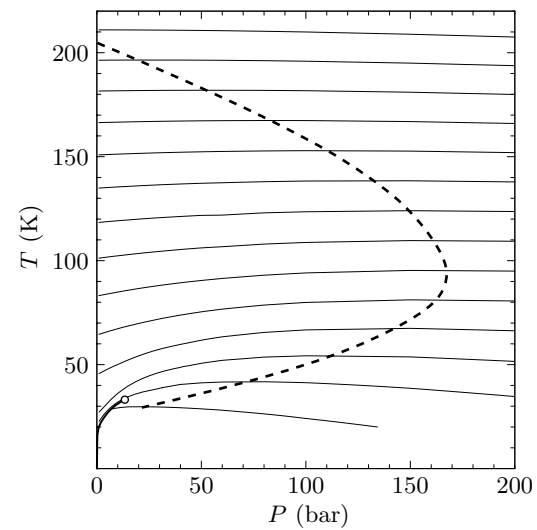


**Figure 4.11.** Schematic diagram of the Hampson-Linde cycle for gas liquefaction. Compressed gas is first cooled (to room temperature is sufficient if it is nitrogen or oxygen) and then passed through a heat exchanger on its way to a throttling valve. The gas cools upon throttling and returns through the heat exchanger to further cool the incoming gas. Eventually the incoming gas becomes cold enough to partially liquefy upon throttling. From then on, new gas must be added at the compressor to replace what is liquefied. Copyright ©2000, Addison-Wesley.

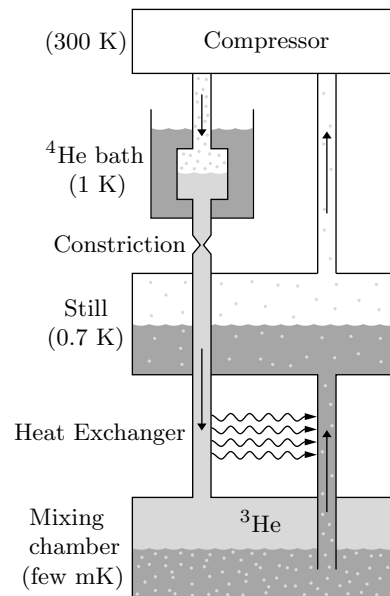
**Figure 4.12.** Lines of constant enthalpy (approximately horizontal, at intervals of 400 J/mol) and inversion curve (dashed) for hydrogen. In a throttling process the enthalpy is constant, so cooling occurs only to the left of the inversion curve, where the enthalpy lines have positive slopes. The heavy solid line at lower-left is the liquid-gas phase boundary. Data from Vargaftik (1975) and Woolley et al. (1948). Copyright ©2000, Addison-Wesley.



	Temperature (K)							
	77 (liq.)	77 (gas)	100	200	300	400	500	600
1 bar	-3407	2161	2856	5800	8717	11,635	14,573	17,554
100 bar			-1946	4442	8174	11,392	14,492	17,575

**Table 4.5.** Molar enthalpy of nitrogen (in joules) at 1 bar and 100 bars.  
 Excerpted from Lide (1994). Copyright ©2000, Addison-Wesley.

**Figure 4.13.** Schematic diagram of a helium dilution refrigerator. The working substance is  $^3\text{He}$  (light gray), which circulates counter-clockwise. The  $^4\text{He}$  (dark gray) does not circulate. Copyright ©2000, Addison-Wesley.



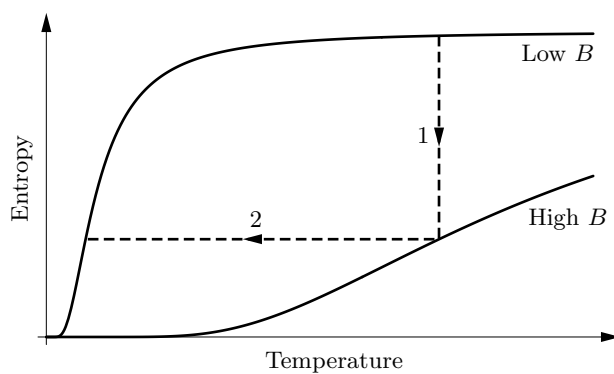


**Figure 4.14.** Entropy as a function of temperature for an ideal two-state paramagnet, at two different values of the magnetic field strength. (These curves were plotted from the formula derived in Problem 3.23.) The magnetic cooling process consists of an isothermal increase in the field strength (step 1), followed by an adiabatic decrease (step 2). Copyright ©2000, Addison-Wesley.

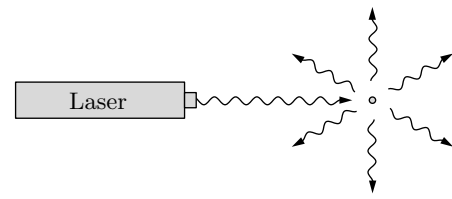


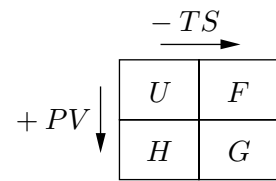
**Figure 4.15.** An atom that continually absorbs and reemits laser light feels a force from the direction of the laser, because the absorbed photons all come from the same direction while the emitted photons come out in all directions. Copyright ©2000, Addison-Wesley.

# 5 Free Energy and Chemical Thermodynamics



**Figure 5.1.** To create a rabbit out of nothing and place it on the table, the magician need not summon up the entire enthalpy,  $H = U + PV$ . Some energy, equal to  $TS$ , can flow in spontaneously as heat; the magician must provide only the difference,  $G = H - TS$ , as work. Drawing by Karen Thurber. Copyright ©2000, Addison-Wesley.

**Figure 5.2.** To get  $H$  from  $U$  or  $G$  from  $F$ , add  $PV$ ; to get  $F$  from  $U$  or  $G$  from  $H$ , subtract  $TS$ . Copyright ©2000, Addison-Wesley.



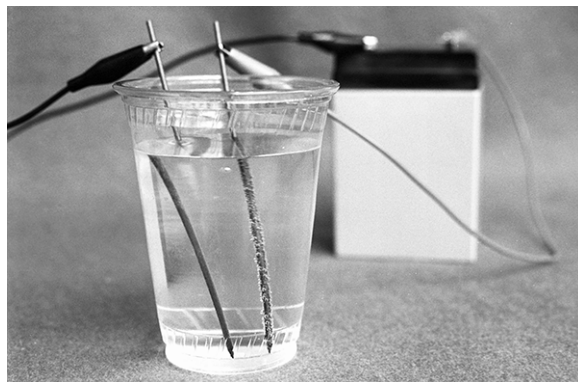


**Figure 5.3.** To separate water into hydrogen and oxygen, just run an electric current through it. In this home experiment the electrodes are mechanical pencil leads (graphite). Bubbles of hydrogen (too small to see) form at the negative electrode (left) while bubbles of oxygen form at the positive electrode (right). Copyright ©2000, Addison-Wesley.

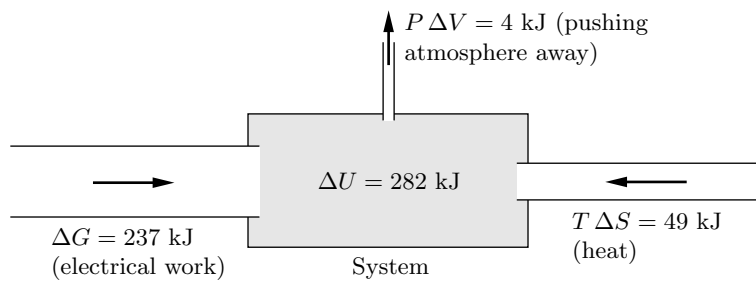


**Figure 5.4.** Energy-flow diagram for electrolysis of one mole of water. Under ideal conditions, 49 kJ of energy enter as heat ( $T\Delta S$ ), so the electrical work required is only 237 kJ:  $\Delta G = \Delta H - T\Delta S$ . The difference between  $\Delta H$  and  $\Delta U$  is  $P\Delta V = 4 \text{ kJ}$ , the work done to make room for the gases produced. Copyright ©2000, Addison-Wesley.

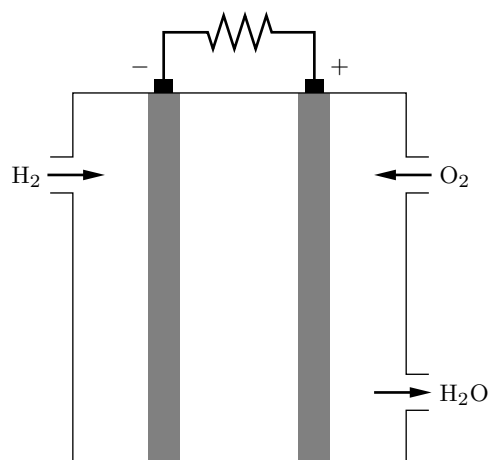


**Figure 5.5.** In a hydrogen fuel cell, hydrogen and oxygen gas pass through porous electrodes and react to form water, removing electrons from one electrode and depositing electrons on the other. Copyright ©2000, Addison-Wesley.

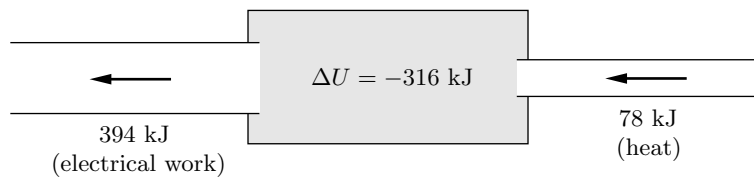


**Figure 5.6.** Energy-flow diagram for a lead-acid cell operating ideally. For each mole that reacts, the system's energy decreases by 316 kJ and its entropy increases by 260 J/K. Because of the entropy increase, the system can absorb 78 kJ of heat from the environment; the maximum work performed is therefore 394 kJ. (Because no gases are involved in this reaction, volume changes are negligible so  $\Delta U \approx \Delta H$  and  $\Delta F \approx \Delta G$ .) Copyright ©2000, Addison-Wesley.

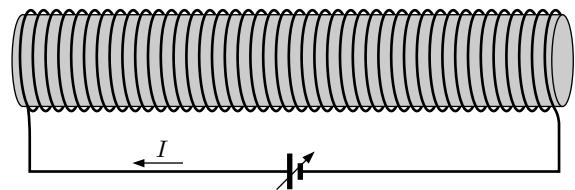
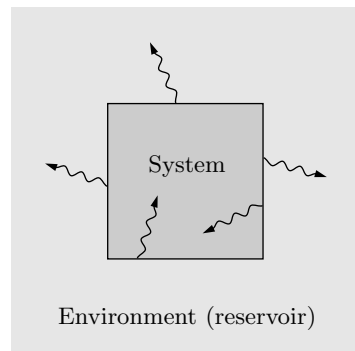


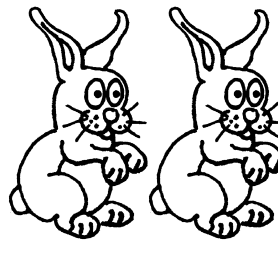
**Figure 5.7.** A long solenoid, surrounding a magnetic specimen, connected to a power supply that can change the current, performing magnetic work.  
Copyright ©2000, Addison-Wesley.

**Figure 5.8.** For a system that can exchange energy with its environment, the total entropy of both tends to increase. Copyright ©2000, Addison-Wesley.



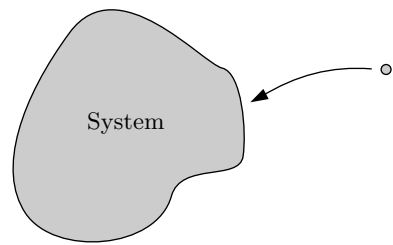


$V, U, S, P, T$

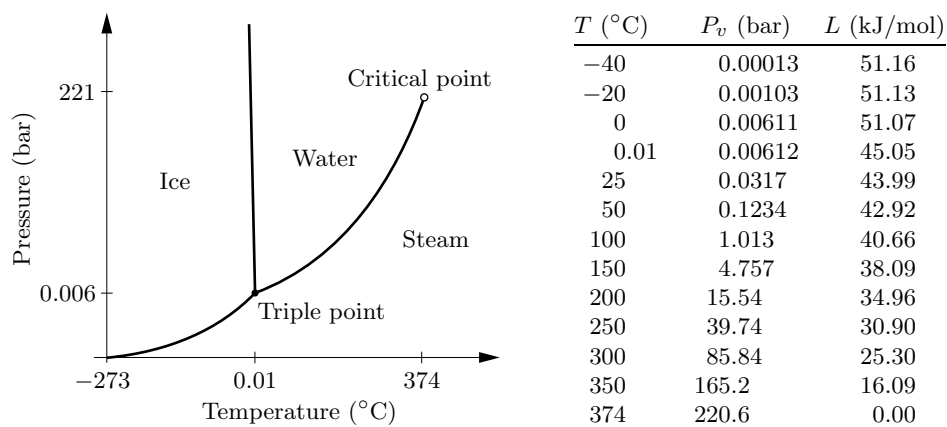


$2V, 2U, 2S, P, T$

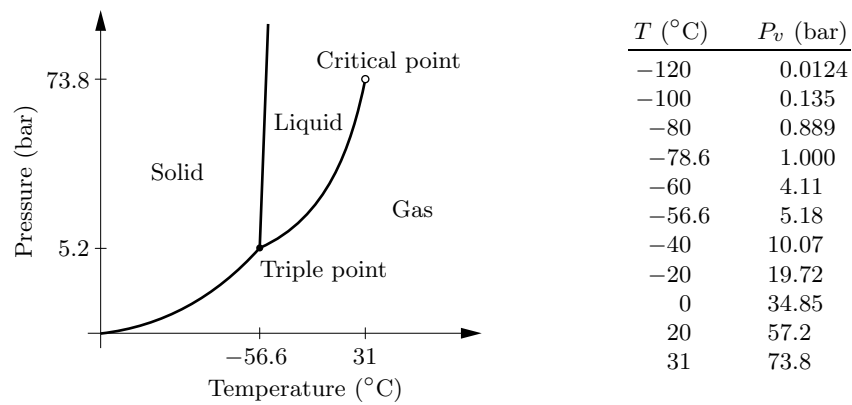
**Figure 5.9.** Two rabbits have twice as much volume, energy, and entropy as one rabbit, but not twice as much pressure or temperature. Drawing by Karen Thurber. Copyright ©2000, Addison-Wesley.



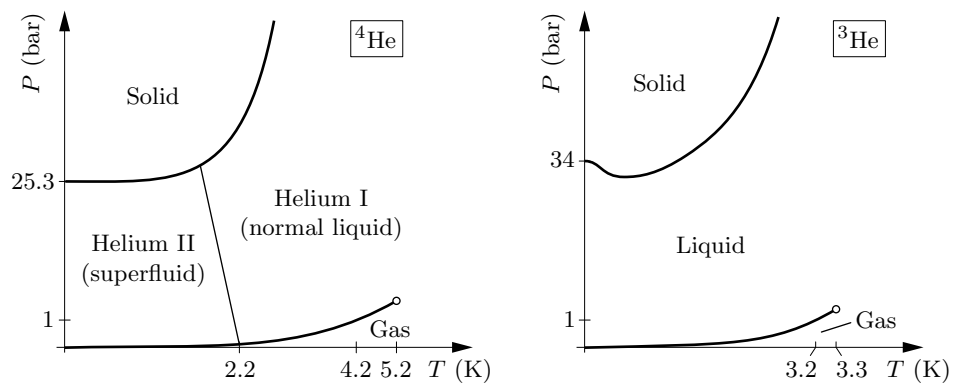
**Figure 5.10.** When you add a particle to a system, holding the temperature and pressure fixed, the system's Gibbs free energy increases by  $\mu$ . Copyright ©2000, Addison-Wesley.



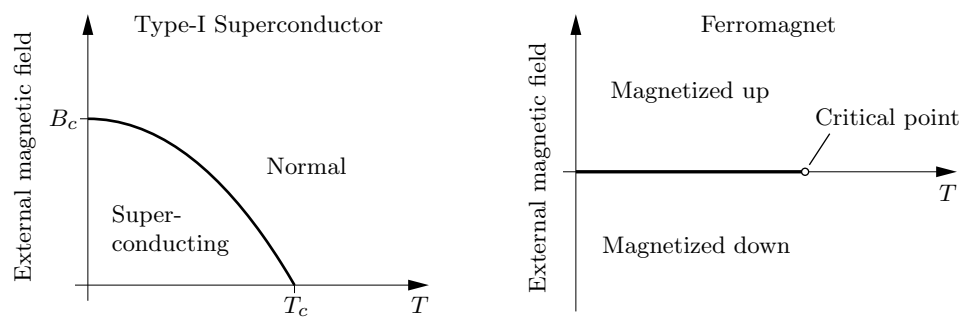
**Figure 5.11.** Phase diagram for  $\text{H}_2\text{O}$  (not to scale). The table gives the vapor pressure and molar latent heat for the solid-gas transformation (first three entries) and the liquid-gas transformation (remaining entries). Data from Keenan et al. (1978) and Lide (1994). Copyright ©2000, Addison-Wesley.



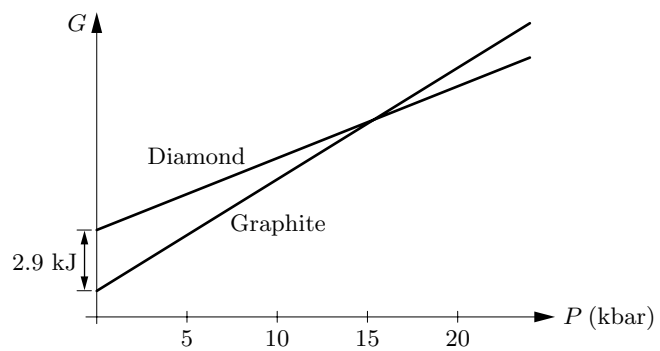
**Figure 5.12.** Phase diagram for carbon dioxide (not to scale). The table gives the vapor pressure along the solid-gas and liquid-gas equilibrium curves. Data from Lide (1994) and Reynolds (1979). Copyright ©2000, Addison-Wesley.



**Figure 5.13.** Phase diagrams of  $^4\text{He}$  (left) and  $^3\text{He}$  (right). Neither diagram is to scale, but qualitative relations between the diagrams are shown correctly. Not shown are the three different solid phases (crystal structures) of each isotope, or the superfluid phases of  $^3\text{He}$  below 3 mK. Copyright ©2000, Addison-Wesley.

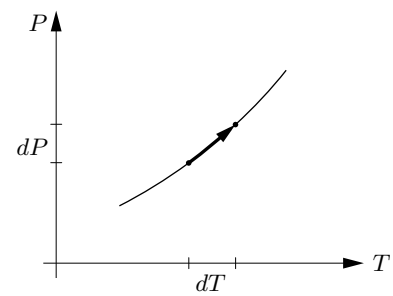


**Figure 5.14.** Left: Phase diagram for a typical type-I superconductor. For lead,  $T_c = 7.2$  K and  $B_c = 0.08$  T. Right: Phase diagram for a ferromagnet, assuming that the applied field and magnetization are always along a given axis. Copyright ©2000, Addison-Wesley.



**Figure 5.15.** Molar Gibbs free energies of diamond and graphite as functions of pressure, at room temperature. These straight-line graphs are extrapolated from low pressures, neglecting the changes in volume as pressure increases. Copyright ©2000, Addison-Wesley.

**Figure 5.16.** Infinitesimal changes in pressure and temperature, related in such a way as to remain on the phase boundary. Copyright ©2000, Addison-Wesley.



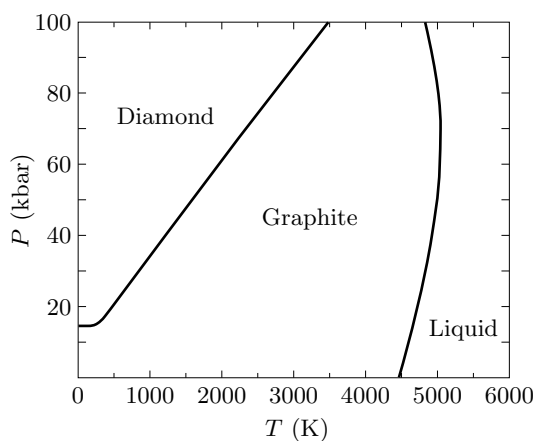


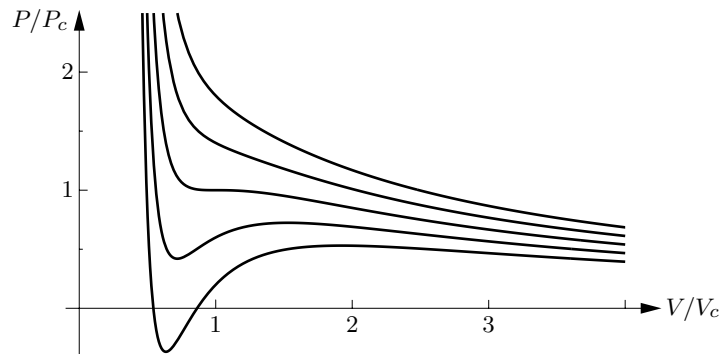
**Figure 5.17.** The experimental phase diagram of carbon. The stability region of the gas phase is not visible on this scale; the graphite-liquid-gas triple point is at the bottom of the graphite-liquid phase boundary, at 110 bars pressure. From David A. Young, *Phase Diagrams of the Elements* (University of California Press, Berkeley, 1991). Copyright ©2000, Addison-Wesley.



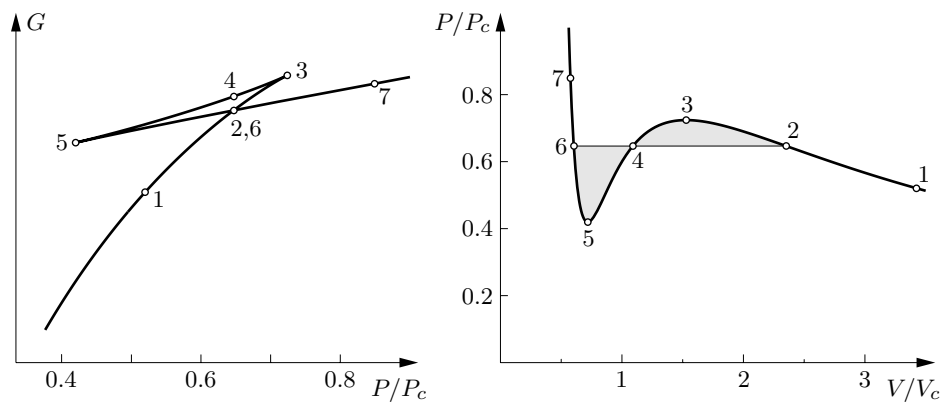
**Figure 5.18.** Cumulus clouds form when rising air expands adiabatically and cools to the dew point (Problem 5.44); the onset of condensation slows the cooling, increasing the tendency of the air to rise further (Problem 5.45). These clouds began to form in late morning, in a sky that was clear only an hour before the photo was taken. By mid-afternoon they had developed into thunderstorms. Copyright ©2000, Addison-Wesley.



**Figure 5.19.** When two molecules come very close together they repel each other strongly. When they are a short distance apart they attract each other. Copyright ©2000, Addison-Wesley.

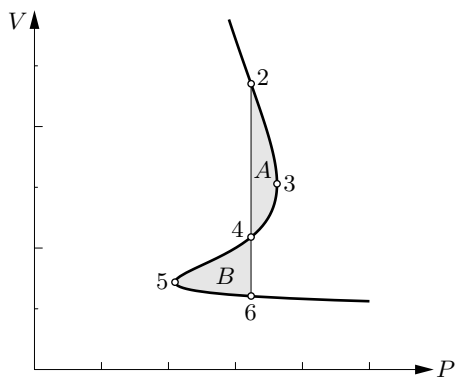


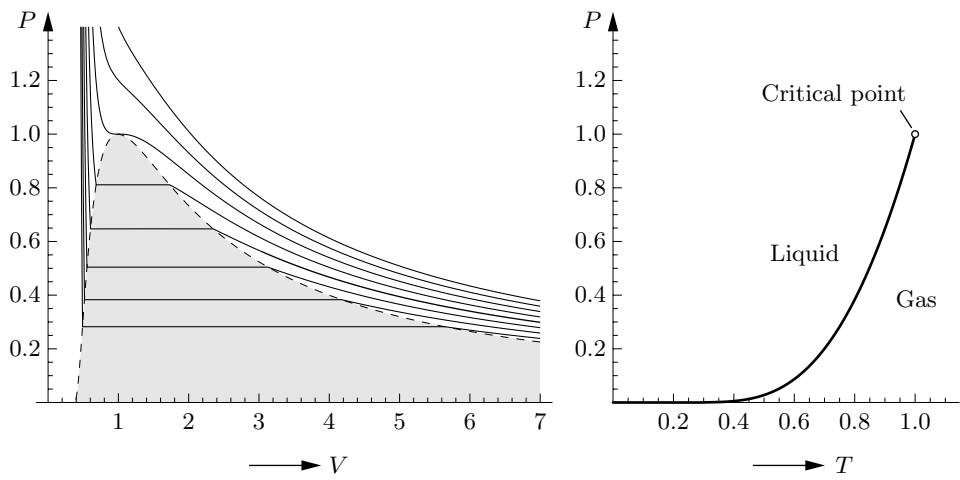
**Figure 5.20.** Isotherms (lines of constant temperature) for a van der Waals fluid. From bottom to top, the lines are for 0.8, 0.9, 1.0, 1.1, and 1.2 times  $T_c$ , the temperature at the critical point. The axes are labeled in units of the pressure and volume at the critical point; in these units the minimum volume ( $N_b$ ) is  $1/3$ . Copyright ©2000, Addison-Wesley.



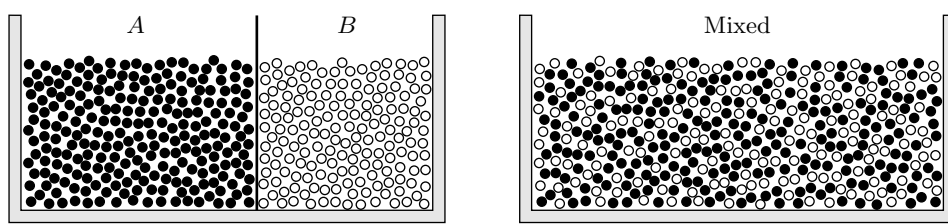
**Figure 5.21.** Gibbs free energy as a function of pressure for a van der Waals fluid at  $T = 0.9T_c$ . The corresponding isotherm is shown at right. States in the range 2-3-4-5-6 are unstable. Copyright ©2000, Addison-Wesley.

**Figure 5.22.** The same isotherm as in Figure 5.21, plotted sideways. Regions *A* and *B* have equal areas.  
Copyright ©2000, Addison-Wesley.

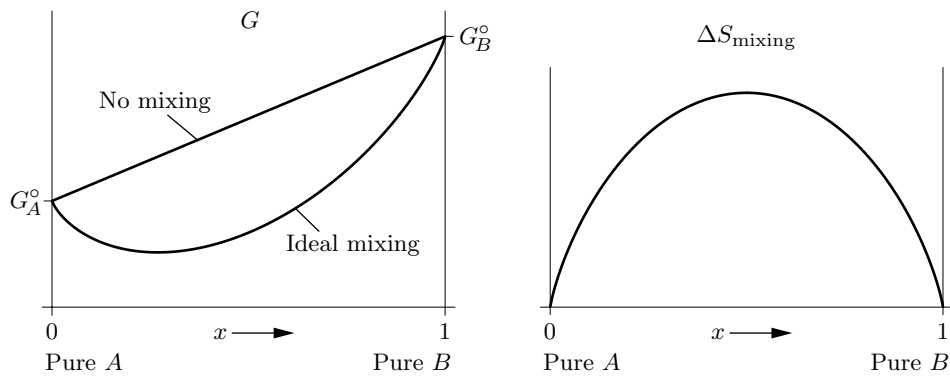




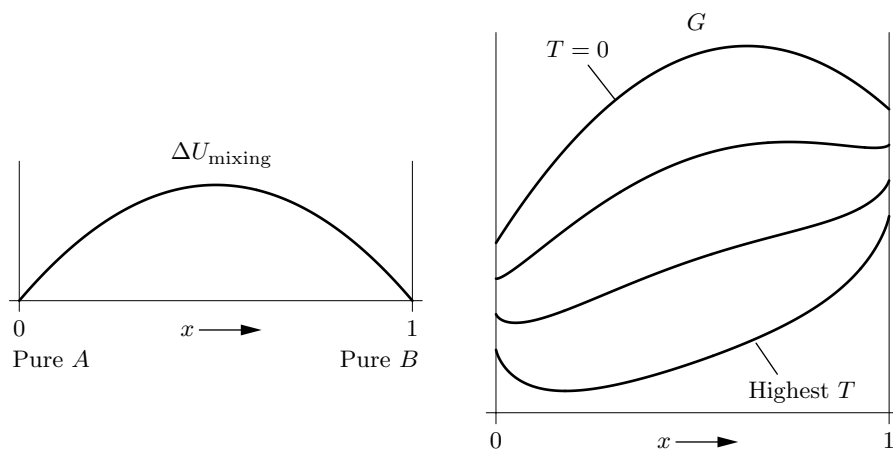
**Figure 5.23.** Complete phase diagrams predicted by the van der Waals model. The isotherms shown at left are for  $T/T_c$  ranging from 0.75 to 1.1 in increments of 0.05. In the shaded region the stable state is a combination of gas and liquid. The full vapor pressure curve is shown at right. All axes are labeled in units of the critical values. Copyright ©2000, Addison-Wesley.



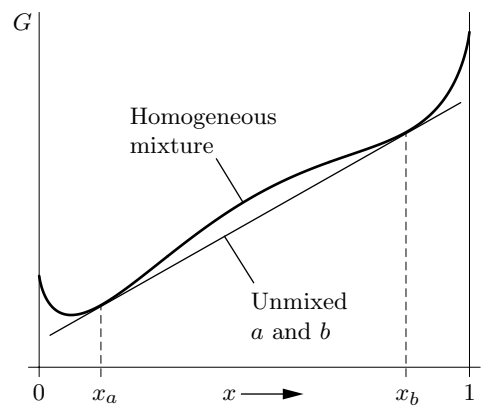
**Figure 5.24.** A collection of two types of molecules, before and after mixing.  
Copyright ©2000, Addison-Wesley.



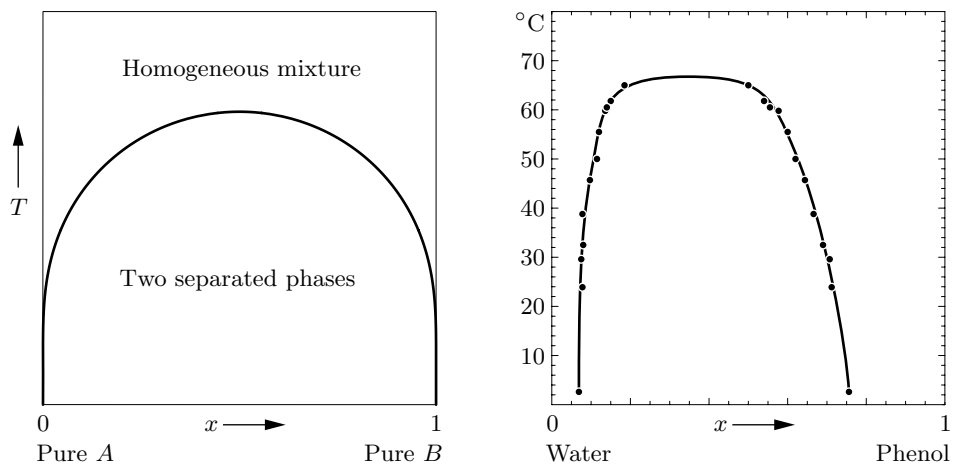
**Figure 5.25.** Before mixing, the free energy of a collection of  $A$  and  $B$  molecules is a linear function of  $x = N_B/(N_A + N_B)$ . After mixing it is a more complicated function; shown here is the case of an “ideal” mixture, whose entropy of mixing is shown at right. Although it isn’t obvious on this scale, the graphs of both  $\Delta S_{\text{mixing}}$  and  $G$  (after mixing) have vertical slopes at the endpoints. Copyright ©2000, Addison-Wesley.



**Figure 5.26.** Mixing  $A$  and  $B$  can often increase the energy of the system; shown at left is the simple case where the mixing energy is a quadratic function (see Problem 5.58). Shown at right is the free energy in this case, at four different temperatures. Copyright ©2000, Addison-Wesley.

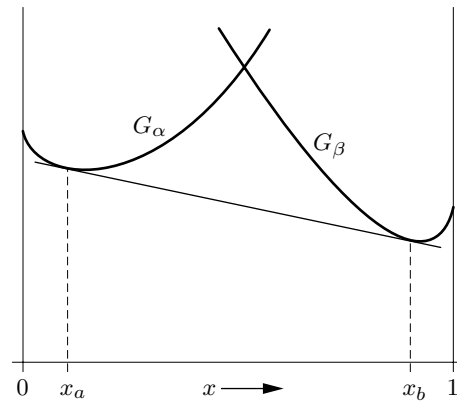


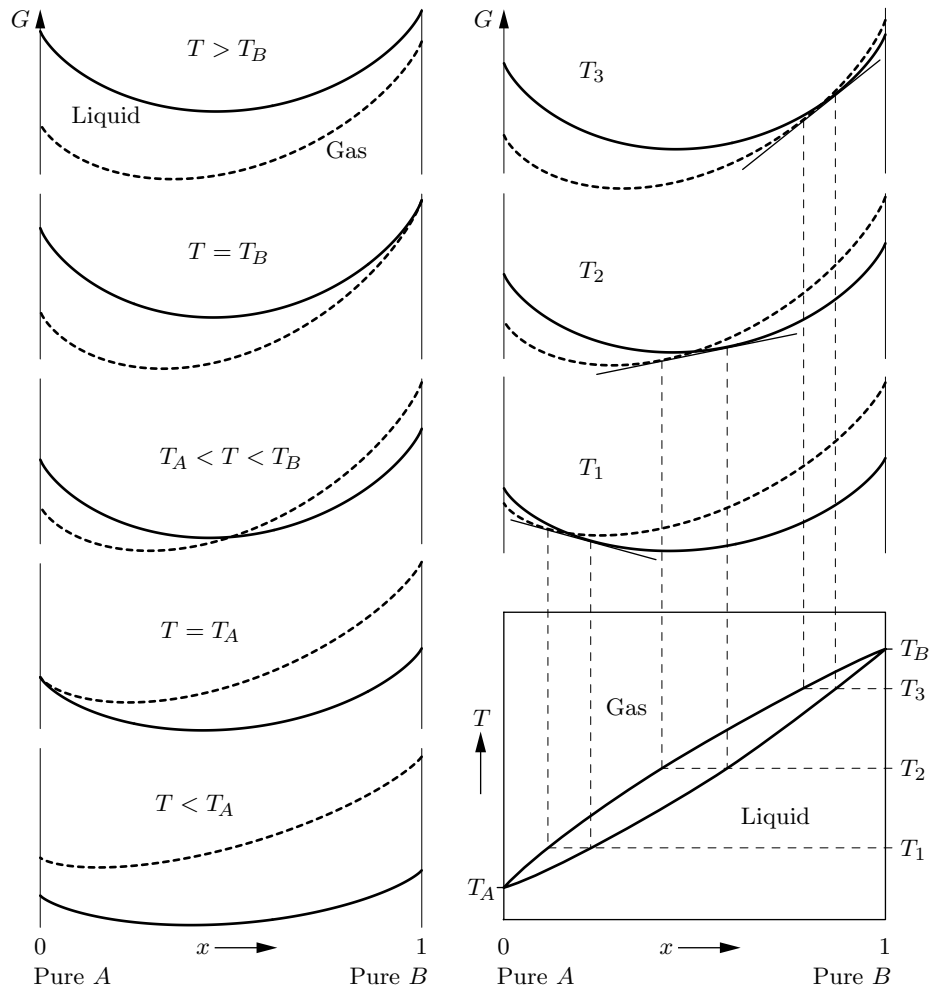
**Figure 5.27.** To construct the equilibrium free energy curve, draw the lowest possible straight line across the concave-down section, tangent to the curve at both ends. At compositions between the tangent points the mixture will spontaneously separate into phases whose compositions are  $x_a$  and  $x_b$ , in order to lower its free energy. Copyright ©2000, Addison-Wesley.



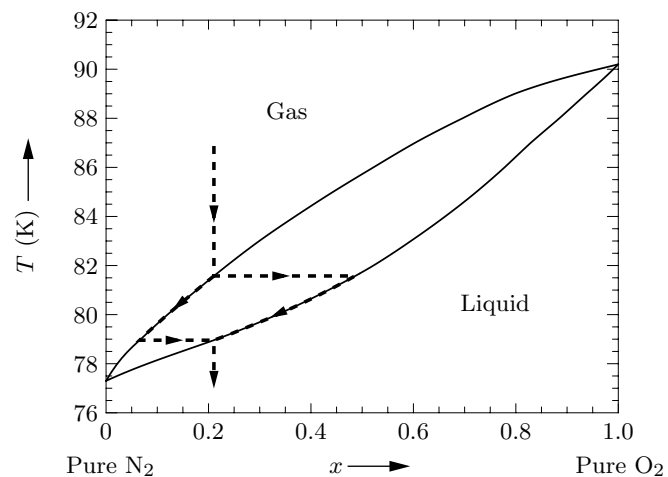
**Figure 5.28.** Left: Phase diagram for the simple model system whose mixing energy is plotted in Figure 5.26. Right: Experimental data for a real system, water + phenol, that shows qualitatively similar behavior. Adapted with permission from Alan N. Campbell and A. Jean R. Campbell, *Journal of the American Chemical Society* **59**, 2481 (1937). Copyright 1937 American Chemical Society. Copyright ©2000, Addison-Wesley.

**Figure 5.29.** Free energy graphs for a mixture of two solids with different crystal structures,  $\alpha$  and  $\beta$ . Again, the lowest possible straight connecting line indicates the range of compositions where an unmixed combination of  $a$  and  $b$  phases is more stable than a homogeneous mixture. Copyright ©2000, Addison-Wesley.

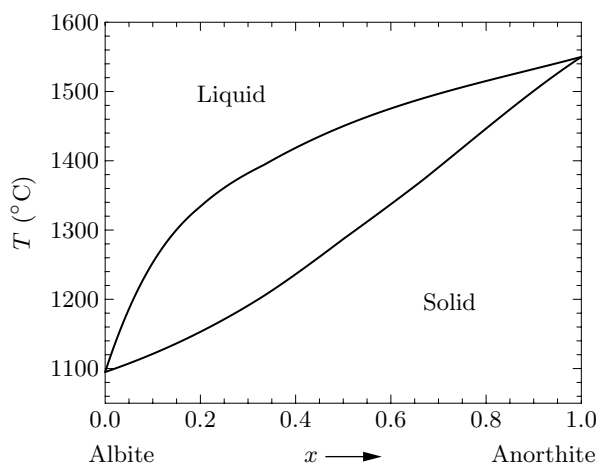




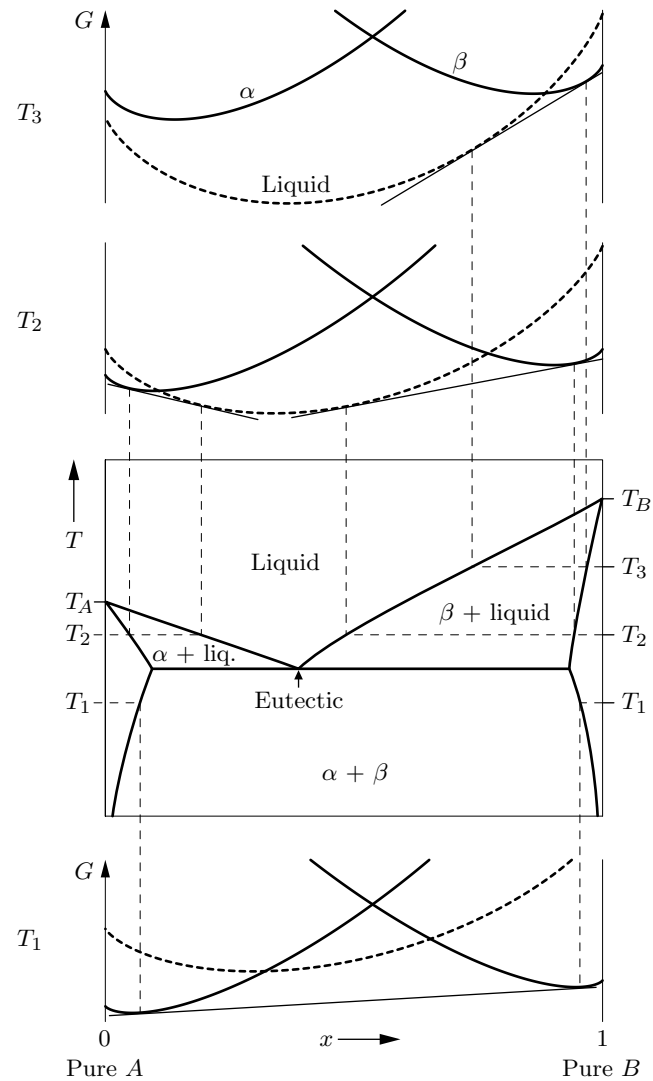
**Figure 5.30.** The five graphs at left show the liquid and gas free energies of an ideal mixture at temperatures above, below, at, and between the boiling points  $T_A$  and  $T_B$ . Three graphs at intermediate temperatures are shown at right, along with the construction of the phase diagram. Copyright ©2000, Addison-Wesley.



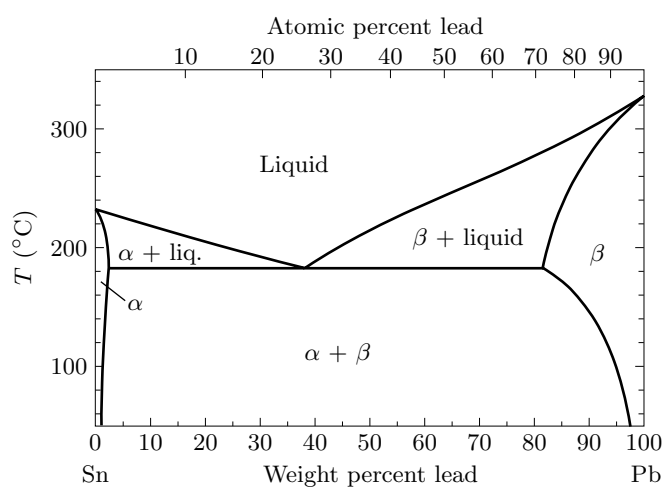
**Figure 5.31.** Experimental phase diagram for nitrogen and oxygen at atmospheric pressure. Data from *International Critical Tables* (volume 3), with endpoints adjusted to values in Lide (1994). Copyright ©2000, Addison-Wesley.



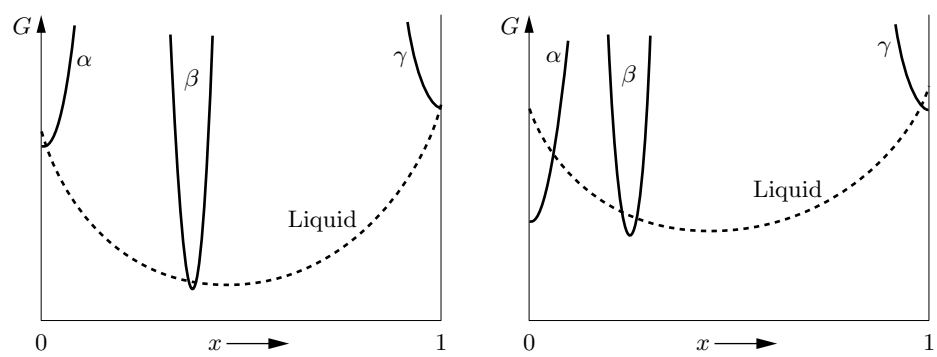
**Figure 5.32.** The phase diagram of plagioclase feldspar (at atmospheric pressure). From N. L. Bowen, “The Melting Phenomena of the Plagioclase Feldspars,” *American Journal of Science* **35**, 577–599 (1913). Copyright ©2000, Addison-Wesley.



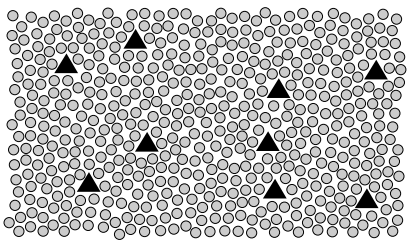
**Figure 5.33.** Construction of the phase diagram of a eutectic system from free energy graphs. Copyright ©2000, Addison-Wesley.



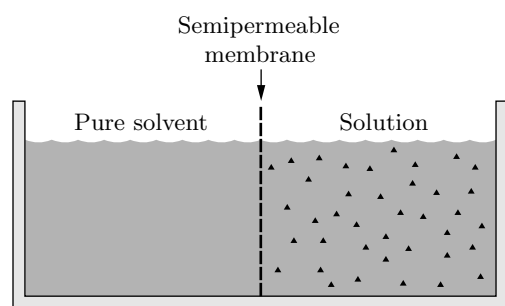
**Figure 5.34.** Phase diagram for mixtures of tin and lead. From Thaddeus B. Massalski, ed., *Binary Alloy Phase Diagrams*, second edition (ASM International, Materials Park, OH, 1990). Copyright ©2000, Addison-Wesley.



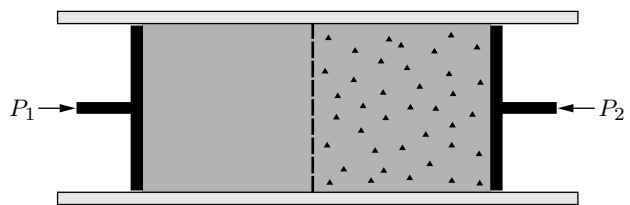
**Figure 5.35.** Free energy diagrams for Problems 5.71 and 5.72. Copyright ©2000, Addison-Wesley.



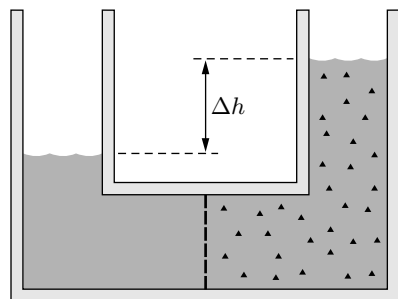
**Figure 5.36.** A dilute solution, in which the solute is much less abundant than the solvent. Copyright ©2000, Addison-Wesley.



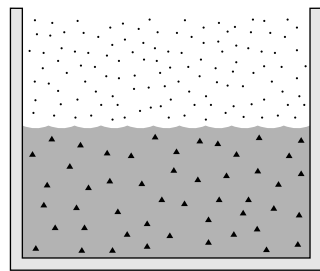
**Figure 5.37.** When a solution is separated by a semipermeable membrane from pure solvent at the same temperature and pressure, solvent will spontaneously flow into the solution. Copyright ©2000, Addison-Wesley.



**Figure 5.38.** To prevent osmosis,  $P_2$  must exceed  $P_1$  by an amount called the **osmotic pressure**. Copyright ©2000, Addison-Wesley.

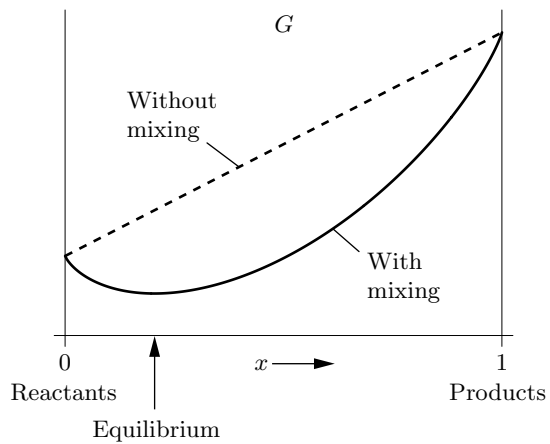


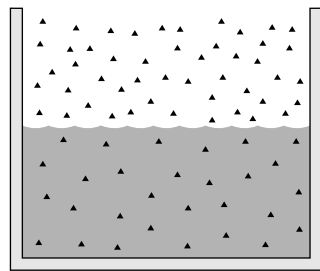
**Figure 5.39.** An experimental arrangement for measuring osmotic pressure. Solvent flows across the membrane from left to right until the difference in fluid level,  $\Delta h$ , is just enough to supply the osmotic pressure. Copyright ©2000, Addison-Wesley.



**Figure 5.40.** The presence of a solute reduces the tendency of a solvent to evaporate. Copyright ©2000, Addison-Wesley.

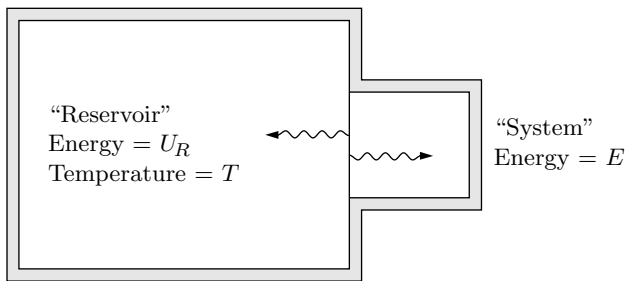
**Figure 5.41.** If reactants and products remained separate, the free energy would be a linear function of the extent of the reaction. With mixing, however,  $G$  has a minimum somewhere between  $x = 0$  and  $x = 1$ . Copyright ©2000, Addison-Wesley.



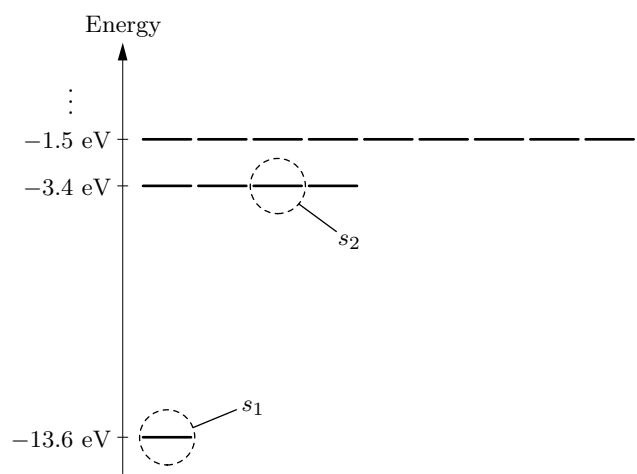


**Figure 5.42.** The dissolution of a gas in a liquid, such as oxygen in water, can be treated as a chemical reaction with its own equilibrium constant. Copyright ©2000, Addison-Wesley.

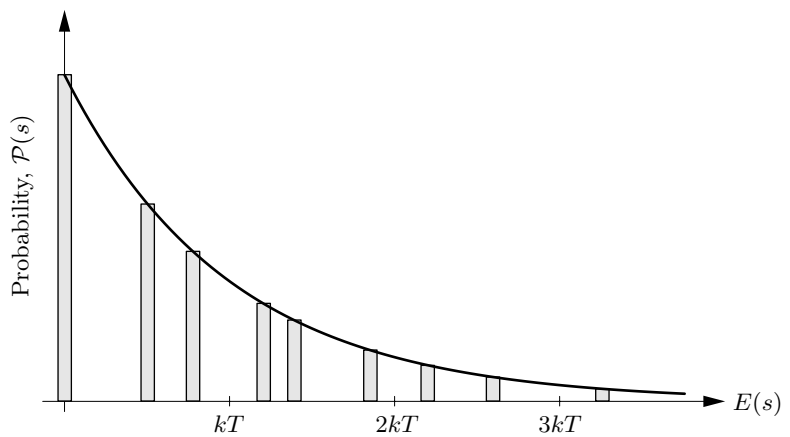
# 6 Boltzmann Statistics



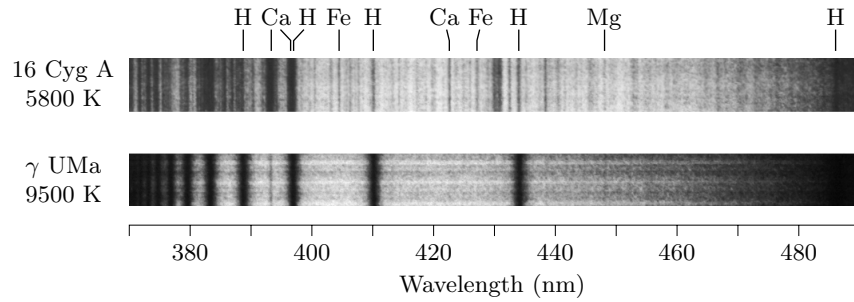
**Figure 6.1.** A “system” in thermal contact with a much larger “reservoir” at some well-defined temperature. Copyright ©2000, Addison-Wesley.



**Figure 6.2.** Energy level diagram for a hydrogen atom, showing the three lowest energy levels. There are four independent states with energy  $-3.4 \text{ eV}$ , and nine independent states with energy  $-1.5 \text{ eV}$ . Copyright ©2000, Addison-Wesley.

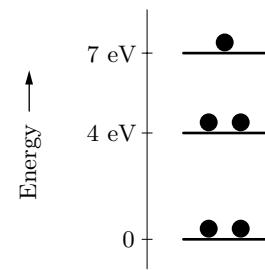


**Figure 6.3.** Bar graph of the relative probabilities of the states of a hypothetical system. The horizontal axis is energy. The smooth curve represents the Boltzmann distribution, equation 6.8, for one particular temperature. At lower temperatures it would fall off more suddenly, while at higher temperatures it would fall off more gradually. Copyright ©2000, Addison-Wesley.

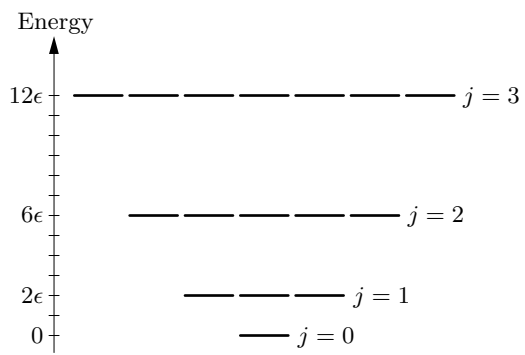


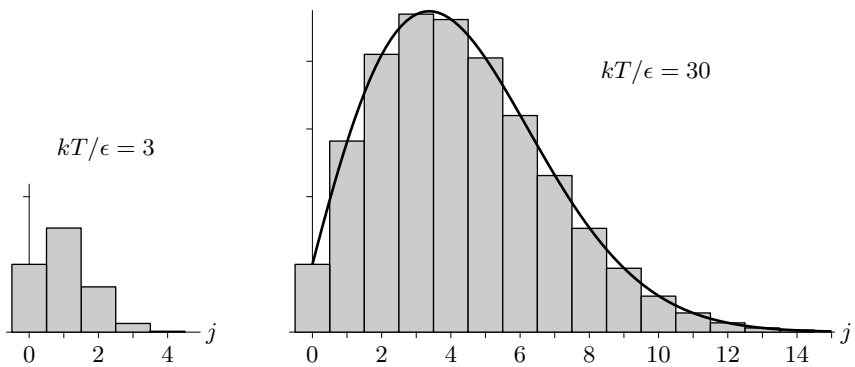
**Figure 6.4.** Photographs of the spectra of two stars. The upper spectrum is of a sunlike star (in the constellation Cygnus) with a surface temperature of about 5800 K; notice that the hydrogen absorption lines are clearly visible among a number of lines from other elements. The lower spectrum is of a hotter star (in Ursa Major, the Big Dipper), with a surface temperature of 9500 K. At this temperature a much larger fraction of the hydrogen atoms are in their first excited states, so the hydrogen lines are much more prominent than any others. Reproduced with permission from Helmut A. Abt et al., *An Atlas of Low-Dispersion Grating Stellar Spectra* (Kitt Peak National Observatory, Tucson, AZ, 1968). Copyright ©2000, Addison-Wesley.

**Figure 6.5.** Five hypothetical atoms distributed among three different states. Copyright ©2000, Addison-Wesley.

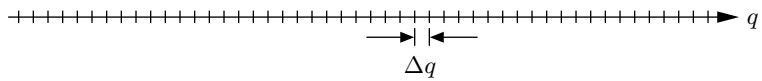


**Figure 6.6.** Energy level diagram for the rotational states of a diatomic molecule. Copyright ©2000, Addison-Wesley.

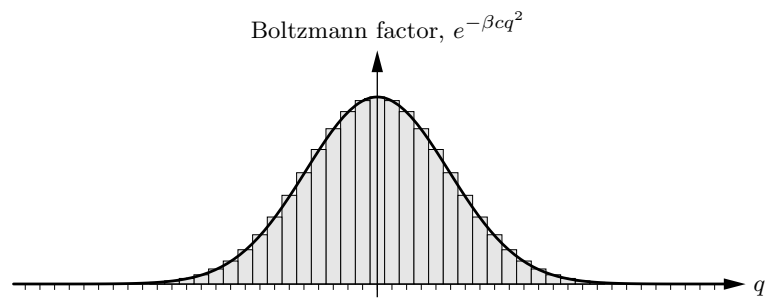




**Figure 6.7.** Bar-graph representations of the partition sum 6.30, for two different temperatures. At high temperatures the sum can be approximated as the area under a smooth curve. Copyright ©2000, Addison-Wesley.

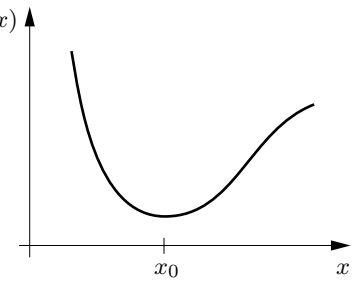


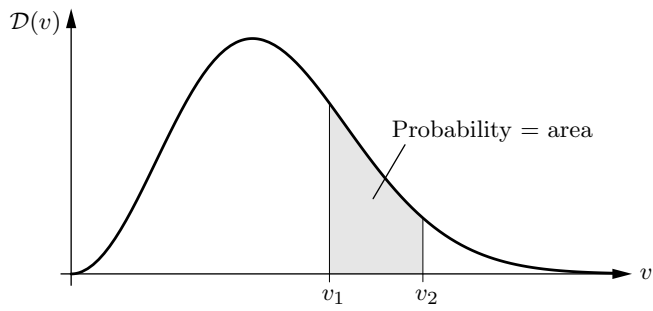
**Figure 6.8.** To count states over a continuous variable  $q$ , pretend that they're discretely spaced, separated by  $\Delta q$ . Copyright ©2000, Addison-Wesley.



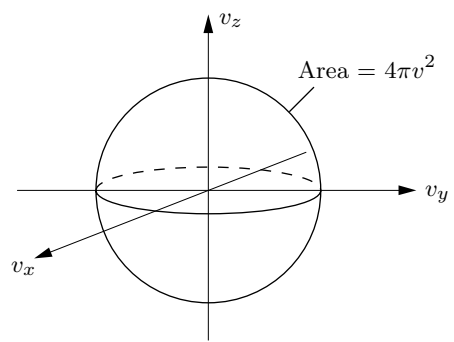
**Figure 6.9.** The partition function is the area under a bar graph whose height is the Boltzmann factor,  $e^{-\beta cq^2}$ . To calculate this area, we pretend that the bar graph is a smooth curve. Copyright ©2000, Addison-Wesley.

**Figure 6.10.** A one-dimensional potential well. The higher the temperature, the farther the particle will stray from the equilibrium point. Copyright ©2000, Addison-Wesley.

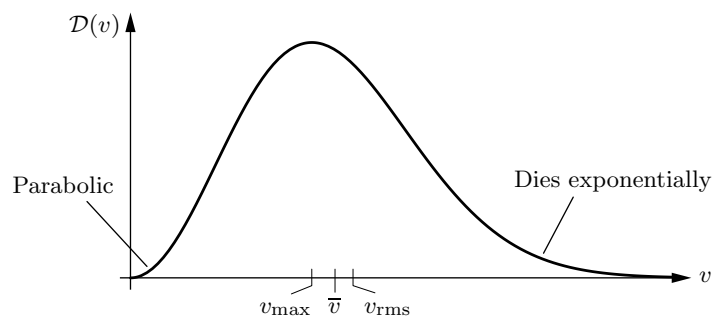




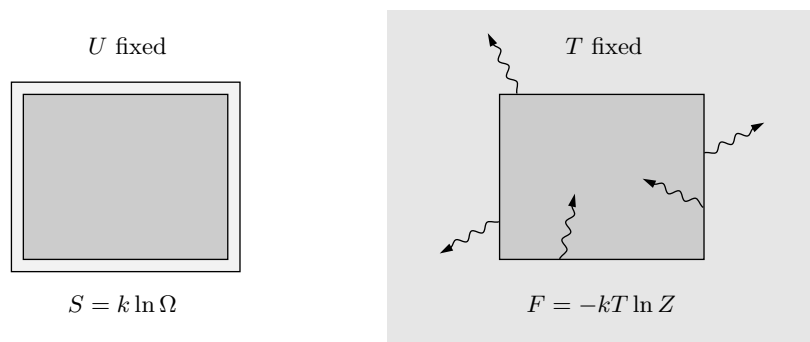
**Figure 6.11.** A graph of the relative probabilities for a gas molecule to have various speeds. More precisely, the vertical scale is defined so that the area under the graph within any interval equals the probability of the molecule having a speed in that interval. Copyright ©2000, Addison-Wesley.



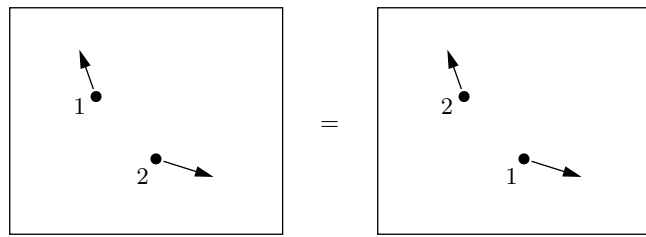
**Figure 6.12.** In “velocity space” each point represents a possible velocity vector. The set of all vectors for a given speed  $v$  lies on the surface of a sphere with radius  $v$ . Copyright ©2000, Addison-Wesley.



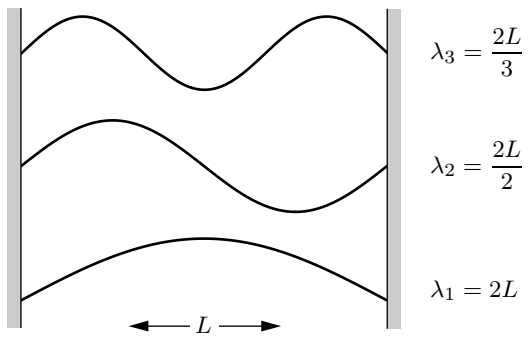
**Figure 6.13.** The Maxwell speed distribution falls off as  $v \rightarrow 0$  and as  $v \rightarrow \infty$ . The average speed is slightly larger than the most likely speed, while the rms speed is a bit larger still. Copyright ©2000, Addison-Wesley.



**Figure 6.14.** For an isolated system (left),  $S$  tends to increase. For a system at constant temperature (right),  $F$  tends to decrease. Like  $S$ ,  $F$  can be written as the logarithm of a statistical quantity, in this case  $Z$ . Copyright ©2000, Addison-Wesley.

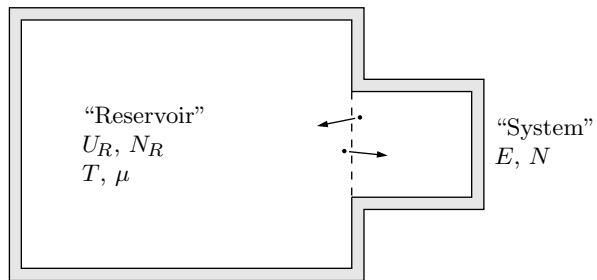


**Figure 6.15.** Interchanging the states of two indistinguishable particles leaves the system in the same state as before. Copyright ©2000, Addison-Wesley.

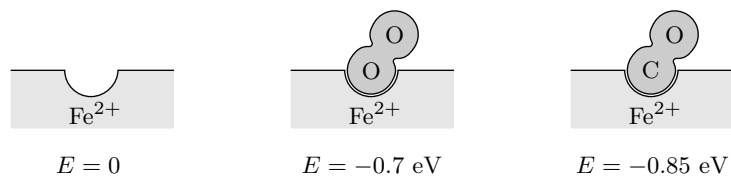


**Figure 6.16.** The three lowest-energy wavefunctions for a particle confined to a one-dimensional box. Copyright ©2000, Addison-Wesley.

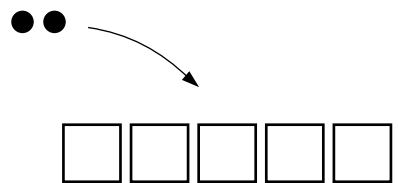
# 7 Quantum Statistics



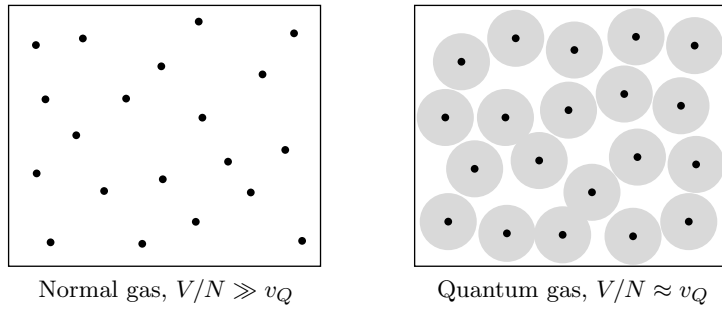
**Figure 7.1.** A system in thermal and diffusive contact with a much larger reservoir, whose temperature and chemical potential are effectively constant. Copyright ©2000, Addison-Wesley.



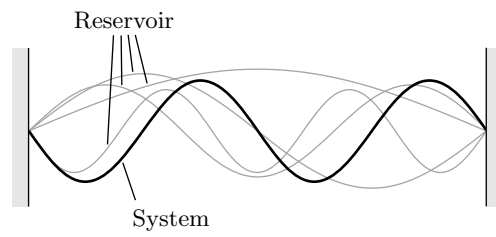
**Figure 7.2.** A single heme site can be unoccupied, occupied by oxygen, or occupied by carbon monoxide. (The energy values are only approximate.) Copyright ©2000, Addison-Wesley.



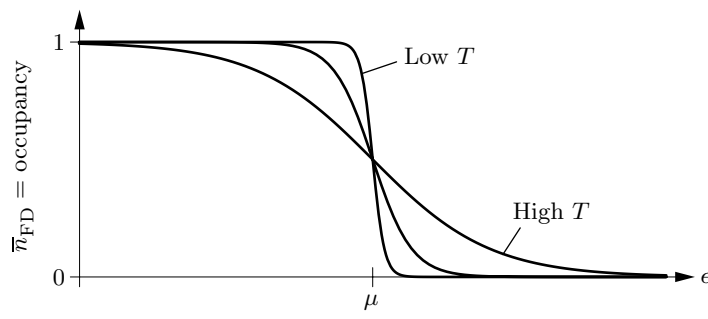
**Figure 7.3.** A simple model of five single-particle states, with two particles that can occupy these states. Copyright ©2000, Addison-Wesley.



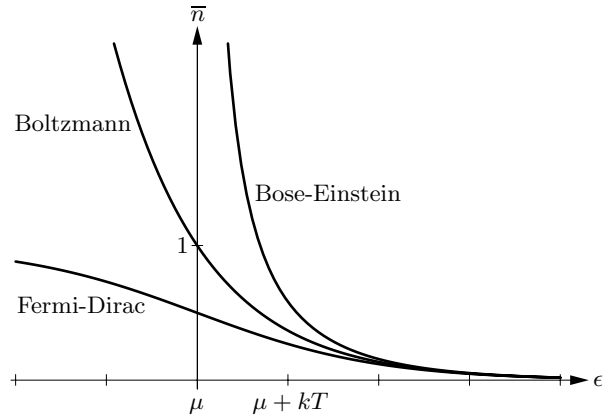
**Figure 7.4.** In a normal gas, the space between particles is much greater than the typical size of a particle's wavefunction. When the wavefunctions begin to "touch" and overlap, we call it a **quantum gas**. Copyright ©2000, Addison-Wesley.



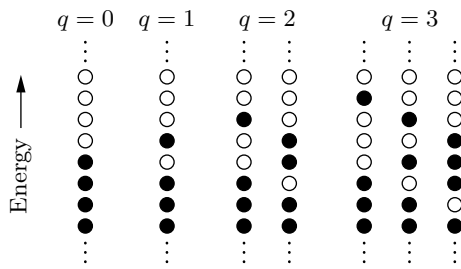
**Figure 7.5.** To treat a quantum gas using Gibbs factors, we consider a “system” consisting of one single-particle state (or wavefunction). The “reservoir” consists of all the other possible single-particle states. Copyright ©2000, Addison-Wesley.



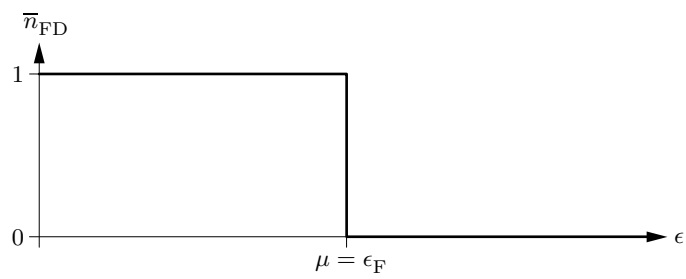
**Figure 7.6.** The Fermi-Dirac distribution goes to 1 for very low-energy states and to zero for very high-energy states. It equals 1/2 for a state with energy  $\mu$ , falling off suddenly for low  $T$  and gradually for high  $T$ . (Although  $\mu$  is fixed on this graph, in the next section we'll see that  $\mu$  normally varies with temperature.)  
Copyright ©2000, Addison-Wesley.



**Figure 7.7.** Comparison of the Fermi-Dirac, Bose-Einstein, and Boltzmann distributions, all for the same value of  $\mu$ . When  $(\epsilon - \mu)/kT \gg 1$ , the three distributions become equal. Copyright ©2000, Addison-Wesley.

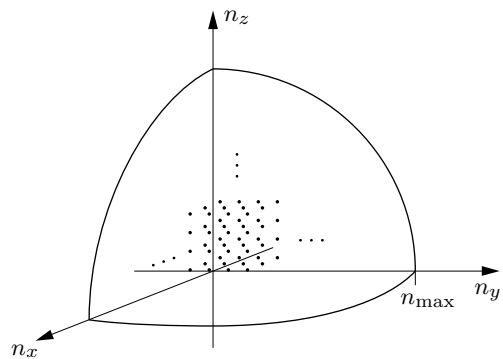


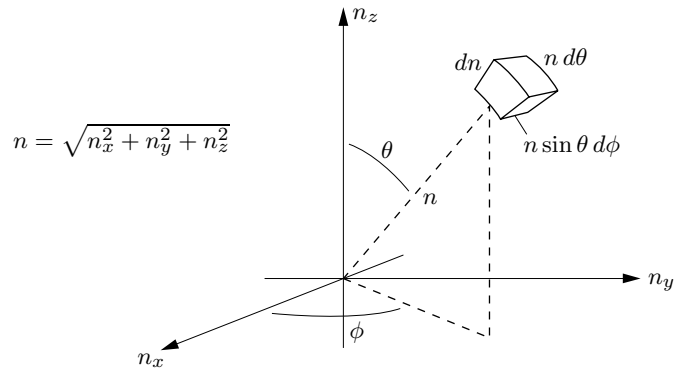
**Figure 7.8.** A representation of the system states of a fermionic system with evenly spaced, nondegenerate energy levels. A filled dot represents an occupied single-particle state, while a hollow dot represents an unoccupied single-particle state. Copyright ©2000, Addison-Wesley.



**Figure 7.9.** At  $T = 0$ , the Fermi-Dirac distribution equals 1 for all states with  $\epsilon < \mu$  and equals 0 for all states with  $\epsilon > \mu$ . Copyright ©2000, Addison-Wesley.

**Figure 7.10.** Each triplet of integers  $(n_x, n_y, n_z)$  represents a pair of definite-energy electron states (one with each spin orientation). The set of all independent states fills the positive octant of  $n$ -space. Copyright ©2000, Addison-Wesley.

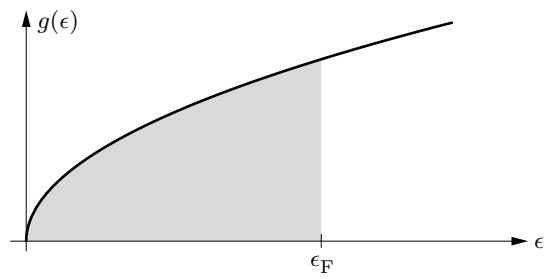




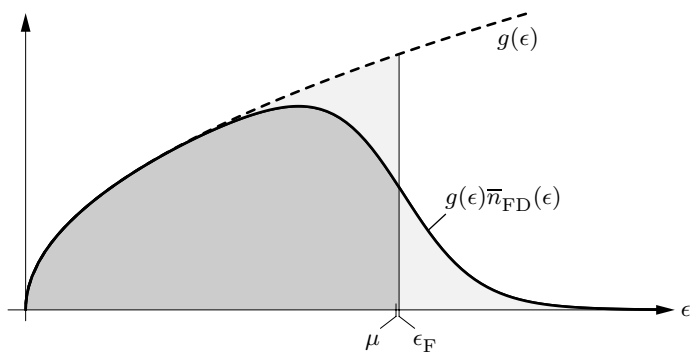
**Figure 7.11.** In spherical coordinates  $(n, \theta, \phi)$ , the infinitesimal volume element is  $(dn)(n d\theta)(n \sin \theta d\phi)$ . Copyright ©2000, Addison-Wesley.

**Figure 7.12.** The double star system Sirius A and B. Sirius A (greatly overexposed in the photo) is the brightest star in our night sky. Its companion, Sirius B, is hotter but very faint, indicating that it must be extremely small—a white dwarf. From the orbital motion of the pair we know that Sirius B has about the same mass as our sun. (UCO/Lick Observatory photo.) Copyright ©2000, Addison-Wesley.



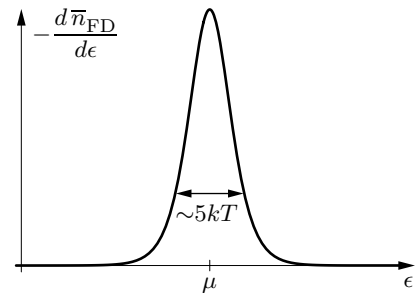


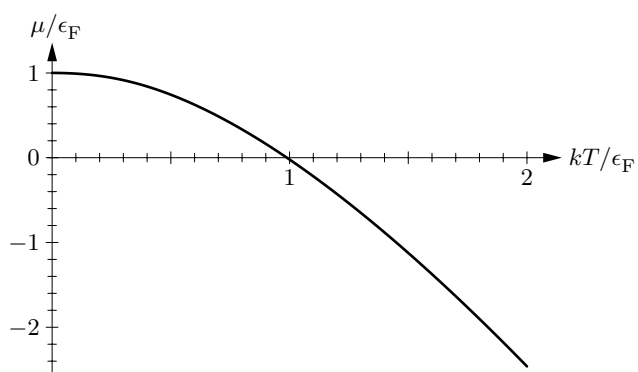
**Figure 7.13.** Density of states for a system of noninteracting, nonrelativistic particles in a three-dimensional box. The number of states within any energy interval is the area under the graph. For a Fermi gas at  $T = 0$ , all states with  $\epsilon < \epsilon_F$  are occupied while all states with  $\epsilon > \epsilon_F$  are unoccupied. Copyright ©2000, Addison-Wesley.



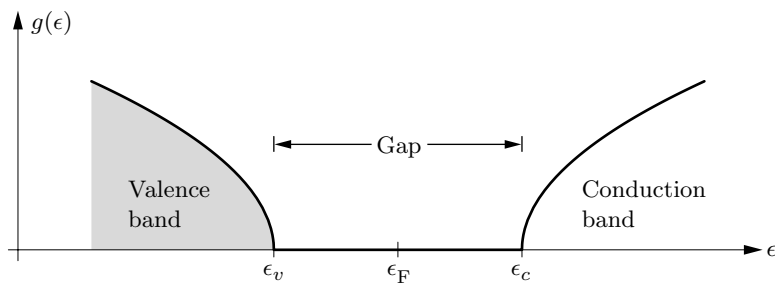
**Figure 7.14.** At nonzero  $T$ , the number of fermions per unit energy is given by the density of states times the Fermi-Dirac distribution. Because increasing the temperature does not change the total number of fermions, the two lightly shaded areas must be equal. Since  $g(\epsilon)$  is greater above  $\epsilon_F$  than below, this means that the chemical potential decreases as  $T$  increases. This graph is drawn for  $T/T_F = 0.1$ ; at this temperature  $\mu$  is about 1% less than  $\epsilon_F$ . Copyright ©2000, Addison-Wesley.

**Figure 7.15.** The derivative of the Fermi-Dirac distribution is negligible everywhere except within a few  $kT$  of  $\mu$ . Copyright ©2000, Addison-Wesley.

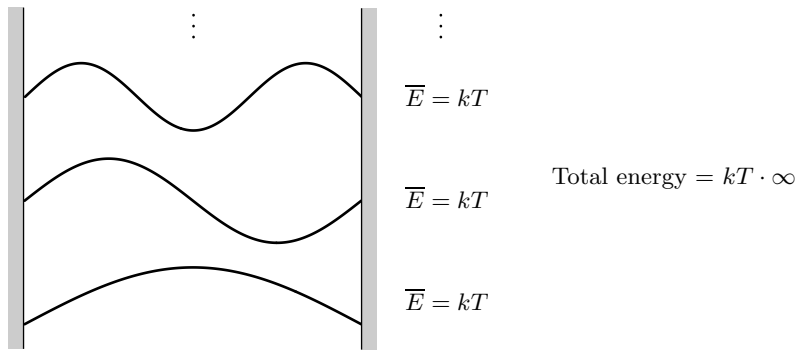




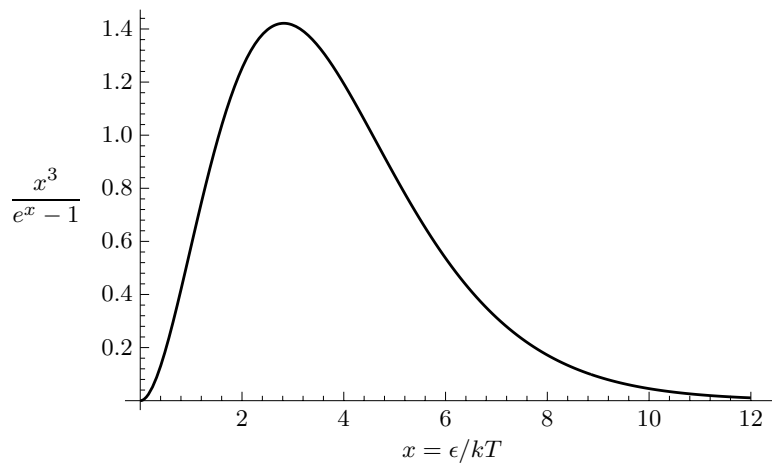
**Figure 7.16.** Chemical potential of a noninteracting, nonrelativistic Fermi gas in a three-dimensional box, calculated numerically as described in Problem 7.32. At low temperatures  $\mu$  is given approximately by equation 7.66, while at high temperatures  $\mu$  becomes negative and approaches the form for an ordinary gas obeying Boltzmann statistics. Copyright ©2000, Addison-Wesley.



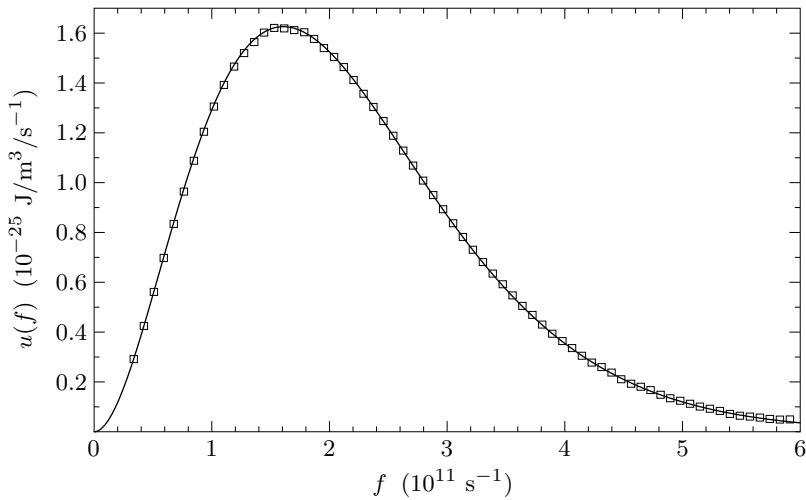
**Figure 7.17.** The periodic potential of a crystal lattice results in a density-of-states function consisting of “bands” (with many states) and “gaps” (with no states). For an insulator or a semiconductor, the Fermi energy lies in the middle of a gap so that at  $T = 0$ , the “valence band” is completely full while the “conduction band” is completely empty. Copyright ©2000, Addison-Wesley.



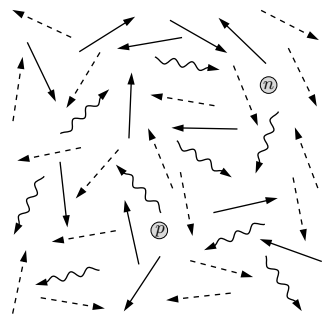
**Figure 7.18.** We can analyze the electromagnetic field in a box as a superposition of standing-wave modes of various wavelengths. Each mode is a harmonic oscillator with some well-defined frequency. Classically, each oscillator should have an average energy of  $kT$ . Since the total number of modes is infinite, so is the total energy in the box. Copyright ©2000, Addison-Wesley.



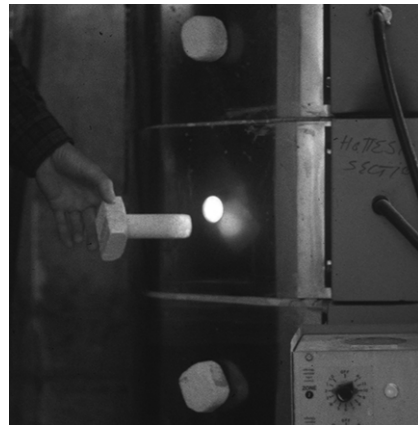
**Figure 7.19.** The Planck spectrum, plotted in terms of the dimensionless variable  $x = \epsilon/kT = hf/kT$ . The area under any portion of this graph, multiplied by  $8\pi(kT)^4/(hc)^3$ , equals the energy density of electromagnetic radiation within the corresponding frequency (or photon energy) range; see equation 7.85. Copyright ©2000, Addison-Wesley.



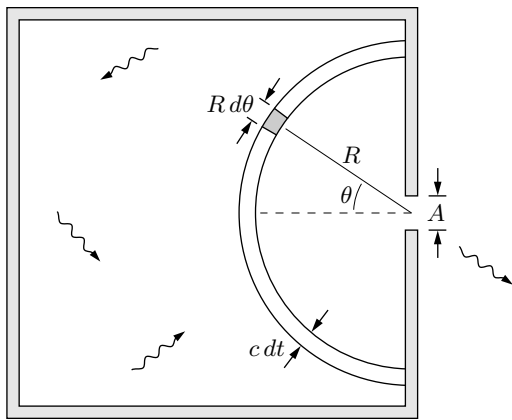
**Figure 7.20.** Spectrum of the cosmic background radiation, as measured by the *Cosmic Background Explorer* satellite. Plotted vertically is the energy density per unit frequency, in SI units. Note that a frequency of  $3 \times 10^{11} \text{ s}^{-1}$  corresponds to a wavelength of  $\lambda = c/f = 1.0 \text{ mm}$ . Each square represents a measured data point. The point-by-point uncertainties are too small to show up on this scale; the size of the squares instead represents a liberal estimate of the uncertainty due to systematic effects. The solid curve is the theoretical Planck spectrum, with the temperature adjusted to 2.735 K to give the best fit. From J. C. Mather et al., *Astrophysical Journal Letters* **354**, L37 (1990); adapted courtesy of NASA/GSFC and the COBE Science Working Group. Subsequent measurements from this experiment and others now give a best-fit temperature of  $2.728 \pm 0.002 \text{ K}$ . Copyright ©2000, Addison-Wesley.



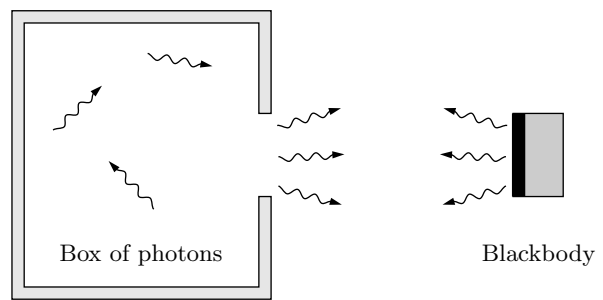
**Figure 7.21.** When the temperature was greater than the electron mass times  $c^2/k$ , the universe was filled with three types of radiation: electrons and positrons (solid arrows); neutrinos (dashed); and photons (wavy). Bathed in this radiation were a few protons and neutrons, roughly one for every billion radiation particles. Copyright ©2000, Addison-Wesley.



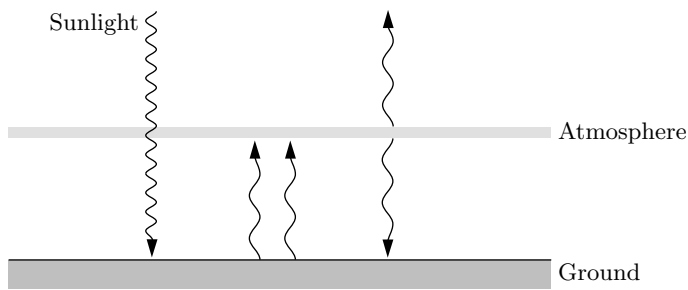
**Figure 7.22.** When you open a hole in a container filled with radiation (here a kiln), the spectrum of the light that escapes is the same as the spectrum of the light inside. The total amount of energy that escapes is proportional to the size of the hole and to the amount of time that passes. Copyright ©2000, Addison-Wesley.



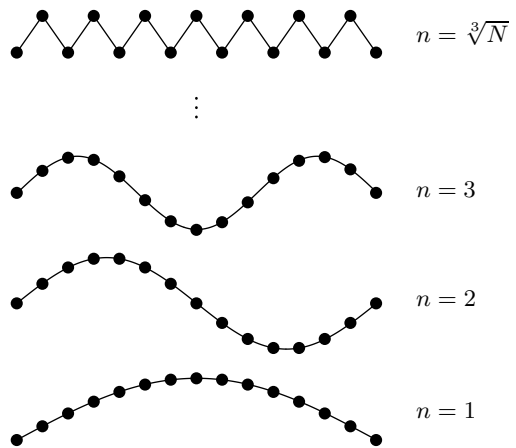
**Figure 7.23.** The photons that escape now were once somewhere within a hemispherical shell inside the box. From a given point in this shell, the probability of escape depends on the distance from the hole and the angle  $\theta$ . Copyright ©2000, Addison-Wesley.



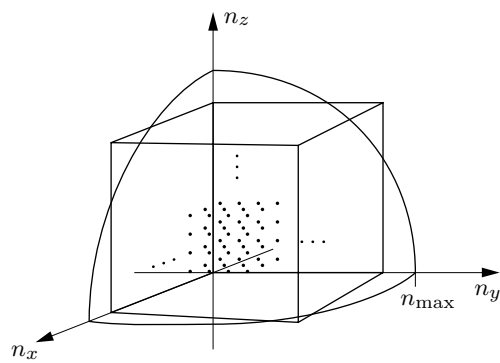
**Figure 7.24.** A thought experiment to demonstrate that a perfectly black surface emits radiation identical to that emitted by a hole in a box of thermal photons.  
Copyright ©2000, Addison-Wesley.



**Figure 7.25.** Earth's atmosphere is mostly transparent to incoming sunlight, but opaque to the infrared light radiated upward by earth's surface. If we model the atmosphere as a single layer, then equilibrium requires that earth's surface receive as much energy from the atmosphere as from the sun. Copyright ©2000, Addison-Wesley.

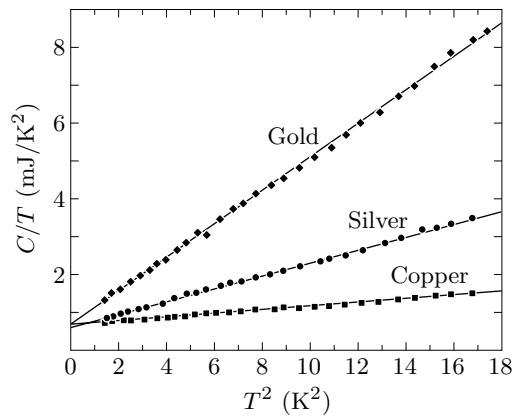


**Figure 7.26.** Modes of oscillation of a row of atoms in a crystal. If the crystal is a cube, then the number of atoms along any row is  $\sqrt[3]{N}$ . This is also the total number of modes along this direction, because each “bump” in the wave form must contain at least one atom. Copyright ©2000, Addison-Wesley.



**Figure 7.27.** The sum in equation 7.106 is technically over a cube in  $n$ -space whose width is  $\sqrt[3]{N}$ . As an approximation, we instead sum over an eighth-sphere with the same total volume. Copyright ©2000, Addison-Wesley.

**Figure 7.28.** Low-temperature measurements of the heat capacities (per mole) of copper, silver, and gold. Adapted with permission from William S. Corak et al., *Physical Review* **98**, 1699 (1955). Copyright ©2000, Addison-Wesley.



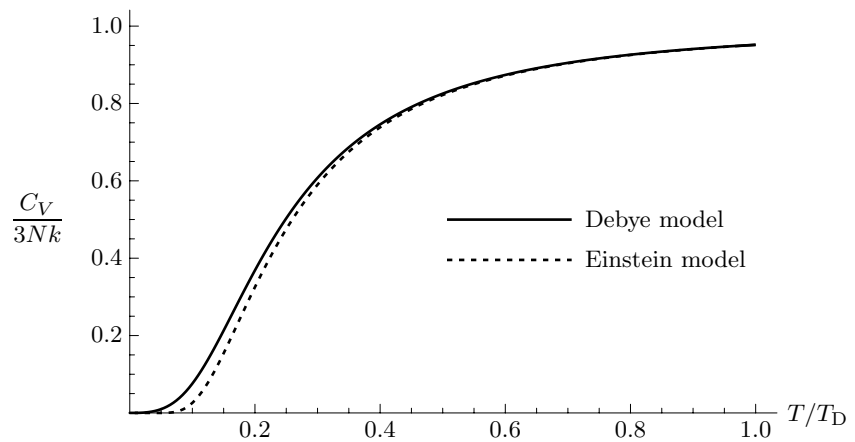


**Figure 7.29.** The Debye prediction for the heat capacity of a solid, with the prediction of the Einstein model plotted for comparison. The constant  $\epsilon$  in the Einstein model has been chosen to obtain the best agreement with the Debye model at high temperatures. Note that the Einstein curve is much flatter than the Debye curve at low temperatures. Copyright ©2000, Addison-Wesley.

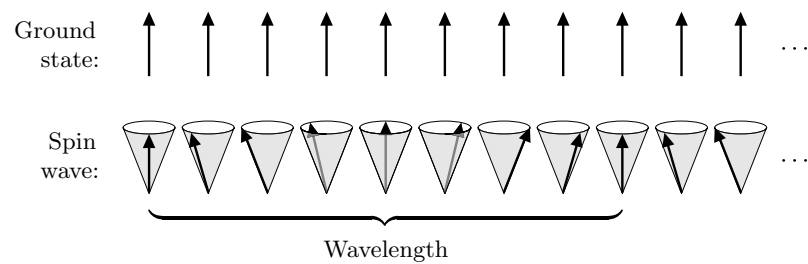


**Figure 7.30.** In the ground state of a ferromagnet, all the elementary dipoles point in the same direction. The lowest-energy excitations above the ground state are **spin waves**, in which the dipoles precess in a conical motion. A long-wavelength spin wave carries very little energy, because the difference in direction between neighboring dipoles is very small. Copyright ©2000, Addison-Wesley.

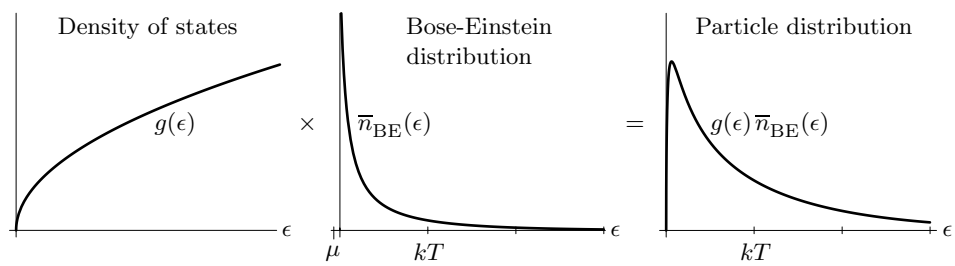


**Figure 7.31.** The distribution of bosons as a function of energy is the product of two functions, the density of states and the Bose-Einstein distribution. Copyright ©2000, Addison-Wesley.

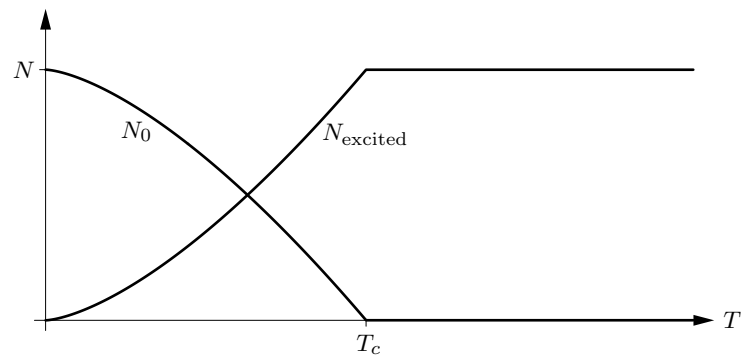


**Figure 7.32.** Number of atoms in the ground state ( $N_0$ ) and in excited states, for an ideal Bose gas in a three-dimensional box. Below  $T_c$  the number of atoms in excited states is proportional to  $T^{3/2}$ . Copyright ©2000, Addison-Wesley.

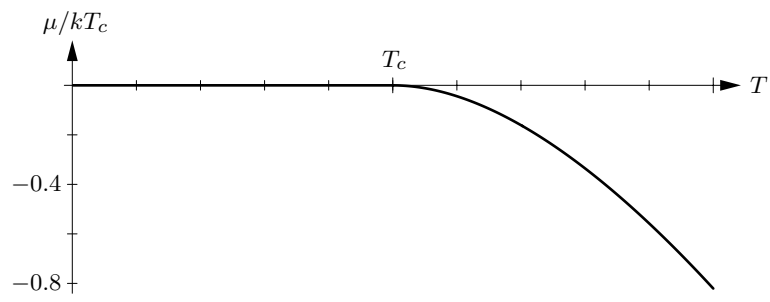


**Figure 7.33.** Chemical potential of an ideal Bose gas in a three-dimensional box. Below the condensation temperature,  $\mu$  differs from zero by an amount that is too small to show on this scale. Above the condensation temperature  $\mu$  becomes negative; the values plotted here were calculated numerically as described in Problem 7.69. Copyright ©2000, Addison-Wesley.

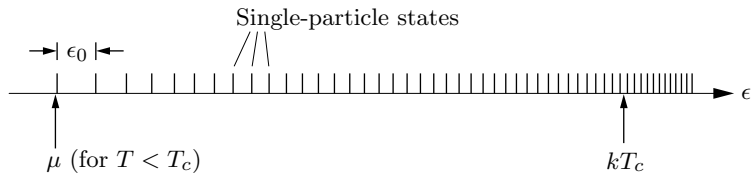


**Figure 7.34.** Schematic representation of the energy scales involved in Bose-Einstein condensation. The short vertical lines mark the energies of various single-particle states. (Aside from growing closer together (on average) with increasing energy, the locations of these lines are not quantitatively accurate.) The condensation temperature (times  $k$ ) is many times larger than the spacing between the lowest energy levels, while the chemical potential, when  $T < T_c$ , is only a tiny amount below the ground-state energy. Copyright ©2000, Addison-Wesley.

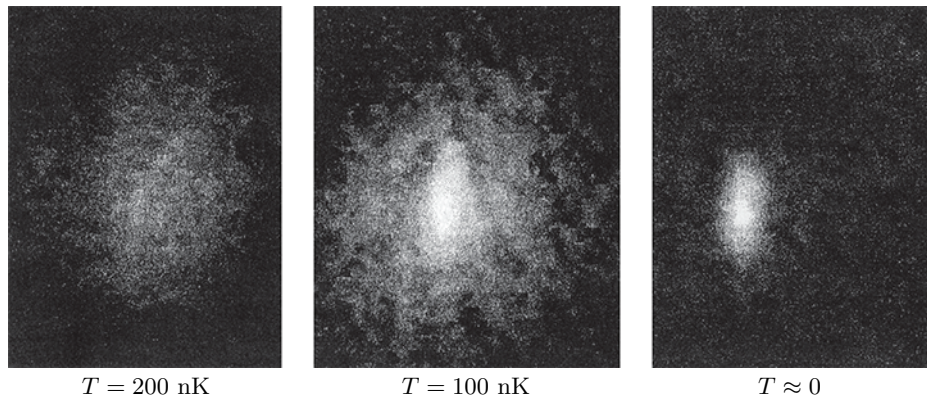


**Figure 7.35.** Evidence for Bose-Einstein condensation of rubidium-87 atoms. These images were made by turning off the magnetic field that confined the atoms, letting the gas expand for a moment, and then shining light on the expanded cloud to map its distribution. Thus, the positions of the atoms in these images give a measure of their *velocities* just before the field was turned off. Above the condensation temperature (left), the velocity distribution is broad and isotropic, in accord with the Maxwell-Boltzmann distribution. Below the condensation temperature (center), a substantial fraction of the atoms fall into a small, elongated region in velocity space. These atoms make up the condensate; the elongation occurs because the trap is narrower in the vertical direction, causing the ground-state wavefunction to be narrower in position space and thus wider in velocity space. At the lowest temperatures achieved (right), essentially all of the atoms are in the ground-state wavefunction. From Carl E. Wieman, *American Journal of Physics* **64**, 854 (1996). Copyright ©2000, Addison-Wesley.

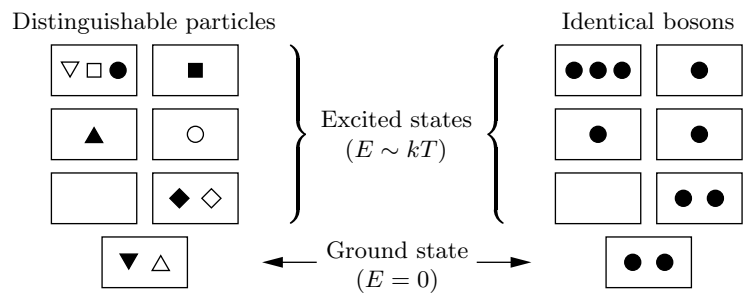


**Figure 7.36.** When most particles are in excited states, the Boltzmann factor for the entire system is always very small (of order  $e^{-N}$ ). For distinguishable particles, the number of arrangements among these states is so large that system states of this type are still very probable. For identical bosons, however, the number of arrangements is much smaller. Copyright ©2000, Addison-Wesley.

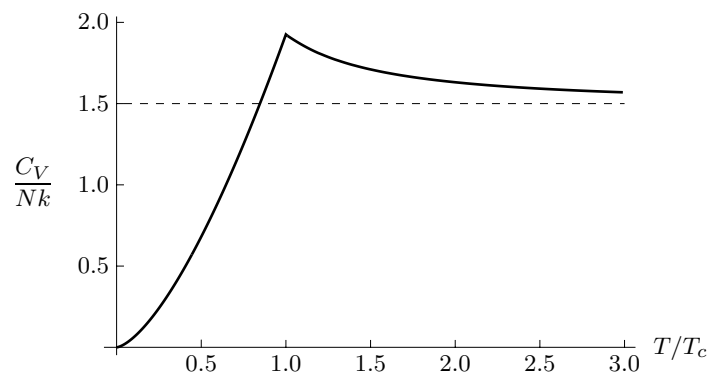


**Figure 7.37.** Heat capacity of an ideal Bose gas in a three-dimensional box. Copyright ©2000, Addison-Wesley.

# 8 Systems of Interacting Particles

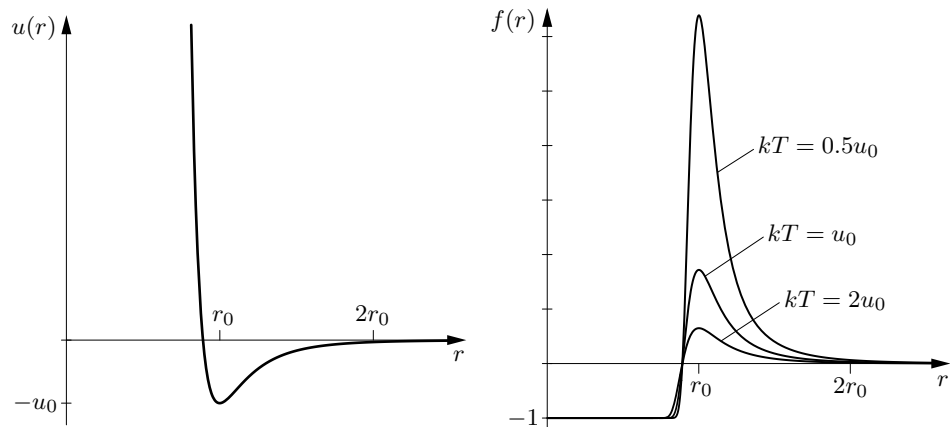


**Figure 8.1.** Left: The Lennard-Jones intermolecular potential function, with a strong repulsive region at small distances and a weak attractive region at somewhat larger distances. Right: The corresponding Mayer  $f$ -function, for three different temperatures. Copyright ©2000, Addison-Wesley.

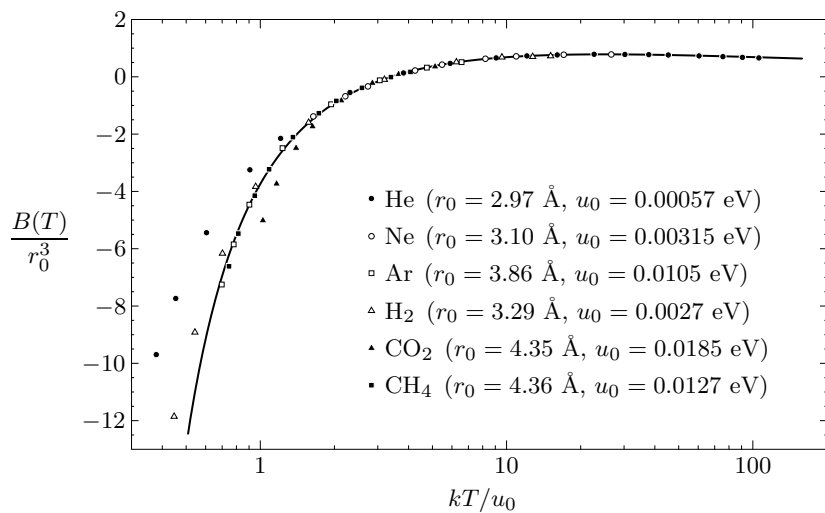


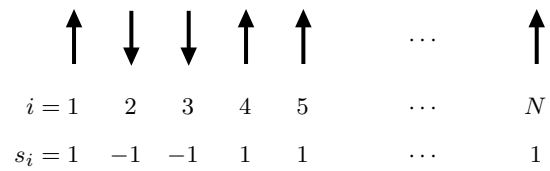
**Figure 8.2.** Measurements of the second virial coefficients of selected gases, compared to the prediction of equation 8.36 with  $u(r)$  given by the Lennard-Jones function. Note that the horizontal axis is logarithmic. The constants  $r_0$  and  $u_0$  have been chosen separately for each gas to give the best fit. For carbon dioxide, the poor fit is due to the asymmetric shape of the molecules. For hydrogen and helium, the discrepancies at low temperatures are due to quantum effects. Data from J. H. Dymond and E. B. Smith, *The Virial Coefficients of Pure Gases and Mixtures: A Critical Compilation* (Oxford University Press, Oxford, 1980). Copyright ©2000, Addison-Wesley.

↑	↓	↓	↓	↑	↑	↑	↑	↑	↓
↓	↓	↓	↓	↑	↑	↑	↑	↑	↓
↑	↑	↑	↓	↓	↑	↑	↓	↓	↓
↑	↓	↑	↑	↑	↑	↑	↑	↓	↑
↑	↑	↑	↑	↑	↑	↓	↑	↑	↑
↑	↑	↑	↑	↑	↑	↓	↑	↑	↑
↓	↑	↑	↑	↑	↑	↑	↓	↑	↓
↑	↑	↑	↑	↑	↑	↑	↑	↑	↑
↑	↑	↓	↑	↑	↓	↓	↑	↑	↑
↓	↑	↑	↑	↑	↓	↓	↓	↓	↑

**Figure 8.3.** One of the many possible states of a two-dimensional Ising model on a  $10 \times 10$  square lattice. Copyright ©2000, Addison-Wesley.

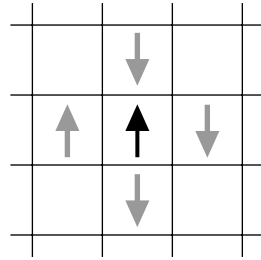
↓	↓	↑	↓
↑	↑	↑	↑
↓	↑	↑	↑
↓	↓	↓	↑

**Figure 8.4.** One particular state of an Ising model on a  $4 \times 4$  square lattice (Problem 8.15). Copyright ©2000, Addison-Wesley.



**Figure 8.5.** A one-dimensional Ising model with  $N$  elementary dipoles. Copyright ©2000, Addison-Wesley.

**Figure 8.6.** The four neighbors of this particular dipole have an average  $s$  value of  $(+1-3)/4 = -1/2$ . If the central dipole points up, the energy due to its interactions with its neighbors is  $+2\epsilon$ , while if it points down, the energy is  $-2\epsilon$ . Copyright ©2000, Addison-Wesley.



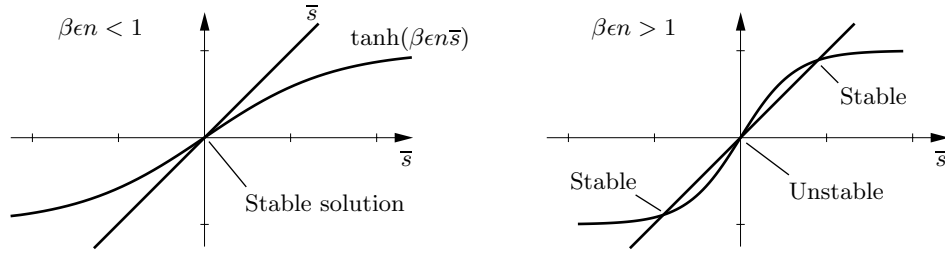


**Figure 8.7.** Graphical solution of equation 8.50. The slope of the tanh function at the origin is  $\beta\epsilon n$ . When this quantity is less than 1, there is only one solution, at  $\bar{s} = 0$ ; when this quantity is greater than 1, the  $\bar{s} = 0$  solution is unstable but there are also two nontrivial stable solutions. Copyright ©2000, Addison-Wesley.

```

program ising                                Monte Carlo simulation of a 2D Ising
                                              model using the Metropolis algorithm

size = 10                                     Width of square lattice
T = 2.5                                       Temperature in units of  $\epsilon/k$ 

initialize                                     Main iteration loop

for iteration = 1 to 100*size^2 do
    i = int(rand*size+1)                      Choose a random row number
    j = int(rand*size+1)                      and a random column number
    deltaU(i,j,Ediff)                        Compute  $\Delta U$  of hypothetical flip
    if Ediff <= 0 then
        s(i,j) = -s(i,j)                      If flipping reduces the energy ...
        colorsquare(i,j)                      then flip it!
    else
        if rand < exp(-Ediff/T) then
            s(i,j) = -s(i,j)                  otherwise the Boltzmann factor
            colorsquare(i,j)                  gives the probability of flipping
        end if
        end if
    next iteration                            Now go back and start over ...
end program

subroutine deltaU(i,j,Ediff)                  Compute  $\Delta U$  of flipping a dipole
                                              (note periodic boundary conditions)

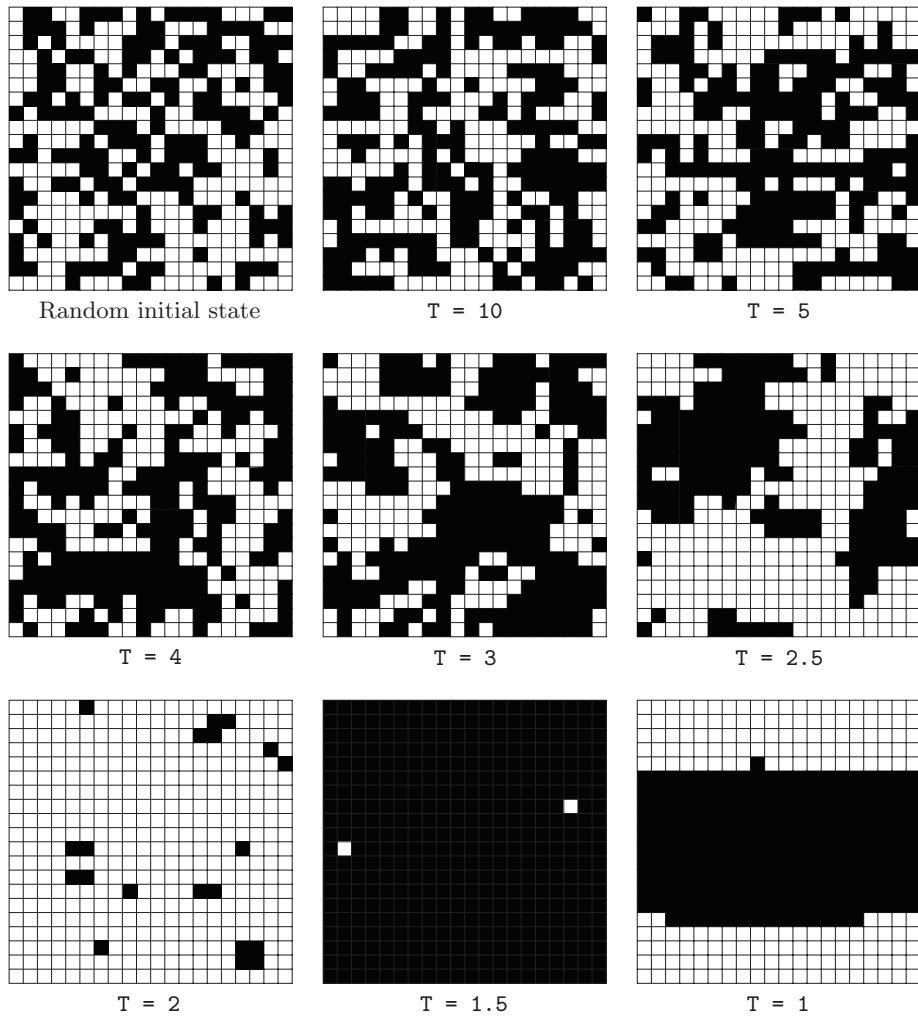
    if i = 1 then top = s(size,j) else top = s(i-1,j)
    if i = size then bottom = s(1,j) else bottom = s(i+1,j)
    if j = 1 then left = s(i,size) else left = s(i,j-1)
    if j = size then right = s(i,1) else right = s(i,j+1)
    Ediff = 2*s(i,j)*(top+bottom+left+right)
end subroutine

subroutine initialize                         Initialize to a random array
                                             
    for i = 1 to size
        for j = 1 to size
            if rand < .5 then s(i,j) = 1 else s(i,j) = -1
            colorsquare(i,j)
        next j
    next i
end subroutine

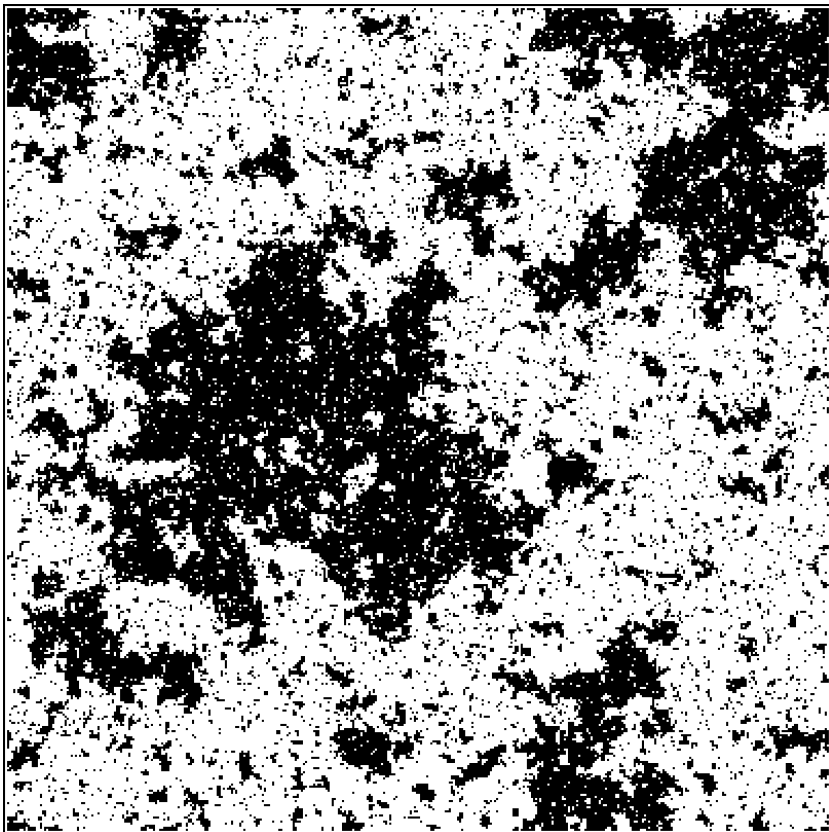
subroutine colorsquare(i,j)                  Color a square according to  $s$  value
                                              (implementation depends on system)

```

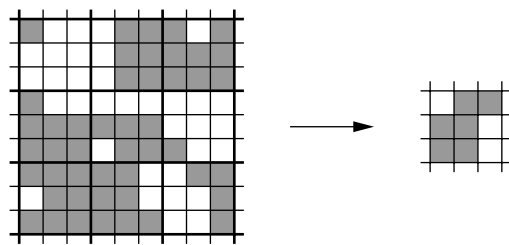
**Figure 8.8.** A pseudocode program to simulate a two-dimensional Ising model, using the Metropolis algorithm. Copyright ©2000, Addison-Wesley.



**Figure 8.9.** Graphical output from eight runs of the `ising` program, at successively lower temperatures. Each black square represents an “up” dipole and each white square represents a “down” dipole. The variable  $T$  is the temperature in units of  $\epsilon/k$ . Copyright ©2000, Addison-Wesley.



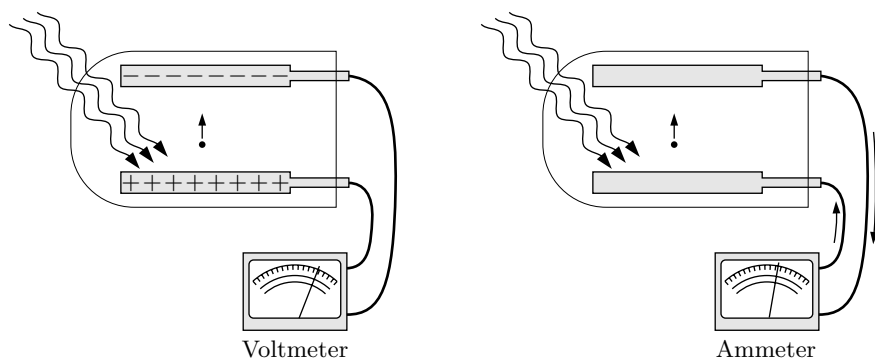
**Figure 8.10.** A typical state generated by the `ising` program after a few billion iterations on a  $400 \times 400$  lattice at  $T = 2.27$  (the critical temperature). Notice that there are clusters of all possible sizes, from individual dipoles up to the size of the lattice itself. Copyright ©2000, Addison-Wesley.



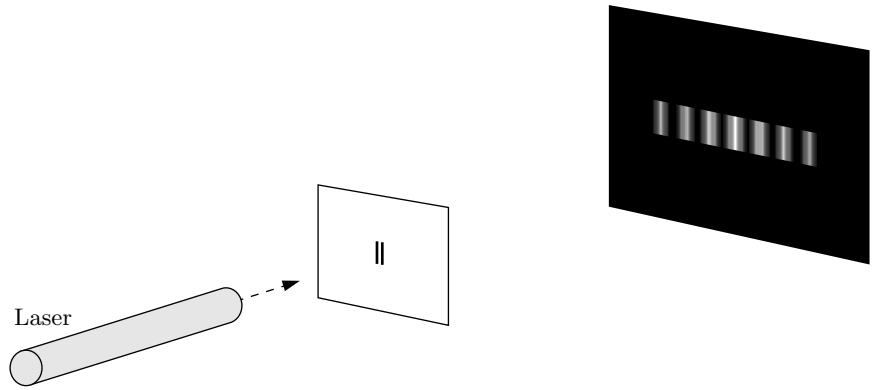
**Figure 8.11.** In a **block spin transformation**, we replace each block of nine dipoles with a single dipole whose orientation is determined by “majority rule.” Copyright ©2000, Addison-Wesley.

# A

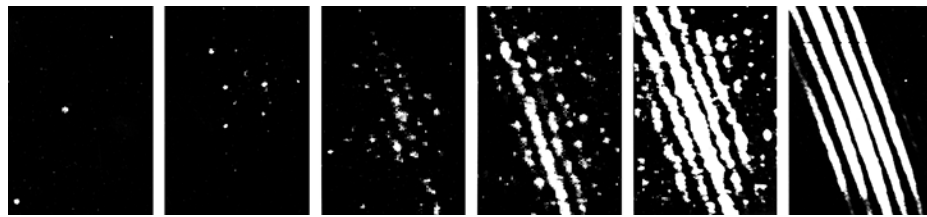
## Elements of Quantum Mechanics



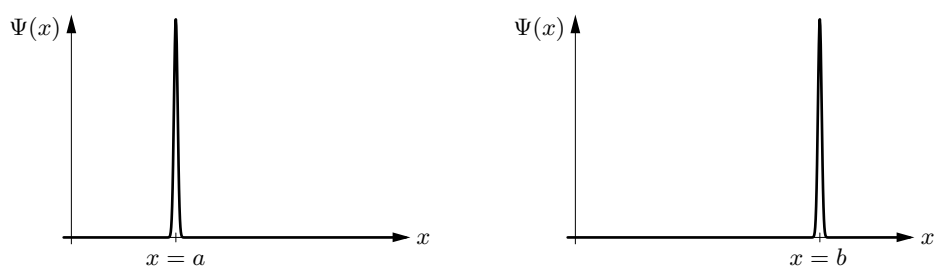
**Figure A.1.** Two experiments to study the photoelectric effect. When an ideal voltmeter (with essentially infinite resistance) is connected to the circuit, electrons accumulate on the anode and repel other electrons; the voltmeter measures the *energy* (per unit charge) that an electron needs in order to cross. When an ammeter is connected, it measures the *number* of electrons (per unit time) that collect on the anode and then circulate back to the cathode. Copyright ©2000, Addison-Wesley.



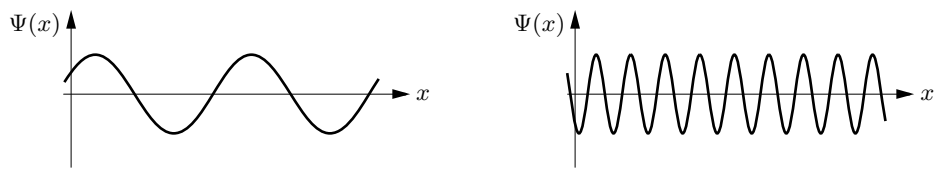
**Figure A.2.** In a two-slit interference experiment, monochromatic light (often from a laser) is aimed at a pair of slits in a screen. An interference pattern of dark and light bands appears on the viewing screen some distance away. Copyright ©2000, Addison-Wesley.



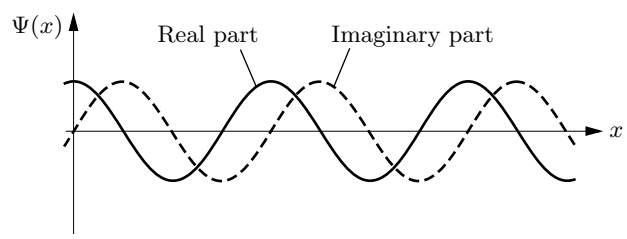
**Figure A.3.** These images were produced using the beam of an electron microscope. A positively charged wire was placed in the path of the beam, causing the electrons to bend around either side and interfere as if they had passed through a double slit. The current in the electron beam increases from one image to the next, showing that the interference pattern is built up from the statistically distributed light flashes of individual electrons. From P. G. Merli, G. F. Missiroli, and G. Pozzi, *American Journal of Physics* **44**, 306 (1976). Copyright ©2000, Addison-Wesley.



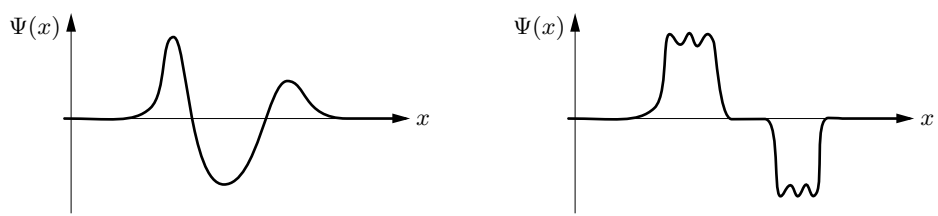
**Figure A.4.** Wavefunctions for states in which a particle's position is well defined (at  $x = a$  and  $x = b$ , respectively). When a particle is in such a state, its momentum is completely undefined. Copyright ©2000, Addison-Wesley.



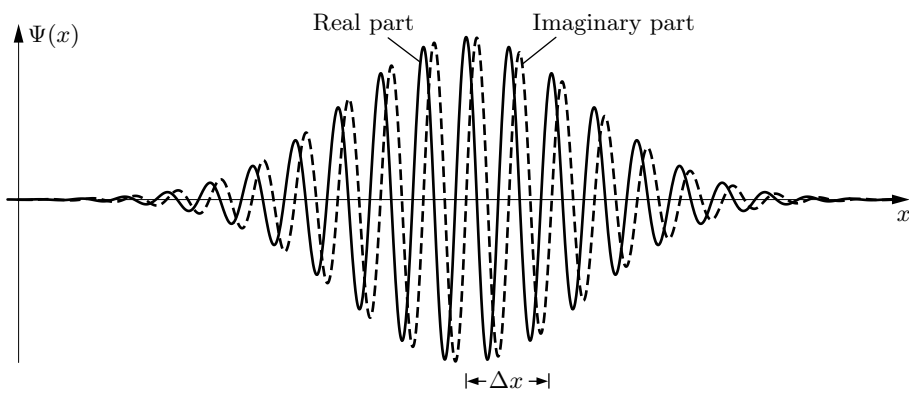
**Figure A.5.** Wavefunctions for states in which a particle's momentum is well defined (with small and large values, respectively). When a particle is in such a state, its position is completely undefined. Copyright ©2000, Addison-Wesley.



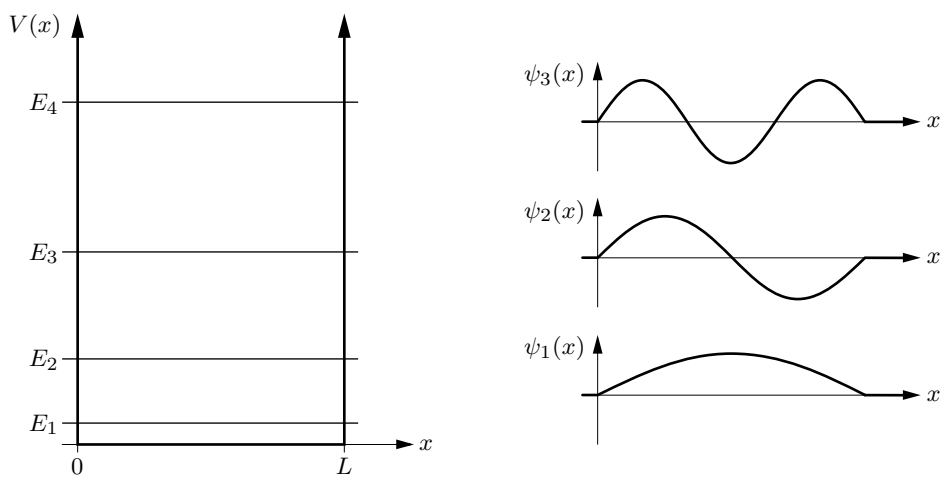
**Figure A.6.** A more complete illustration of the wavefunction of a particle with well-defined momentum, showing both the “real” and “imaginary” parts of the function. Copyright ©2000, Addison-Wesley.



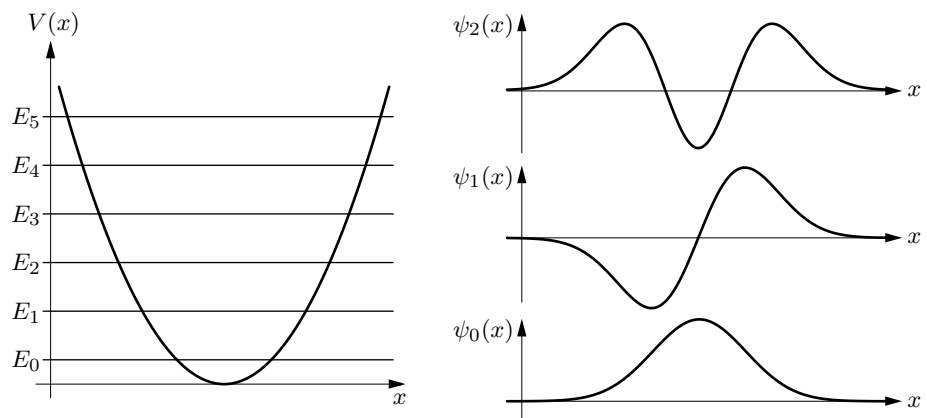
**Figure A.7.** Other possible wavefunctions for which neither the position nor the momentum of the particle is well defined. Copyright ©2000, Addison-Wesley.



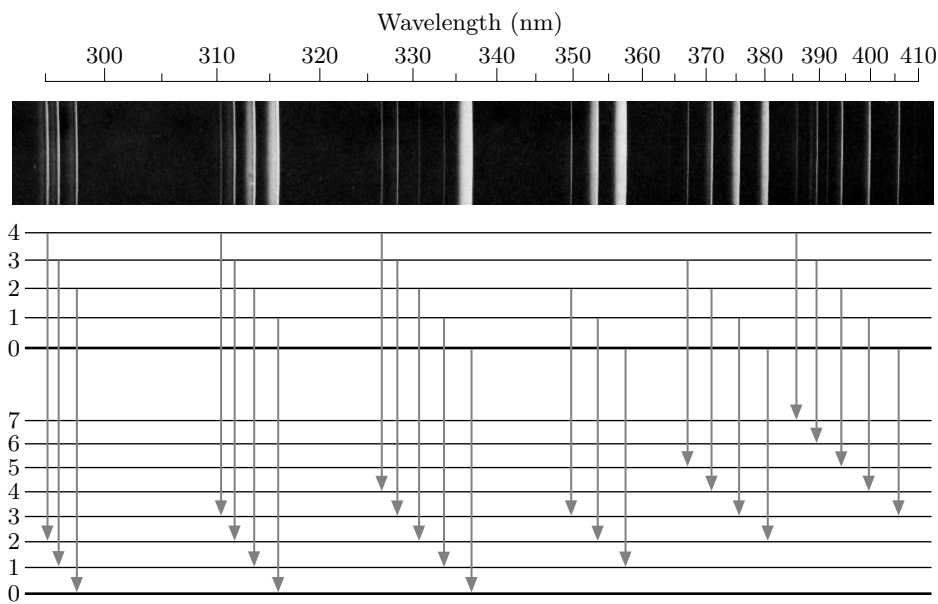
**Figure A.8.** A **wavepacket**, for which both  $x$  and  $p_x$  are defined approximately but not precisely. The “width” of the wavepacket is quantified by  $\Delta x$ , technically the standard deviation of the square of the wavefunction. (As you can see,  $\Delta x$  is actually a few times smaller than the “full” width.) Copyright ©2000, Addison-Wesley.



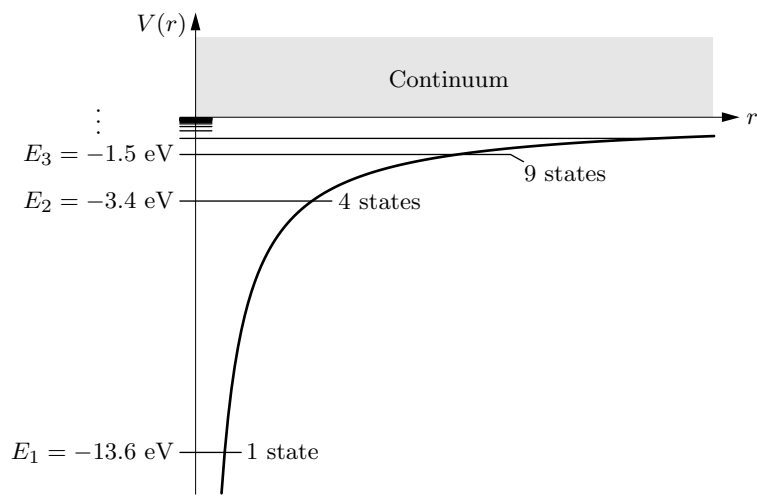
**Figure A.9.** A few of the lowest energy levels and corresponding definite-energy wavefunctions for a particle in a one-dimensional box. Copyright ©2000, Addison-Wesley.



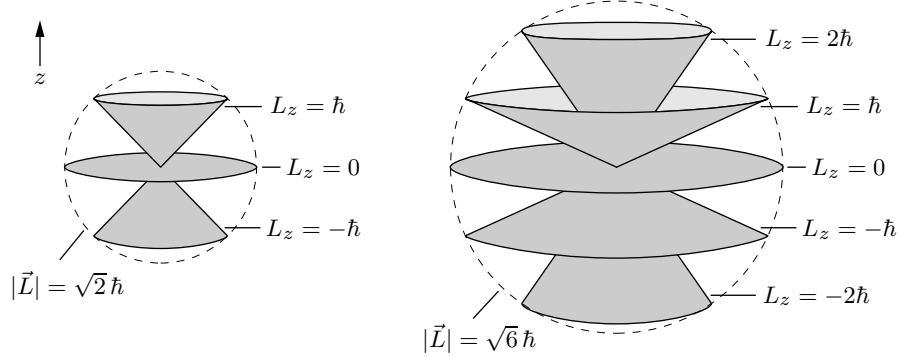
**Figure A.10.** A few of the lowest energy levels and corresponding wavefunctions for a one-dimensional quantum harmonic oscillator. Copyright ©2000, Addison-Wesley.



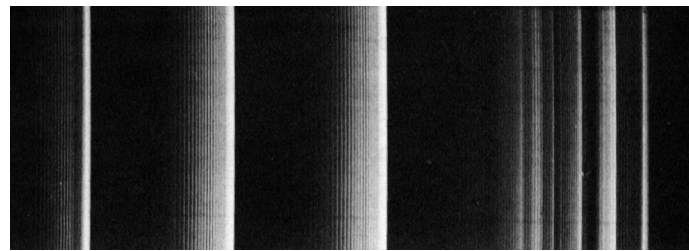
**Figure A.11.** A portion of the emission spectrum of molecular nitrogen,  $\text{N}_2$ . The energy level diagram shows the transitions corresponding to the various spectral lines. All of the lines shown are from transitions between the same pair of electronic states. In either electronic state, however, the molecule can also have one or more “units” of vibrational energy; these numbers are labeled at left. The spectral lines are grouped according to the number of units of vibrational energy gained or lost. The splitting within each group of lines occurs because the vibrational levels are spaced farther apart in one electronic state than in the other. From Gordon M. Barrow, *Introduction to Molecular Spectroscopy* (McGraw-Hill, New York, 1962). Photo originally provided by J. A. Marquisee. Copyright ©2000, Addison-Wesley.



**Figure A.12.** Energy level diagram for a hydrogen atom. The heavy curve is the potential energy function, proportional to  $-1/r$ . In addition to the discretely spaced negative-energy states, there is a continuum of positive-energy (ionized) states. Copyright ©2000, Addison-Wesley.

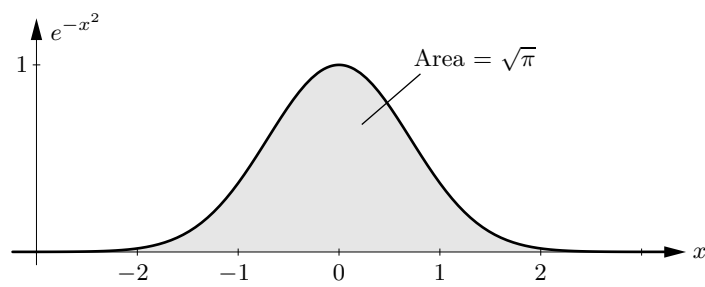


**Figure A.13.** A particle with well-defined  $|\vec{L}|$  and  $L_z$  has completely undefined  $L_x$  and  $L_y$ , so we can visualize its angular momentum “vector” as a cone, smeared over all possible  $L_x$  and  $L_y$  values. Shown here are the allowed states for  $\ell = 1$  and  $\ell = 2$ . Copyright ©2000, Addison-Wesley.



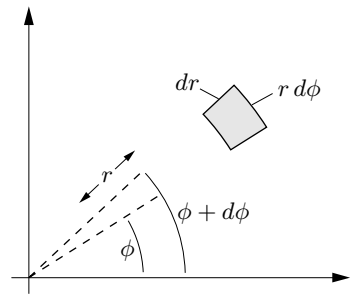
**Figure A.14.** Enlargement of a portion of the  $\text{N}_2$  spectrum shown in Figure A.11, covering approximately the range 370–390 nm. Each of the broad lines is actually split into a “band” of many narrow lines, due to the multiplicity of rotational levels for each vibrational level. From Gordon M. Barrow, *Introduction to Molecular Spectroscopy* (McGraw-Hill, New York, 1962). Photo originally provided by J. A. Marquisee. Copyright ©2000, Addison-Wesley.

# B Mathematical Results



**Figure B.1.** The Gaussian function  $e^{-x^2}$ , whose integral from  $-\infty$  to  $\infty$  is  $\sqrt{\pi}$ .  
Copyright ©2000, Addison-Wesley.

**Figure B.2.** In polar coordinates, the infinitesimal area element is  $(dr)(r d\phi)$ .  
Copyright ©2000, Addison-Wesley.



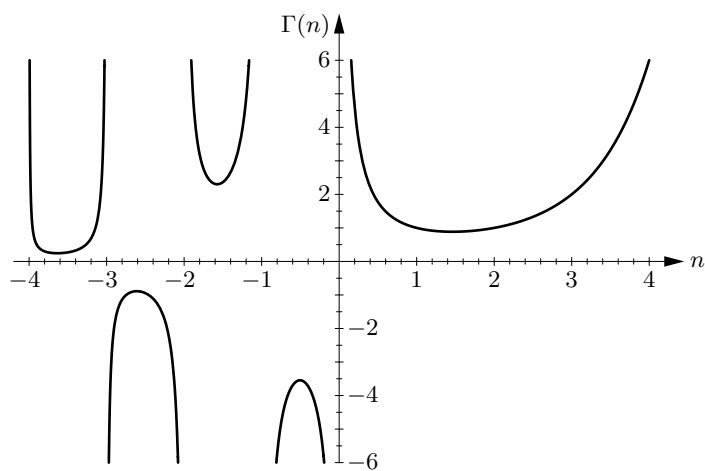


**Figure B.3.** The gamma function,  $\Gamma(n)$ . For positive integer arguments,  $\Gamma(n) = (n-1)!$ . For positive nonintegers,  $\Gamma(n)$  can be computed from equation B.12, while for negative nonintegers,  $\Gamma(n)$  can be computed from equation B.14. Copyright ©2000, Addison-Wesley.

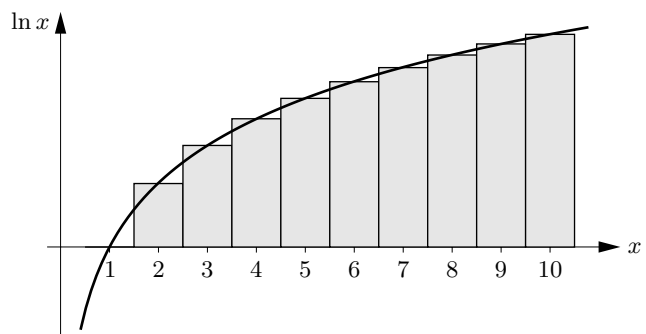


**Figure B.4.** The area under the bar graph, up to any integer  $n$ , equals  $\ln n!$ . When  $n$  is large, this area can be approximated by the area under the smooth curve of the logarithm function. Copyright ©2000, Addison-Wesley.

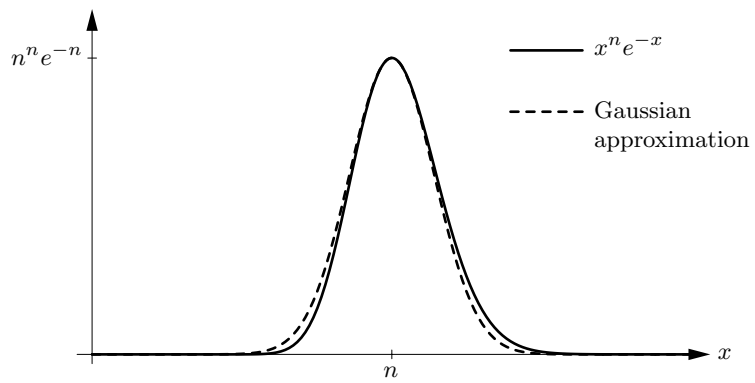


**Figure B.5.** The function  $x^n e^{-x}$  (solid curve), plotted for  $n = 50$ . The area under this curve is  $n!$ . The dashed curve shows the best Gaussian fit, whose area gives Stirling's approximation to  $n!$ . Copyright ©2000, Addison-Wesley.

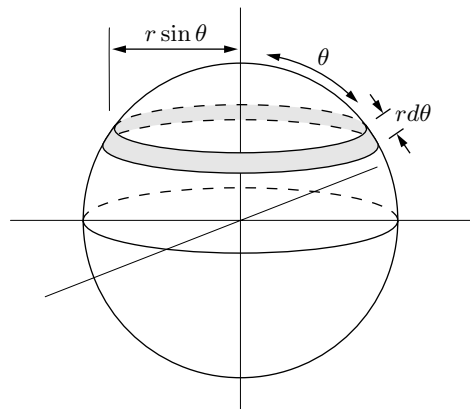


**Figure B.6.** To calculate the area of a sphere, divide it into loops and integrate. To calculate the area of a hypersphere, do the same thing. Copyright ©2000, Addison-Wesley.

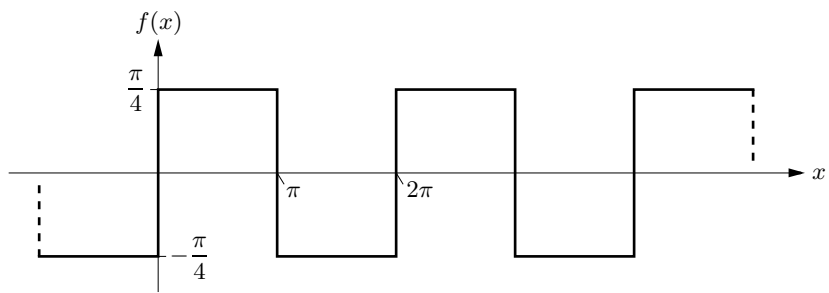


**Figure B.7.** A square-wave function with period  $2\pi$  and amplitude  $\pi/4$ . The Fourier series for this function yields values of  $\zeta(n)$  when  $n$  is an even integer.  
Copyright ©2000, Addison-Wesley.

# Reference Data

## Physical Constants

$$\begin{aligned}k &= 1.381 \times 10^{-23} \text{ J/K} \\&= 8.617 \times 10^{-5} \text{ eV/K} \\N_A &= 6.022 \times 10^{23} \\R &= 8.315 \text{ J/mol}\cdot\text{K} \\h &= 6.626 \times 10^{-34} \text{ J}\cdot\text{s} \\&= 4.136 \times 10^{-15} \text{ eV}\cdot\text{s} \\c &= 2.998 \times 10^8 \text{ m/s} \\G &= 6.673 \times 10^{-11} \text{ N}\cdot\text{m}^2/\text{kg}^2 \\e &= 1.602 \times 10^{-19} \text{ C} \\m_e &= 9.109 \times 10^{-31} \text{ kg} \\m_p &= 1.673 \times 10^{-27} \text{ kg}\end{aligned}$$

## Unit Conversions

$$\begin{aligned}1 \text{ atm} &= 1.013 \text{ bar} = 1.013 \times 10^5 \text{ N/m}^2 \\&= 14.7 \text{ lb/in}^2 = 760 \text{ mm Hg} \\(T \text{ in } ^\circ\text{C}) &= (T \text{ in K}) - 273.15 \\(T \text{ in } ^\circ\text{F}) &= \frac{9}{5}(T \text{ in } ^\circ\text{C}) + 32 \\1 \text{ }^\circ\text{R} &= \frac{5}{9} \text{ K} \\1 \text{ cal} &= 4.186 \text{ J} \\1 \text{ Btu} &= 1054 \text{ J} \\1 \text{ eV} &= 1.602 \times 10^{-19} \text{ J} \\1 \text{ u} &= 1.661 \times 10^{-27} \text{ kg}\end{aligned}$$

The atomic number (top left) is the number of protons in the nucleus. The atomic mass (bottom) is weighted by isotopic abundances in the earth's surface. Atomic masses are relative to the mass of the carbon-12 isotope, defined to be exactly 12 unified atomic mass units (u). Uncertainties range from 1 to 9 in the last digit quoted. Relative isotopic abundances often vary considerably, both in natural and commercial samples. A number in parentheses is the mass of the longest-lived isotope of that element—no stable isotope exists. However, although Th, Pa, and U have no stable isotopes, they do have characteristic terrestrial compositions, and meaningful weighted masses can be given. For elements 110–112, the mass numbers of known isotopes are given. From the Review of Particle Physics by the Particle Data Group, *The European Physical Journal C3*, 73 (1998).

1 IA	Periodic Table of the Elements																	
1 <b>H</b> Hydrogen 1.00794	2 <b>He</b> Helium 4.002602	3 <b>Li</b> Lithium 6.941	4 <b>Be</b> Beryllium 9.012182	5	6	7	8	9	10	11	12	13 <b>Al</b> Boron 10.811	14 <b>Si</b> Silicon 12.0107	15 <b>P</b> Phosph. 14.00674	16 <b>S</b> Sulfur 28.0855	17 <b>Cl</b> Chlorine 30.973761	2 <b>He</b> Helium 4.002602	
11 <b>Na</b> Sodium 22.989770	12 <b>Mg</b> Magnesium 24.3050	3 <b>Sc</b> Scandium 44.955910	4 <b>Ti</b> Titanium 47.867	5 <b>V</b> Vanadium 50.9415	6 <b>Cr</b> Chromium 51.9961	7 <b>Mn</b> Manganese 54.938049	8 <b>Fe</b> Iron 55.845	9 <b>Co</b> Cobalt 58.933200	10 <b>Ni</b> Nickel 58.6934	11 <b>Cu</b> Copper 63.546	12 <b>Zn</b> Zinc 65.39	13 <b>Ga</b> Gallium 69.723	14 <b>Ge</b> German. 72.61	15 <b>As</b> Arsenic 74.92160	16 <b>Se</b> Selenium 78.96	17 <b>Br</b> Bromine 79.904	18 <b>Ar</b> Argon 39.948	
19 <b>K</b> Potassium 39.0983	20 <b>Ca</b> Calcium 40.078	21 <b>Sc</b> Scandium 44.955910	22 <b>Ti</b> Titanium 47.867	23 <b>V</b> Vanadium 50.9415	24 <b>Cr</b> Chromium 51.9961	25 <b>Mn</b> Manganese 54.938049	26 <b>Fe</b> Iron 55.845	27 <b>Co</b> Cobalt 58.933200	28 <b>Ni</b> Nickel 58.6934	29 <b>Cu</b> Copper 63.546	30 <b>Zn</b> Zinc 65.39	31 <b>Ga</b> Gallium 69.723	32 <b>Ge</b> German. 72.61	33 <b>As</b> Arsenic 74.92160	34 <b>Se</b> Selenium 78.96	35 <b>Br</b> Bromine 79.904	36 <b>Kr</b> Krypton 83.80	
37 <b>Rb</b> Rubidium 85.4678	38 <b>Sr</b> Strontium 87.62	39 <b>Y</b> Yttrium 88.90585	40 <b>Zr</b> Zirconium 91.224	41 <b>Nb</b> Niobium 92.90638	42 <b>Mo</b> Molybd. (97.907215)	43 <b>Tc</b> Technet. 95.94	44 <b>Ru</b> Ruthen. 101.07	45 <b>Rh</b> Rhodium 102.90550	46 <b>Pd</b> Palladium 106.42	47 <b>Ag</b> Silver 107.8682	48 <b>Cd</b> Cadmium 112.411	49 <b>In</b> Indium 114.818	50 <b>Sn</b> Tin 118.710	51 <b>Sb</b> Antimony 121.760	52 <b>Te</b> Tellurium 127.60	53 <b>I</b> Iodine 126.90447	54 <b>Xe</b> Xenon 131.29	
55 <b>Cs</b> Cesium 132.90545	56 <b>Ba</b> Barium 137.327	57–71 Lanthanides 178.49	72 <b>Hf</b> Hafnium 180.9479	73 <b>Ta</b> Tantalum 183.84	74 <b>W</b> Tungsten 186.207	75 <b>Re</b> Rhenium 190.23	76 <b>Os</b> Osmium 192.217	77 <b>Ir</b> Iridium 195.078	78 <b>Pt</b> Platinum 196.96655	79 <b>Au</b> Gold 200.59	80 <b>Hg</b> Mercury 204.3833	81 <b>Tl</b> Thallium 207.2	82 <b>Pb</b> Lead 208.98038	83 <b>Bi</b> Bismuth (208.982415)	84 <b>Po</b> Polonium (209.987131)	85 <b>At</b> Astatine (222.017570)	86 <b>Rn</b>	
87 <b>Fr</b> Francium (223.019731)	88 <b>Ra</b> Radium (226.025402)	89–103 Actinides (261.1089)	104 <b>Rf</b> Rutherford. (262.1144)	105 <b>Db</b> Dubnium (263.1186)	106 <b>Sg</b> Seaborg. (262.1231)	107 <b>Bh</b> Bohrium (265.1306)	108 <b>Hs</b> Hassium (266.1378)	109 <b>Mt</b> Meitner. (269, 273)	110	111	112							
Lanthanide series		57 <b>La</b> Lanthanum 138.9055	58 <b>Ce</b> Cerium 140.116	59 <b>Pr</b> Praseodym. 140.90765	60 <b>Nd</b> Neodym. 144.24	61 <b>Pm</b> Prometh. (144.912745)	62 <b>Sm</b> Samarium 150.36	63 <b>Eu</b> Europium 151.964	64 <b>Gd</b> Gadolin. 157.25	65 <b>Tb</b> Terbium 158.92534	66 <b>Dy</b> Dyspros. 162.50	67 <b>Ho</b> Holmium 164.93032	68 <b>Er</b> Erbium 167.26	69 <b>Tm</b> Thulium 168.93421	70 <b>Yb</b> Ytterbium 173.04	71 <b>Lu</b> Lutetium 174.967		
Actinide series		89 <b>Ac</b> Actinium (227.027747)	90 <b>Th</b> Thorium 232.0381	91 <b>Pa</b> Protactin. 231.03588	92 <b>U</b> Uranium 238.0289	93 <b>Np</b> Neptunium (237.048166)	94 <b>Pu</b> Plutonium (244.064197)	95 <b>Am</b> Americium (243.061372)	96 <b>Cm</b> Curium (247.070346)	97 <b>Bk</b> Berkelium (247.070298)	98 <b>Cf</b> Californ. Einstein. (251.079579)	99 <b>Es</b> Einstein. Fermium (252.08297)	100 <b>Fm</b> Fermium (257.095096)	101 <b>Md</b> Mendelev. (258.098427)	102 <b>No</b> Nobelium (259.1011)	103 <b>Lr</b> Lawrenc. (262.1098)		

## Thermodynamic Properties of Selected Substances

All of the values in this table are for one mole of material at 298 K and 1 bar. Following the chemical formula is the form of the substance, either solid (s), liquid (l), gas (g), or aqueous solution (aq). When there is more than one common solid form, the mineral name or crystal structure is indicated. Data for aqueous solutions are at a standard concentration of 1 mole per kilogram water. The enthalpy and Gibbs free energy of formation,  $\Delta_f H$  and  $\Delta_f G$ , represent the changes in  $H$  and  $G$  upon forming one mole of the material starting with elements in their most stable pure states (e.g., C (graphite), O<sub>2</sub> (g), etc.). To obtain the value of  $\Delta H$  or  $\Delta G$  for another reaction, subtract  $\Delta_f$  of the reactants from  $\Delta_f$  of the products. For ions in solution there is an ambiguity in dividing thermodynamic quantities between the positive and negative ions; by convention, H<sup>+</sup> is assigned the value zero and all others are chosen to be consistent with this value. Data from Atkins (1998), Lide (1994), and Anderson (1996). Please note that, while these data are sufficiently accurate and consistent for the examples and problems in this textbook, not all of the digits shown are necessarily significant; for research purposes you should always consult original literature to determine experimental uncertainties.

Substance (form)	$\Delta_f H$ (kJ)	$\Delta_f G$ (kJ)	$S$ (J/K)	$C_P$ (J/K)	$V$ (cm <sup>3</sup> )
Al (s)	0	0	28.33	24.35	9.99
Al <sub>2</sub> SiO <sub>5</sub> (kyanite)	-2594.29	-2443.88	83.81	121.71	44.09
Al <sub>2</sub> SiO <sub>5</sub> (andalusite)	-2590.27	-2442.66	93.22	122.72	51.53
Al <sub>2</sub> SiO <sub>5</sub> (sillimanite)	-2587.76	-2440.99	96.11	124.52	49.90
Ar (g)	0	0	154.84	20.79	
C (graphite)	0	0	5.74	8.53	5.30
C (diamond)	1.895	2.900	2.38	6.11	3.42
CH <sub>4</sub> (g)	-74.81	-50.72	186.26	35.31	
C <sub>2</sub> H <sub>6</sub> (g)	-84.68	-32.82	229.60	52.63	
C <sub>3</sub> H <sub>8</sub> (g)	-103.85	-23.49	269.91	73.5	
C <sub>2</sub> H <sub>5</sub> OH (l)	-277.69	-174.78	160.7	111.46	58.4
C <sub>6</sub> H <sub>12</sub> O <sub>6</sub> (glucose)	-1273	-910	212	115	
CO (g)	-110.53	-137.17	197.67	29.14	
CO <sub>2</sub> (g)	-393.51	-394.36	213.74	37.11	
H <sub>2</sub> CO <sub>3</sub> (aq)	-699.65	-623.08	187.4		
HCO <sub>3</sub> <sup>-</sup> (aq)	-691.99	-586.77	91.2		
Ca <sup>2+</sup> (aq)	-542.83	-553.58	-53.1		
CaCO <sub>3</sub> (calcite)	-1206.9	-1128.8	92.9	81.88	36.93
CaCO <sub>3</sub> (aragonite)	-1207.1	-1127.8	88.7	81.25	34.15
CaCl <sub>2</sub> (s)	-795.8	-748.1	104.6	72.59	51.6
Cl <sub>2</sub> (g)	0	0	223.07	33.91	
Cl <sup>-</sup> (aq)	-167.16	-131.23	56.5	-136.4	17.3
Cu (s)	0	0	33.150	24.44	7.12
Fe (s)	0	0	27.28	25.10	7.11

Substance (form)	$\Delta_f H$ (kJ)	$\Delta_f G$ (kJ)	$S$ (J/K)	$C_P$ (J/K)	$V$ (cm <sup>3</sup> )
H <sub>2</sub> (g)	0	0	130.68	28.82	
H (g)	217.97	203.25	114.71	20.78	
H <sup>+</sup> (aq)	0	0	0	0	
H <sub>2</sub> O (l)	-285.83	-237.13	69.91	75.29	18.068
H <sub>2</sub> O (g)	-241.82	-228.57	188.83	33.58	
He (g)	0	0	126.15	20.79	
Hg (l)	0	0	76.02	27.98	14.81
N <sub>2</sub> (g)	0	0	191.61	29.12	
NH <sub>3</sub> (g)	-46.11	-16.45	192.45	35.06	
Na <sup>+</sup> (aq)	-240.12	-261.91	59.0	46.4	-1.2
NaCl (s)	-411.15	-384.14	72.13	50.50	27.01
NaAlSi <sub>3</sub> O <sub>8</sub> (albite)	-3935.1	-3711.5	207.40	205.10	100.07
NaAlSi <sub>2</sub> O <sub>6</sub> (jadeite)	-3030.9	-2852.1	133.5	160.0	60.40
Ne (g)	0	0	146.33	20.79	
O <sub>2</sub> (g)	0	0	205.14	29.38	
O <sub>2</sub> (aq)	-11.7	16.4	110.9		
OH <sup>-</sup> (aq)	-229.99	-157.24	-10.75	-148.5	
Pb (s)	0	0	64.81	26.44	18.3
PbO <sub>2</sub> (s)	-277.4	-217.33	68.6	64.64	
PbSO <sub>4</sub> (s)	-920.0	-813.0	148.5	103.2	
SO <sub>4</sub> <sup>2-</sup> (aq)	-909.27	-744.53	20.1	-293	
HSO <sub>4</sub> <sup>-</sup> (aq)	-887.34	-755.91	131.8	-84	
SiO <sub>2</sub> ( $\alpha$ quartz)	-910.94	-856.64	41.84	44.43	22.69
H <sub>4</sub> SiO <sub>4</sub> (aq)	-1449.36	-1307.67	215.13	468.98	